4

Result and Discussion

The major objective of this research work targeted on the investigation of the IEDDA reaction chemistry of the diene 2-oxo-2*H*-pyrido[1, 2-*a*]pyrimidin-3(4*H*)-ylidene acetic acid (**3**). To achieve this, diene was synthesized by the procedure reported in **(N. R. Campbell and J. H. Hunt, 1947 and Venugopal & Sundaram, 2016)**.

4.1. PREPARATION OF 2-OXO-2*H*-PYRIDO [1, 2-*a*] PYRIMIDIN-3(4*H*)-YLIDENE ACETIC ACID

The target diene 2-oxo-2*H*-pyrido [1, 2-*a*] pyrimidin-3(4*H*)-ylidene acetic acid **3** was synthesized from aconic acid **2** and 2-aminopyridine **1** in the presence of alcohol at room temperature. The reaction progressed with high yield giving rise to the target diene **3** in one synthetic operation **Scheme 11**.

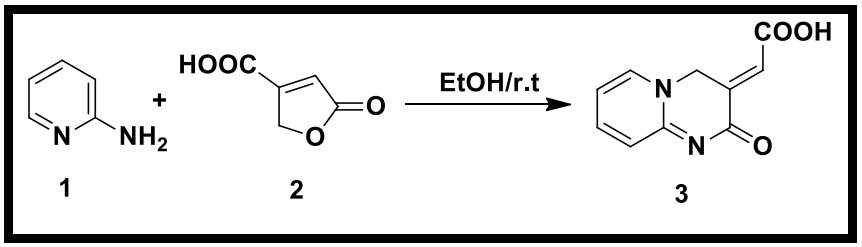

Scheme 11: Preparation of 2-oxo-2*H*-pyrido[1, 2-*a*]pyrimidin-3(4*H*)-ylidene acetic acid

4.1.1 Selectivity

4.1.1. a Regioselectivity of IEDDA

IEDDA reaction as that of DA reaction will give different regioisomers depending upon the substituent pattern of dienes and dienophiles. The regiochemistry of the reaction is governed by *ortho-para* rule. If the EWG is present at C_1 of diene, the addition will proceed so as to position the EDG of dienophile *ortho* to EWG group of diene. If the substitution is present at position 2 of the diene, the product will be formed in such a way that EWG and EDG are *para* to each other. These rules are derived from FMO analysis or Zwitter Ionic Models **(Houk, 1973)**. The target diene **(3)** of the present work has two electron withdrawing centres, C_{11} carboxylic group and C_2 carbonyl group adjacent to ring nitrogen.

The target diene (3) of the present work has two electron withdrawing centers, (C_{11}) carboxylic group and C_2 carbonyl group adjacent to ring nitrogen.

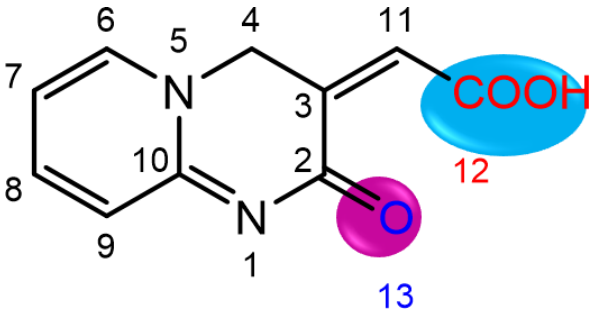

Based on the resonance of the parent nuclei Pyrido [1, 2-*a*] pyrimidin-2-ones **(Alanine et al., 2016)** of the diene the C_2 carbonyl group acquires negative charge

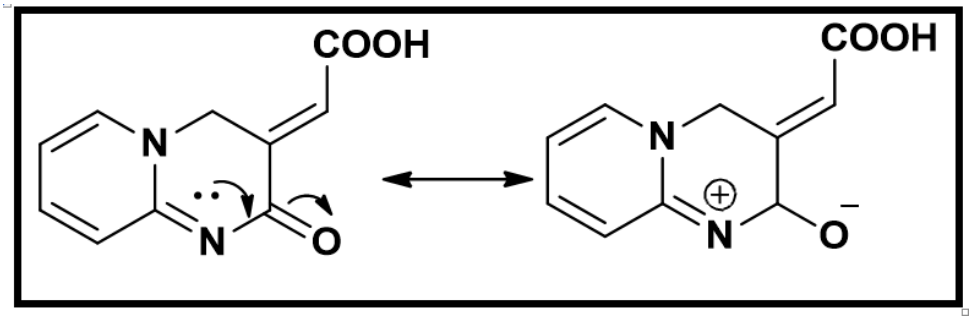

Figure 8: Resonance Structures of diene (3)

Therefore, the carboxylic acid moiety of the target will act as more electron withdrawing centre compared to C_2 carbonyl. Hence the IEDDA reaction of **(3)** may proceed with regioselective cycloaddition across the C_{11} carbon of the diene with the dienophile carbon possessing EDG.

4.1.1. b Endo/Exo Selectivity of IEDDA

Stereoselectivity of IEDDA reaction is governed by *endo*-rule. The *endo* adducts are favoured products because of the secondary orbital interaction, that occurs between π system of the diene and π system with the dienophilc double bond **(Png et al., 2017)**. The expected *endo* and *exo* isomer of the reaction between diene(3) and dienophiles (4,6,8,10 and 12) are depicted in **Figure 9.**

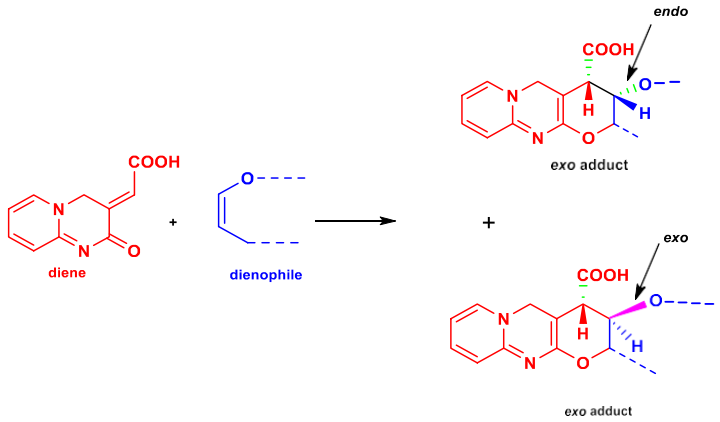

Figure 9: Possible *endo-exo* isomers of diene (3)

4.1.1 Selection of Dienophile

Butyl vinyl ether **(4),** 1-phenyl-3-methyl-pyrazolone **(6),** 1-methyl-1-cyclohexene **(8),** 3, 4-Dihydro-2H-pyran **(10)** and 1-morpholinocyclohexene **(12)** were selected for the IEDDA reaction with target diene **(3)** based on the previously reported IEDDA reaction**.**

Structure of the Dienophiles	
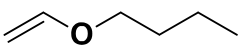 1-(vinyloxy)butane **(4)** **(Stepanova & Maslivets, 2015)**	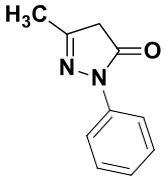 3-methyl-1-phenyl-1*H*-pyrazol-5(4*H*)-one **(6)**
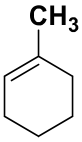 1-methylcyclohex-1-ene (8) **(Gardiner et al., 2015)**	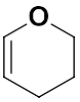 3,4-dihydro-2*H*-pyran (10) **(Babu & Perumal, 1998)**
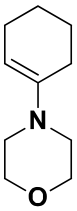 4-(cyclohex-1-en-1-yl)morpholine (12)	

4.2. SYNTHESIS OF 3-BUTOXY-2,3,4,5-TETRAHYDRO PYRANO[2, 3-*d*]PYRIDO [1, 2-*a*] PYRIMIDINE-4-CARBOXYLIC ACID

The reaction between 2-oxo-2*H*-pyrido[1,2-*a*] pyrimidin-3(4*H*)-ylidiene acetic acid **(3)** and the selected dienophile butyl vinyl ether **(4)** has been carried out in presence of various catalysts using different solvents to optimize the reaction conditions.

4.2.1. Optimization of the Reaction Condition for IEDDA

Optimizing the reaction conditions for the organic synthesis are keys to get successful and reproducible synthetic products. The reaction conditions such as presence of catalyst, solvent, reaction time and temperature are highly sensitive to get the desired products. By undertaking optimization, it is easy to tune the yield and purity of the desired products and can also eliminate the by-product formation.

The present study IEDDA reaction started with the diene 2-oxo-2*H*-pyrido [1, 2-*a*] pyrimidin-3(4*H*) -ylidene acetic acid **(3)** and the dienophile butyl vinyl ether **(4)** as the model substrates for the scrutinization and optimization of the reaction conditions. The reaction without catalyst at room temperature was carried out for 24h. The TLC examination of the reaction mixture showed no product formation.

Generally, IEDDA reaction requires rugged conditions. To improve the reactivity of the diene the LUMO energy must be lowered. This task of lowering of LUMO energy is accomplished by coordination with a Lewis acid which act as a catalyst for this IEDDA adduct forming reaction. Verities of Lewis acid catalyst based on Copper **(Li *et al.*, 2016 and Yang *et al.*, 2022)**, Indium **(Prajapati & Gohain, 2006)** Boron trifluoride **(Schnell *et al.*, 2021)** and Iron **(Tanaka *et al.*, 2019)** have been reported in the literatures for IEDDA reaction.

4.2.1.1. Selection of Reaction Catalyst

These results and reported literatures prompted the investigation of this reaction with the possible Lewis acid catalysts. Different Lewis acid catalyst viz., Aluminium Chloride ($AlCl_3$) Zinc Chloride ($ZnCl_2$) and Indium(III) Chloride ($InCl_3$) has been taken for the IEDDA adduct formation reaction in water at room temperatures under air. The details of the reaction conditions and resulted yields are tabulated in **Table 1.** The results clearly revealed that presence of catalyst was the essential criteria for the IEDDA adduct formation reaction to

occur. Among the chosen catalysts, indium(III) chloride yielded better results than the others. So further optimization was done with indium(III) chloride catalyst.

Table 1: Optimization of Reaction Catalyst

Entry	Catalyst	Solvent	Temperature/Time	Yield (%)
1.	-	Water	25°C/12h	n.d.
2.	-	Water	25°C/24h	n.d.
3.	$AlCl_3$	Water	25°C/12h	12
4.	$ZnCl_2$	Water	25°C/12h	20
5.	$InCl_3$	Water	25°C/12h	22

★ n.d-not detected

4.2.1.2. Optimization of Reactants to Catalyst Concentrations

After selecting the catalyst, the parameters such as catalyst loading and reaction concentrations in molar ratios were investigated. As the Diels Alder reaction usually required the dienes and dienophiles in the 1:1 equiv molar ratio with one reactive centre, the molar ratio of the reactant to catalyzed has be optimized with different ratios viz 1:1:1 [diene (1) : dienophile (1) : catalyst (1)]; 1:1:2 1:1:5 and 1:1:10. The studied reaction parameters and conditions with the respective yields of the reaction products are presented in **Table 2.**

Table 2: Optimization of Reactants & Catalyst Concentrations

Entry	Catalyst	Solvent	Temperature/ Time	Molar Ratios Diene : Dienophile : Catalyst	Yield (%)
1.	$InCl_3$	Water	25°C/12h	1:1:1	6
2.	$InCl_3$	Water	25°C/12h	1:1:2	15
3.	$InCl_3$	Water	25°C/12h	1:1:5	18
4.	$InCl_3$	Water	25°C/12h	1:1:10	22

Gratifyingly, the reaction proceeded to afford the IEDDA adduct in moderate yield, when the substrates 2-oxo-2*H*-pyrido [1, 2-*a*] pyrimidin-3(4*H*) -ylidene acetic acid and butyl vinyl ether were reacted with indium (III) chloride in 1:1:10 molar ratio in water. Hence further optimizations were carried out with indium (III) chloride in 1:1:10 molar ratios.

4.2.1.3. Optimization of Reaction Medium - Solvent

Influence of solvent on the formation of IEDDA adduct was also optimized with various solvents such as water, CH_3CN and DMF. Surprisingly, the use of DMF as a solvent led to an increase in the yield to 30%, when the substrates 2-oxo-2*H*-pyrido [1, 2-*a*]

pyrimidin-3(4*H*) -ylidene acetic acid **(3)** and butyl vinyl ether **(4)** were reacted with indium(III) chloride at 25^{o}C for 12 h. In order to study the influence of DMF on the reaction a trial run was carried out without catalyst with DMF but no products were found even after 24 h of reaction time.

Table 3: Optimization of Reaction Medium - Solvent

Entry	Catalyst	Solvent	Temperature/ Time	Yield (%)
1.	$InCl_3$	Water	25^{o}C/12h	22
2.	$InCl_3$	CH_3CN	25^{o}C/12h	n.d.
3.	$InCl_3$	DMF	25^{o}C/12h	30
4.	-	DMF	25^{o}C/24h	n.d.

4.2.1.4. Optimization of Reaction Time and Temperature

Reaction time and temperature were also found to influence the product characteristics. In this IEDDA adduct formation, influence of the reaction time and temperature were investigated by conducting the same reactions with different temperature for various reaction periods. The adopted reaction conditions and obtained results are given in the **Table 4:** On increasing the reaction temperature from 25^{o}C to 50^{o}C the yield increased to about 38%. Further increasing the temperature to 90^{o}C increase the yield of the IEDDA adduct to above 50%.

Table 4: Optimization of Reaction Time and Temperature

Entry	Catalyst	Solvent	Temperature/ Time	Yield (%)
1.	$InCl_3$	DMF	25^{o}C/12h	30
2.	$InCl_3$	DMF	50^{o}C/12h	38
3.	$InCl_3$	DMF	50^{o}C/6h	37
4.	$InCl_3$	DMF	90^{o}C/6h	55
5.	$InCl_3$	DMF	90^{o}C/5h	55
6.	$InCl_3$	DMF	90^{o}C/4h	55
7.	$InCl_3$	DMF	90^{o}C/3h	50
8.	$InCl_3$	DMF	90^{o}C/4½h	55
9.	-	DMF	90^{o}C/4½h	n.d.
10.	-	DMF	90^{o}C/12h	n.d.

However, increasing the reaction temperature to 90^{o}C reflux for 4½h afforded IEDDA adduct in 55% yield respectively. In contrast, no effect was observed for the target reaction

without Lewis acid catalyst adopting the reaction conditions. Thus, the optimized conditions for the IEDDA adduct formation from the target diene were found to be,

Catalyst	Indium (III) Chloride
Molar Ratio	Diene; Dienophile & catalyst (1:1:10) molar ratio
Solvent	Dimethyl formamide (DMF)
Reaction Temperature	90 ^{o} C
Reaction Time Period	4 ½ h

By adopting the optimised conditions, the reaction between 2-oxo-2*H*-pyrido [1, 2-*a*] pyrimidin-3(4*H*) -ylidene acetic acid **(3)** and butyl vinyl ether **(4)** were carried out in DMF solvent at 90^{o}C **Scheme 12**.. A product appeared after 2h and the mixture was held at reflux temperature for a period of 4½ h. TLC analysis of the mixture after 3h showed the gradual diminishing of starting material concentration. After 4½ h the TLC showed no remaining starting material and a single major spot.

The reaction afforded a brown precipitate as a mixture. Under classical conditions the mixture failed to afford a single diastereoisomer after column chromatography. Hencefurther characterization the adducts were carried out after recrystallizing it with ethyl alcohol. The melting point of the adducts was in the range of 280^{0}C – 285^{0}C. Similar reactions were carried out for 7-methyl and 8-methyl substituted 2-oxo-2*H*-pyrido [1, 2-*a*] pyrimidin-3(4*H*) -ylidene acetic acid **(3b and 3c)** and butyl vinyl ether **(4)** maintaining the same optimized conditions **Scheme 12**. However, the time required for complete consumption of the reactants varied substantially. The details of the products formed andtheir resulting yield and melting points are given in **Table 5.**

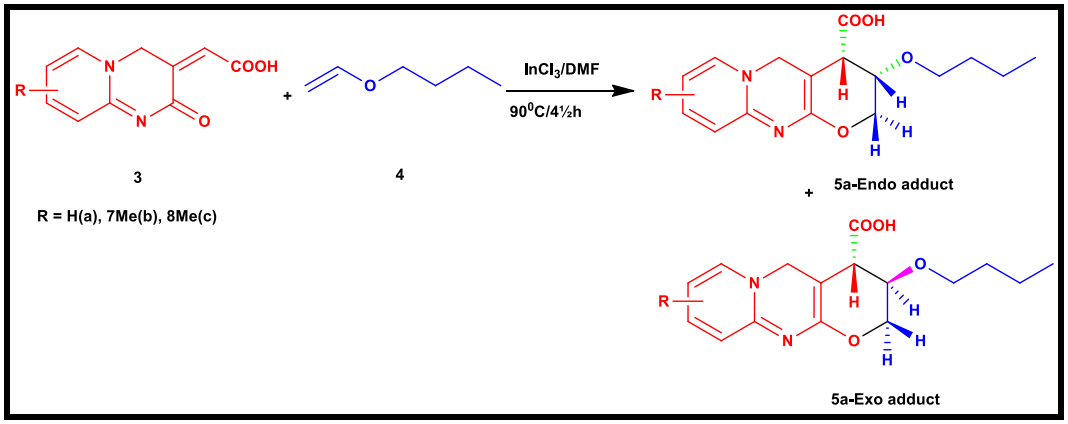

Scheme 12: Synthesis of 3-Butoxy-2, 3, 4, 5-tetrahydropyrano [2, 3-*d*] pyrido[1,2-*a*] pyrimidine-4-carboxylic acid derivatives

Table 5: Reaction Conditions, Melting Point and Yield of 3-Butoxy-2, 3, 4, 5-Tetrahydropyrano [2, 3-*d*]Pyrido[1,2-*a*] Pyrimidine-4-Carboxylic Acid Derivatives

Diene	Dienophile	Temp./Time	Product	Yield/M.P
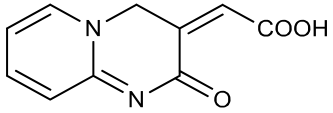	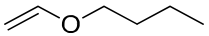	90˚C/4½	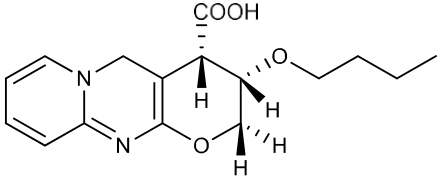	55% /280-285˚C
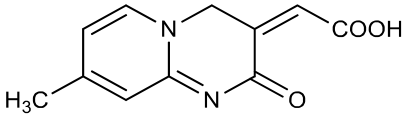		90˚C/5	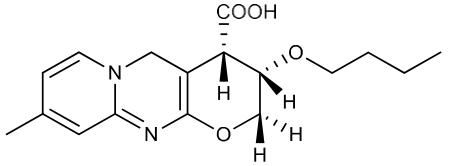	58% /292-297˚C
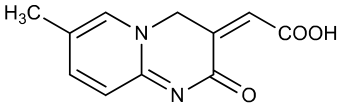		90˚C/5½	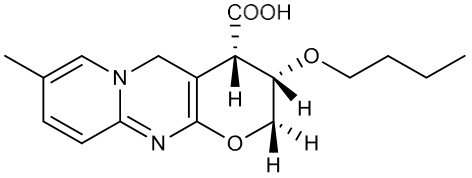	58%/ 298-300˚C

4.2.2. SPECTRAL CHARACTERIZATION OF THE SYNTHESIZED CYCLIC ADDUCT (5a)

4.2.2.1 FT-IR SPECTRUM

The structure of the adduct **5a** was arrived based on FT-IR spectroscopic analysis. Presence of pyridopyrimidine nucleus was confirmed by a absorption bands of C=N and C=C at 1638 cm^{-1},1574 cm^{-1} and 1433 cm^{-1} respectively **(Figure 10)**. A broad intense O-H stretching band centered at 3327 cm^{-1} was an overriding spectral feature of the carboxylic acid. This was also confirmed by the presence of strong intense O-H in plane bend at 1373 cm^{-1} along with medium intense O-H out of plane bend at 988 cm^{-1}.

The strong and medium intense bands at 1686 cm^{-1} and 1294 cm^{-1} were attributed to the -C=O and -C-O stretch of the carboxylic acid moiety respectively. The peak observed at 2959 cm-^{1}, 2922 cm^{-1} and 1148 cm^{-1} corresponds to sp^3 C-H stretch and –C-O-C– groups of vinyl ether. The absence of strong absorption band at 1680-1700 cm^{-1} and the absence of–C=C– stretching at 1600 cm^{-1} confirmed the formation of the proposed product by the use of C=C and C=O of the diene.

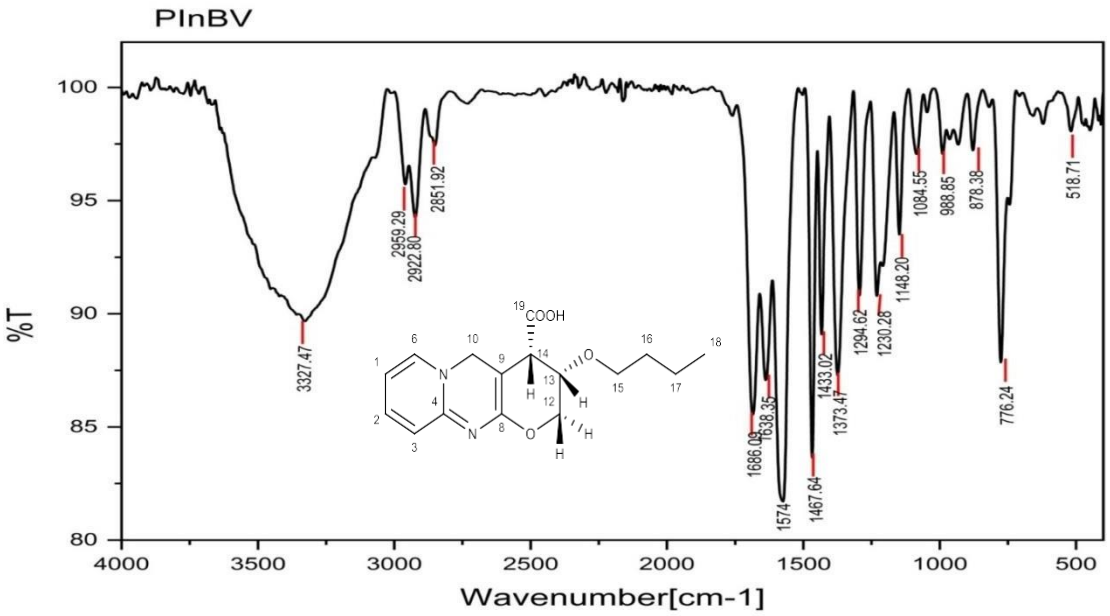

FIGURE 10 : FTIR Spectrum of 3-Butoxy-2,3,4,5-Tetrahydropyrano[2,3-*d*]Pyrido[1,2-*a*] Pyrimidine-4-Carboxylic Acid (5a)

4.2.2.2 ^{1}H NMR SPECTRUM

The ^{1}H NMR **(Figure 11)** spectrum of compound **5a** displayed 11 sets of protons and their assignments are given in **Table 6.** The signal at C_{14}-H was used for the quantification of

the diastereoisomeric ratio. This appeared as two triplets with equal intensity, one at δ2.3 and the other at δ2.6, with J value of 4.0Hz confirming the formation of *endo* and *exo* diastereoisomers in the ratio 1:1. Similar quantification of diastereisomers obtained in IEDDA reaction were reported by various authors **(Gaulon *et al.*, 2004)(Shi et al., 2016)(Sanap & Samant, 2015)(Pałasz *et al.*, 2013)(Di Valentin *et al.*, 2000)(Arvinnezhad *et al.*, 2020).** The ring proton C_{13}-H near to oxygen showed doublet of doublets at δ6.4-6.46 (coupling constant *J* = 4.0 and 8.0 Hz). The low coupling constant J=4.0 Hz observed may be due to the presence of electro negative oxygen atom attached to the C-13 carbon atom **(Stanley *et al.*, 2002)**.

The positive peak at δ 7.3-7.32 with J value 8.0Hz and 4.0Hz corresponding to C_{12}-H appeared as triplet and a far downfield singlet signal at δ 10.2 represent the carboxyl group proton COOH. A multiple around δ 7.05-8.3 corresponded to five aromatic protons of pyridine ring. Aliphatic protons nearer to the oxygen atom were observed as multiplet at

δ 1.03-1.15.

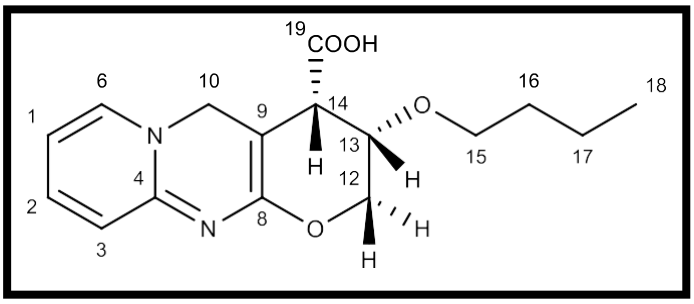

TABLE 6: ^{1}H NMR Assignments of 3-Butoxy-2,3,4,5-Tetrahydropyrano[2,3-*d*]Pyrido[1,2-*a*] Pyrimidine-4-Carboxylic Acid (5a)

^{1}H Shift in ppm	**No. of ^{1}H/ Multiplicity**	**J value (Hz)**	**^{1}H Shift in ppm**	**No. of ^{1}H/ Multiplicity**	**J value (Hz)**
7.75	H^{1} /t	12.0/12.0	6.4	H^{13} /dd	6.0/12.0/12.0
8.38	H^{2} /t	12.0/6.0	2.3/2.6	H^{14} /t	6.0/6.0
7.87	H^{3} /d	6.0	1.15-1.03	H^{15}, H^{16}, H^{17} /m	
7.05	H^{6} /t	12.0/6.0	0.87	H^{18} /t	6.0/6.0
5.08	H^{10} /s		10.2	H^{19} /s	
7.3	H^{12} /t	12.0/6.0			

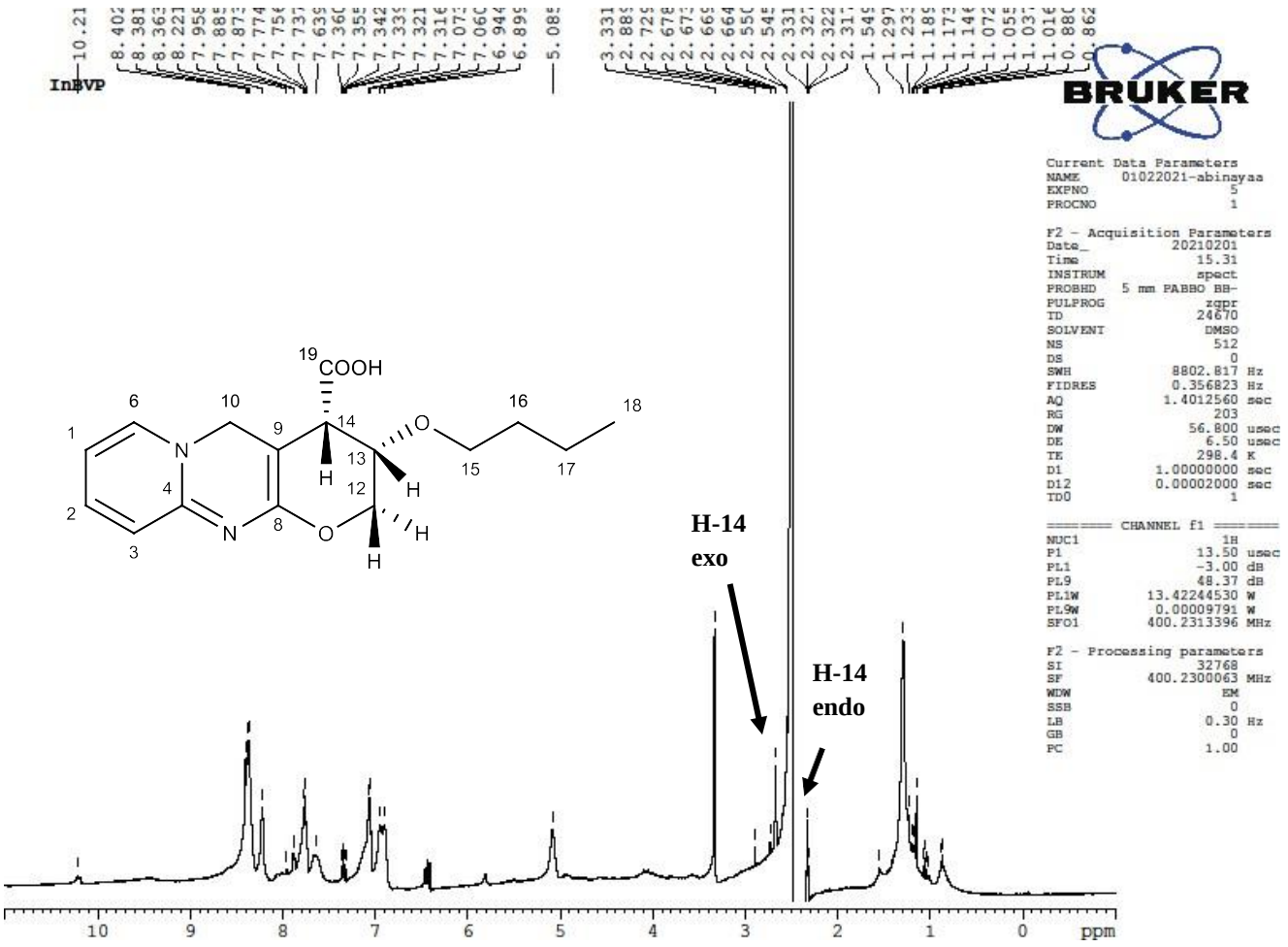

FIGURE 11 : ^{1}H NMR Spectrum of 3-Butoxy-2,3,4,5-Tetrahydropyrano[2,3-*d*]Pyrido[1,2-*a*]Pyrimidine-4-Carboxylic Acid (5a)

^{1}H NMR Spectrum of 3-Butoxy-2,3,4,5-Tetrahydropyrano[2,3-*d*]Pyrido[1,2-*a*]Pyrimidine-4-Carboxylic Acid (5a)

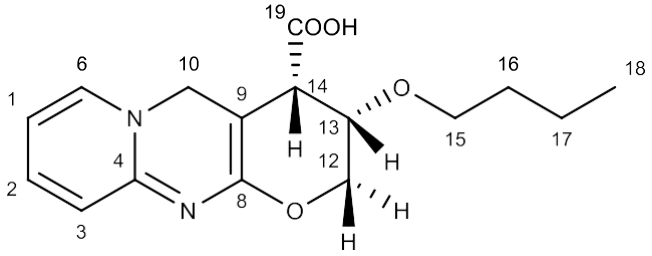

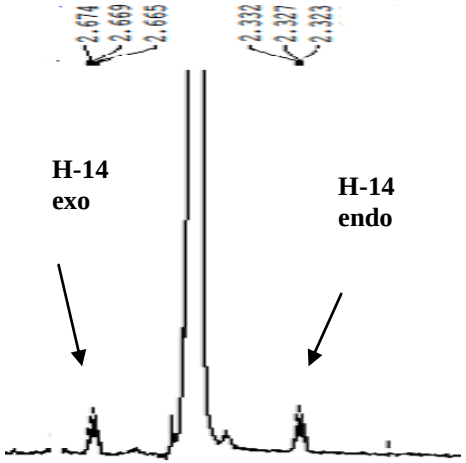

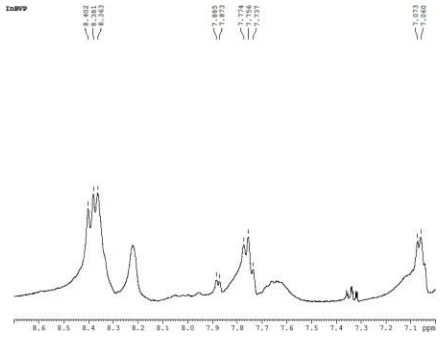

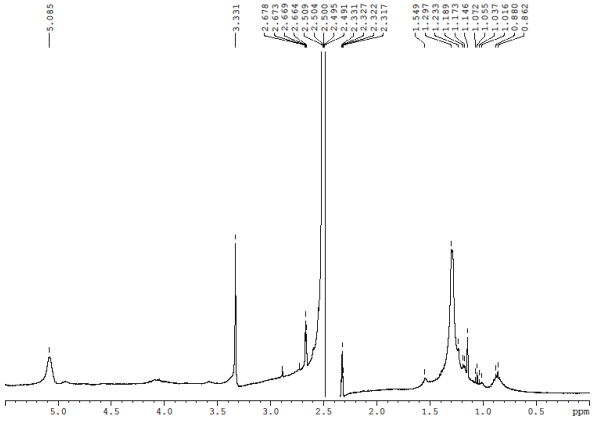

4.2.2.3 ^{13}C NMR SPECTRUM

Further confirmation of the product was found through ^{13}C NMR **(Figure 12)** analysis and their data are given in the **Table 7.** Compound **5a** showed 16 distinct carbons for the 16 chemically non-equivalent carbons**.** The signal for imine carbon (C=N) was observed at δ 152. Among all the skeletal carbons, pyridopyrimidine ring carbons C-1, C-2, C-3, C-4, C-6, C-8, C-9 and C-10 were observed at δ 118,137, 132, 152, 147, 153, 116 and 54 respectively. The three peaks observed in the upfield region at δ 64, 21 and 19 were believed to correspond to the saturated carbons C-15, C-16 and C-17. The C-12 and C-13 carbons appeared somewhat more downfield probably due to the presence of oxygen in the ring **(Stanley *et al.*, 2002)**. The chemical shift of the methyl group carbon appeared at δ 13 further supported this assumption. The peak at δ 168 observed within the expected area for the carboxylic carbon C-19.

Based on the data provided by H^1 and ^{13}C NMR spectroscopy the structure of the adducts formed through IEDDA reaction was confirmed.

TABLE 7: ^{13}C NMR Assignments of 3-Butoxy-2,3,4,5-Tetrahydropyrano[2,3-*d*] Pyrido[1,2-*a*]Pyrimidine-4-Carboxylic Acid (5a)

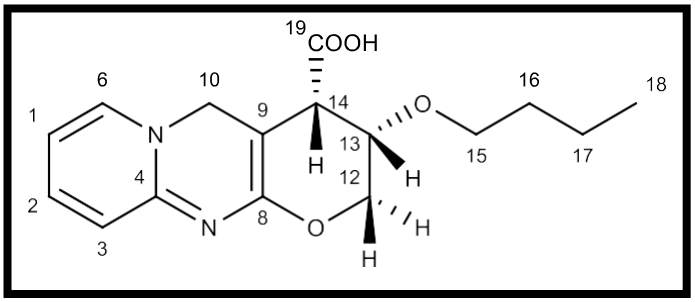

C^{13} shift in ppm	Carbon	C^{13} shift in ppm	Carbon
118	C^{1}	111	C^{12}
137	C^{2}	114	C^{13}
132	C^{3}	29	C^{14}
152	C^{4}	64	C^{15}
147	C^{6}	21	C^{16}
153	C^{8}	19	C^{17}
116	C^{9}	13	C^{18}
54	C^{10}	168	C^{19}

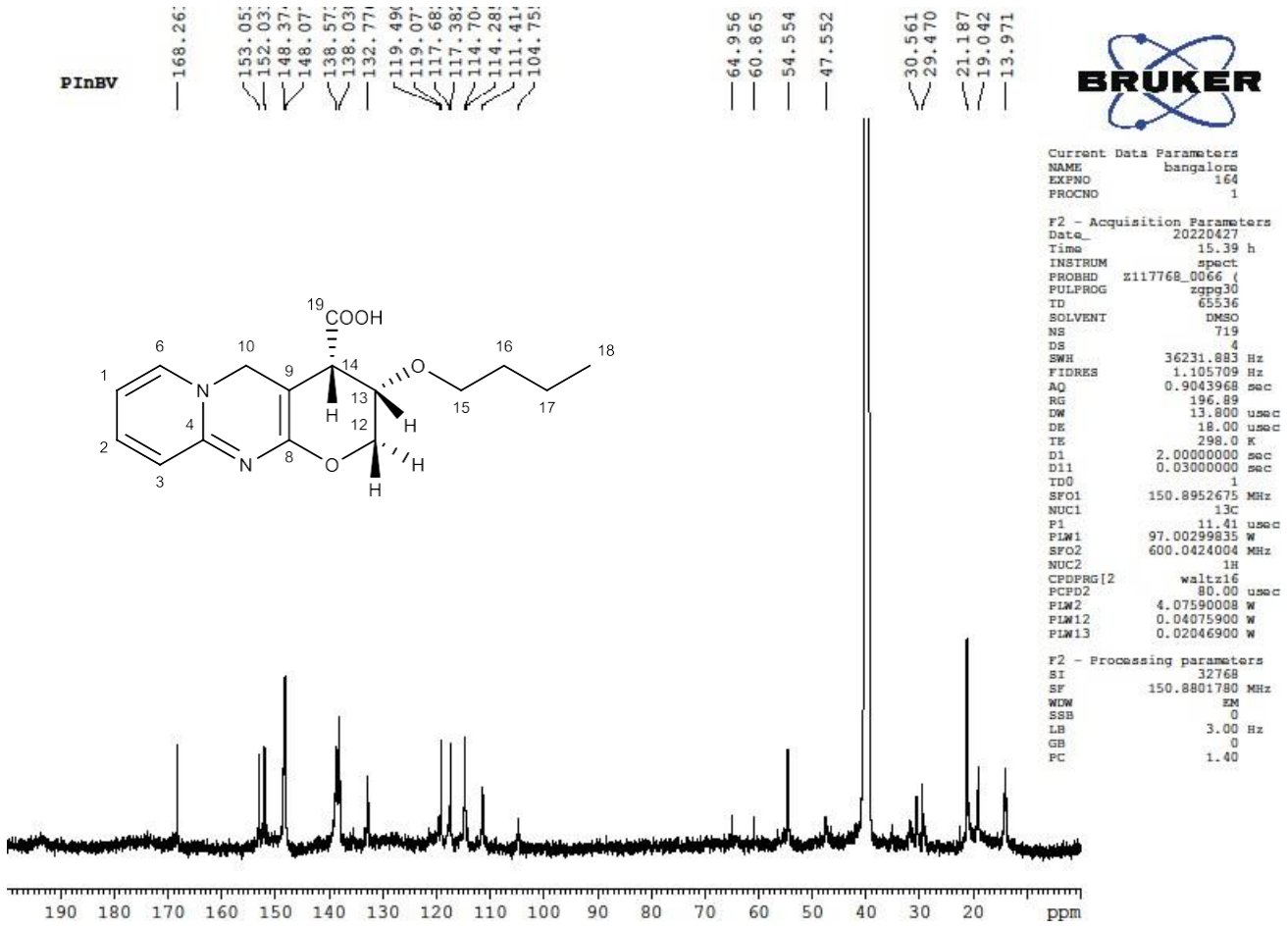

FIGURE 12 : ^{13}C Spectrum of 3-Butoxy-2,3,4,5-Tetrahydropyrano[2,3-*d*]Pyrido [1,2-*a*]Pyrimidine-4-Carboxylic Acid (5a)

4.2.2.4. MASS SPECTRUM

Mass spectrum of the compound 5a was recorded which showed M+2 peak at *m/z* value of 306.03. F**igure-13** showed the mass spectrum of 3-butoxy-2,3,4,5-tetrahydropyrano [2, 3-*d*] pyrido[1, 2-*a*]pyrimidine-4-carboxylic acid **(5a).** Further fragmented peaks were observed at *m/z* values of 261.16, 198.37, and 104.67.

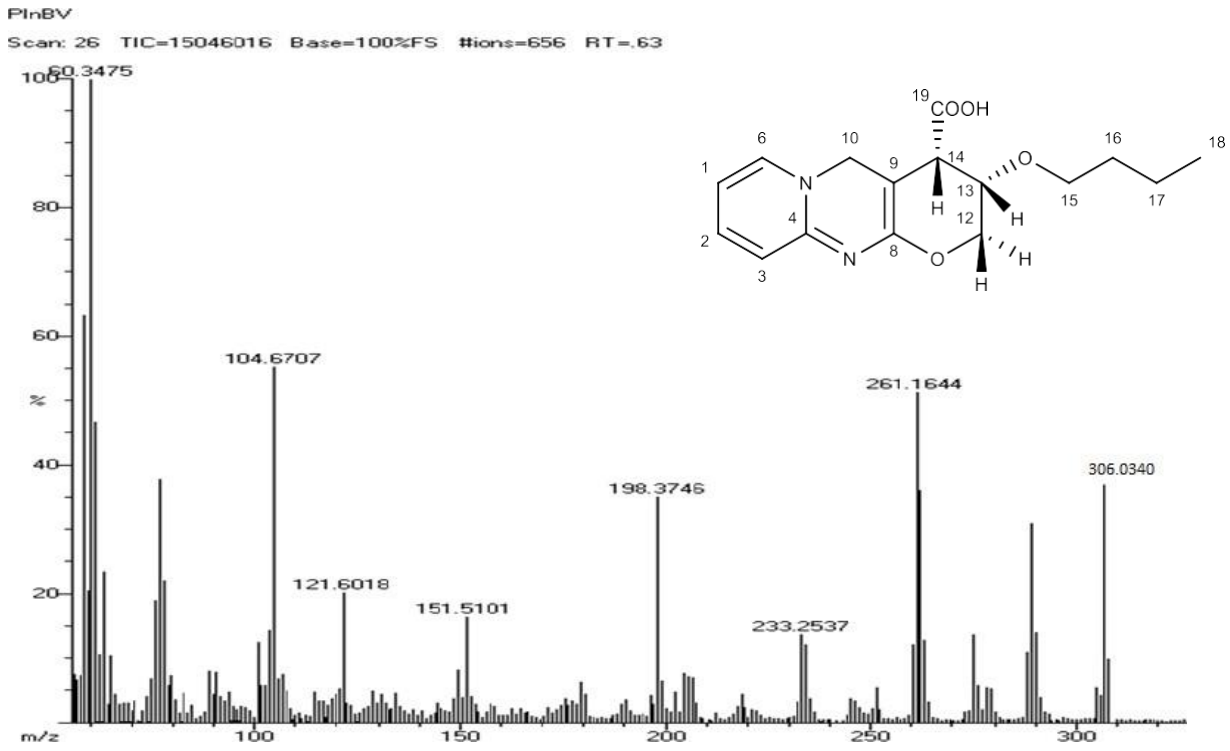

FIGURE 13 : Mass Spectrum of 3-Butoxy-2,3,4,5-Tetrahydropyrano[2,3-*d*] Pyrido[1,2-*a*]Pyrimidine-4-Carboxylic Acid (5a)

4.2.3. SPECTRAL CHARACTERIZATION OF SYNTHESIZED CYCLO ADDUCTS (5b & 5c)

The prepared IEDDA adducts of the 7-methyl and 8-methyl substituted dienes were characterized using FTIR, ^{1}H NMR, ^{13}C NMR and Mass spectrum obtained results are tabulated in **Table 8, 9 and 10**. The spectra of the substituted dienes are given in the **Figures 14, 15, 16, 17, 18, 19 20 and 21.** The spectral observations of the compounds 5b and 5c further confirmed the proposed structure of the adduct 5b and 5c.

TABLE 8: FTIR Assignments of Compounds 5b & 5c

Functional group	Types of vibration	Wave number (cm^{-1})	Intensity
(5b) 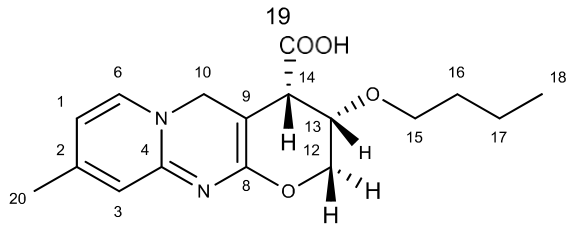			
C=O	Stretch	1683	strong
C=N	Bending	1636	medium
O-H	Stretch	3330	Very broad
O-H	Stretch	1370	strong
O-H	Stretch	932	medium
C-O	Stretch	1294	strong
(5c) 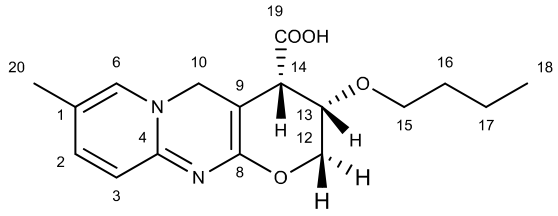			
C=O	Stretch	1691	strong
C=N	Bending	1562	medium
O-H	Stretch	3431	Very broad
O-H	Stretch	1378	strong
O-H	Stretch	824	medium
C-O	Stretch	1293	strong

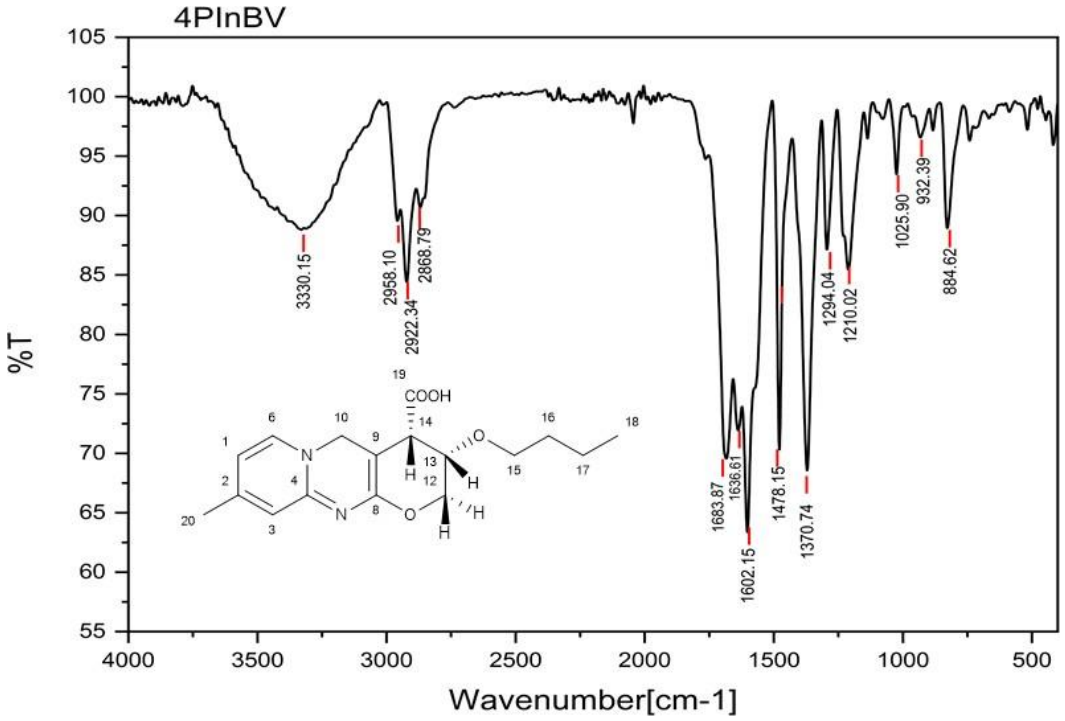

FIGURE 14: FTIR Spectrum of 3-Butoxy-9-Methyl-2,3,4,5-Tetrahydropyrano [2,3-*d*]Pyrido[1,2-*a*]Pyrimidine-4-Carboxylic Acid (5b)

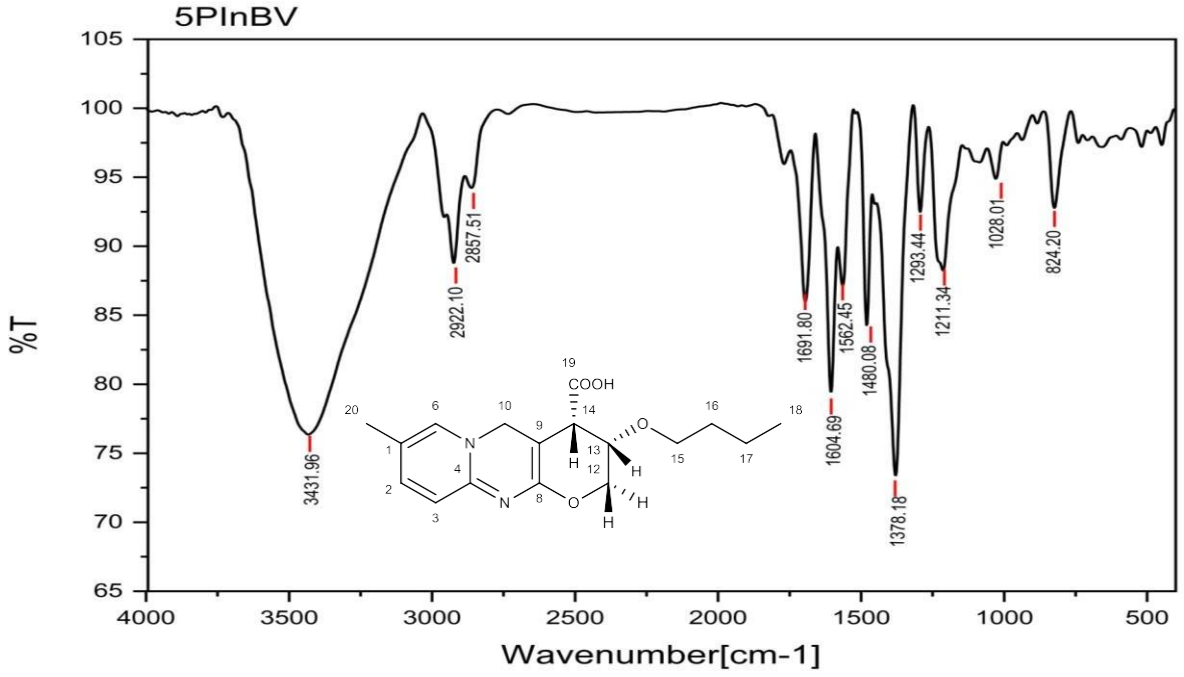

FIGURE 15: FTIR Spectrum of 3-Butoxy-8-Methyl-2,3,4,5-Tetrahydropyrano[2,3-*d*]Pyrido[1,2-*a*]Pyrimidine-4-Carboxylic Acid (5c)

TABLE 9: ^{1}H NMR Assignments of Compounds 5b & 5c

(5b)			**(5c)**		
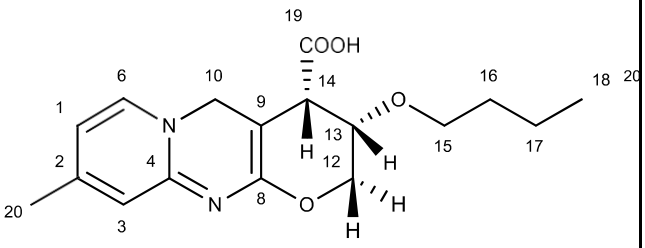			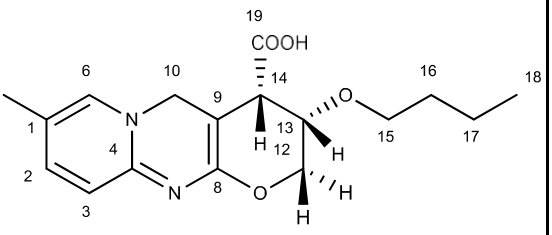		
^{1}H Shift in ppm	**No. of ^{1}H/ Multiplicity**	**J value (Hz)**	**^{1}H Shift in ppm**	**No. of ^{1}H/ Multiplicity**	**J value (Hz)**
7.75	H^{1}, H^{6}/m		8.1	H^{2} , H^{3}/m	
6.8	H^{3}/s		7.3	H^{6}/s	
5.05	H^{10}/s		4.99	H^{10}/s	
6.29	H^{12}/d	30.0	7.5	H^{12}/d	30.0
6.73	H^{13}/dd	12.0/30.0/12.0	6.8	H^{13}/d	12.0/30.0
4.04/3.99	H^{14}/t	6.0/6.0	5.9/5.5	H^{14}/d	12.0
1.53-0.90	H^{15}, H^{16} ,H^{17}/m		1.45-1.62	H^{15} ,H^{16} , H^{17}/m	
0.73	H^{18}/t	6.0/6.0	0.84	H^{18}/t	6.0/6.0
10.15	H^{19}/s		10.06	H^{19}/s	
2.29	H^{20}/s		2.21	H^{20}/s	

TABLE 10: ^{13}C NMR Assignments of Compound 5b & 5c

(5b)				**(5c)**			
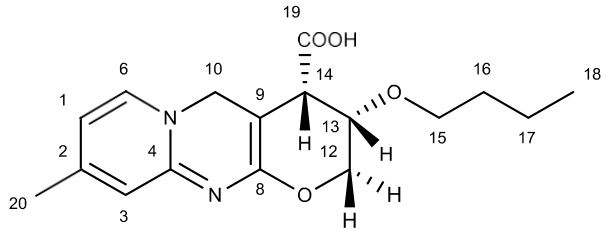				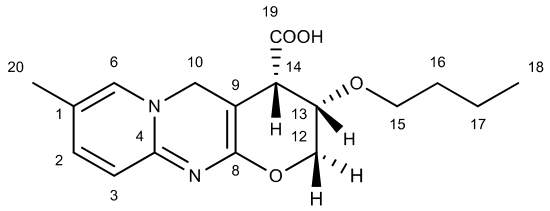			
C*1*^{3} shift in ppm (5b)	**Carbon (5b)**	**C^{13} shift in ppm (5b)**	**Carbon (5b)**	**C^{13} shift in ppm (5c)**	**Carbon (5c)**	**C^{13} shift in ppm (5c)**	**Carbon (5c)**
119	C^{1}	114	C^{13}	128	C^{1}	114	C^{13}
147	C^{2}	29	C^{14}	138	C^{2}	29	C^{14}
132	C^{3}	64	C^{15}	132	C^{3}	54	C^{15}
152	C^{4}	20	C^{16}	150	C^{4}	20	C^{16}
149	C^{6}	18	C^{17}	147	C^{6}	18	C^{17}
151	C^{8}	13	C^{18}	149	C^{8}	13	C^{18}
118	C^{9}	167	C^{19}	126	C^{9}	168	C^{19}
54	C^{10}	20	C^{20}	30	C^{10}	17	C^{20}
111	C^{12}			111	C^{12}		

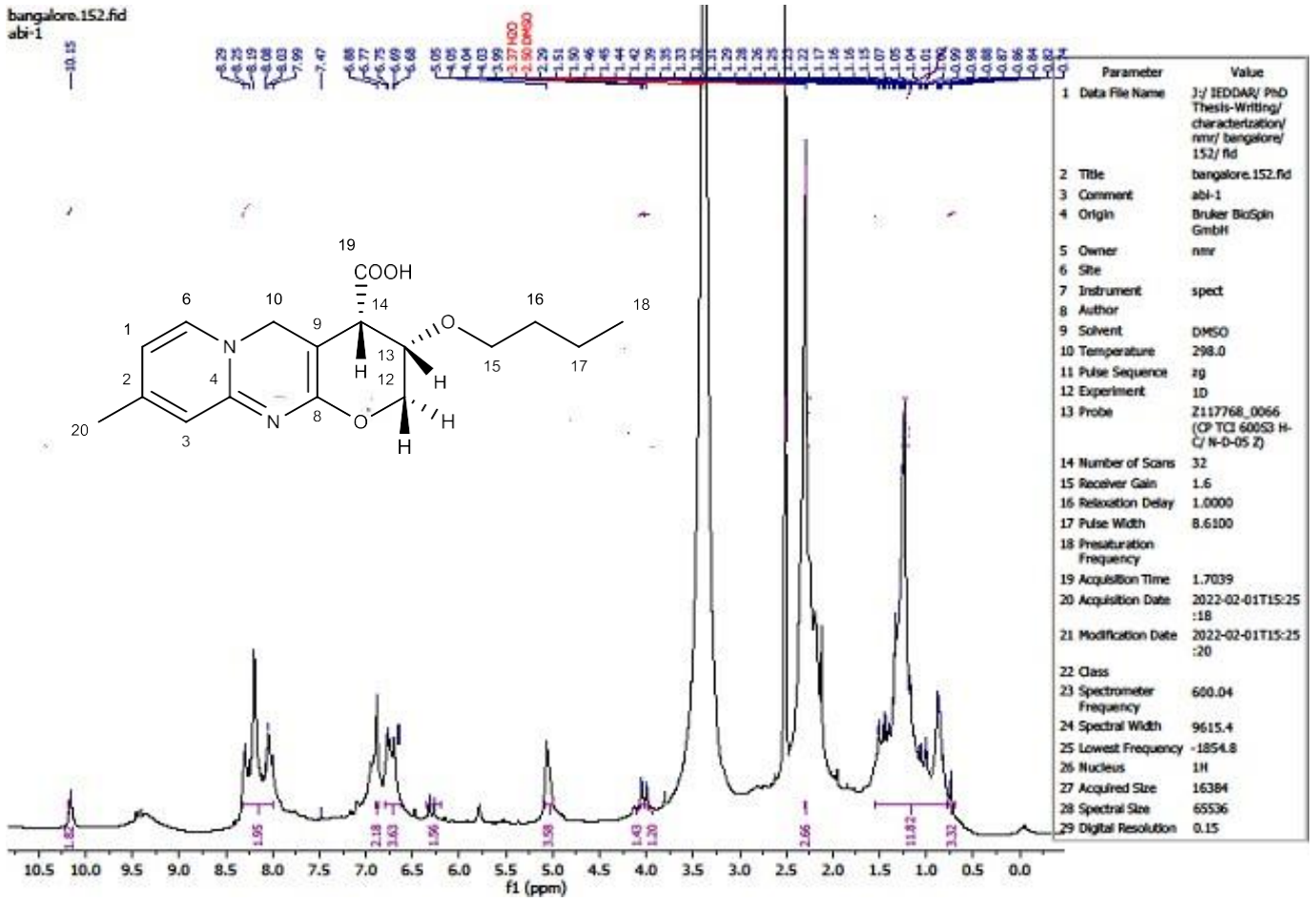

FIGURE 16 : ^{1}HNMR Spectrum of 3-Butoxy-9-Methyl-2,3,4,5-Tetrahydropyrano[2,3-*d*]Pyrido[1,2-*a*]Pyrimidine-4-Carboxylic Acid (5b)

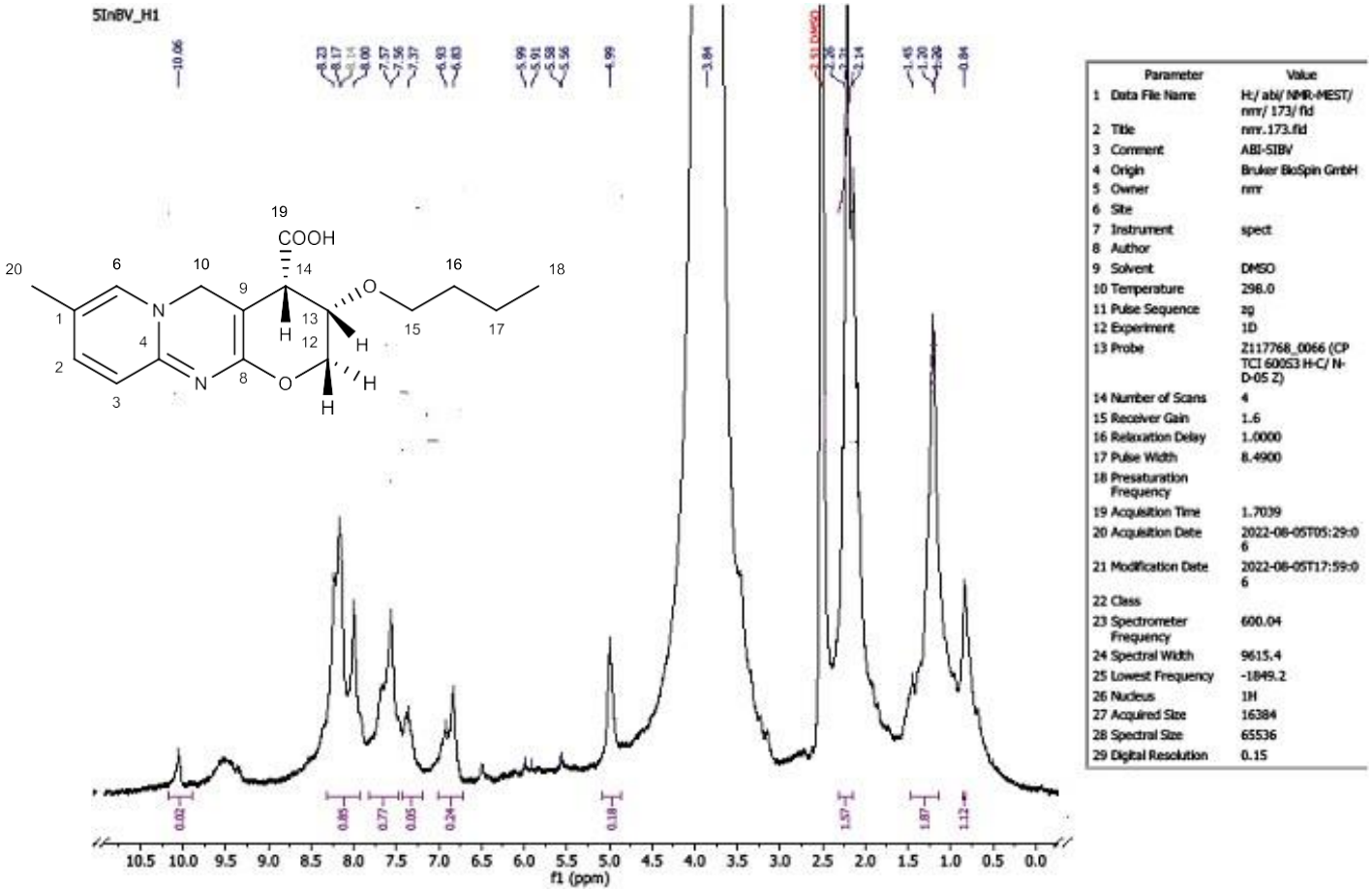

FIGURE 17 : ^{1}HNMR Spectrum of 3-Butoxy-8-Methyl-2,3,4,5-Tetrahydropyrano[2,3-*d*]Pyrido[1,2-*a*]Pyrimidine-4-Carboxylic Acid (5c)

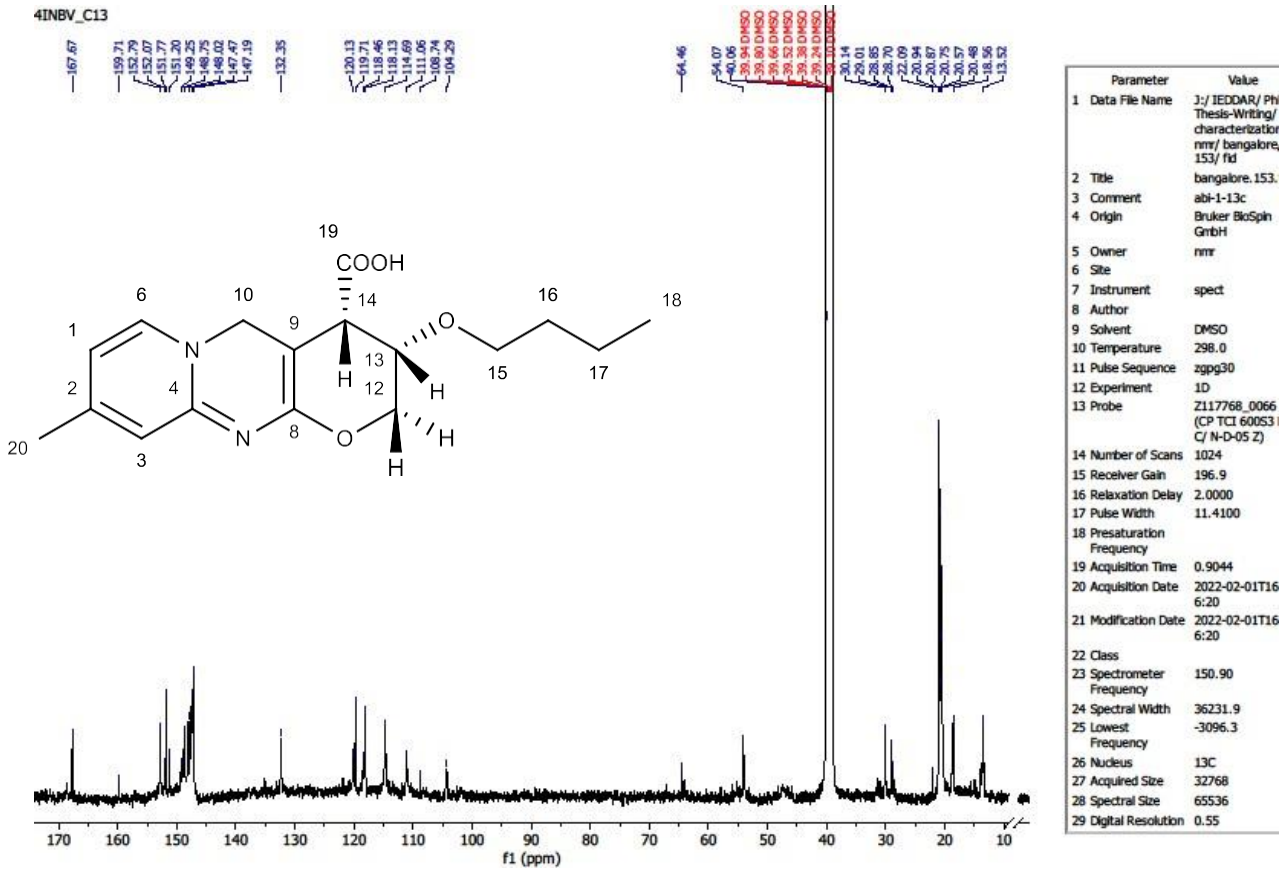

FIGURE 18 : ^{13}C Spectrum of 3-Butoxy-9-Methyl-2,3,4,5-Tetrahydropyrano[2,3-*d*]Pyrido[1,2-*a*]Pyrimidine-4-Carboxylic Acid (5b)

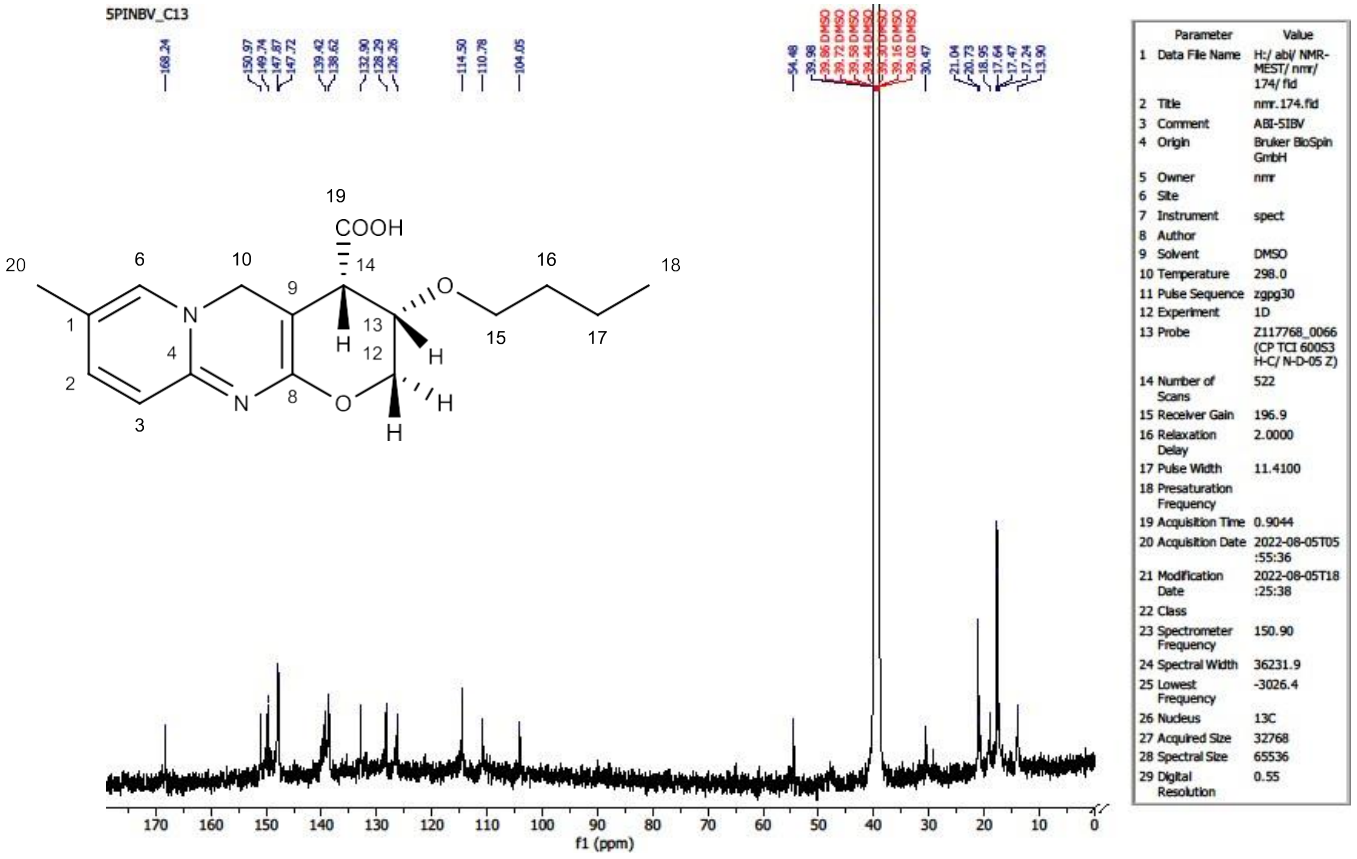

FIGURE 19 : ^{13}C Spectrum of 3-Butoxy-8-Methyl-2,3,4,5-Tetrahydropyrano[2,3-*d*]Pyrido[1,2-*a*]Pyrimidine-4-Carboxylic Acid (5c)

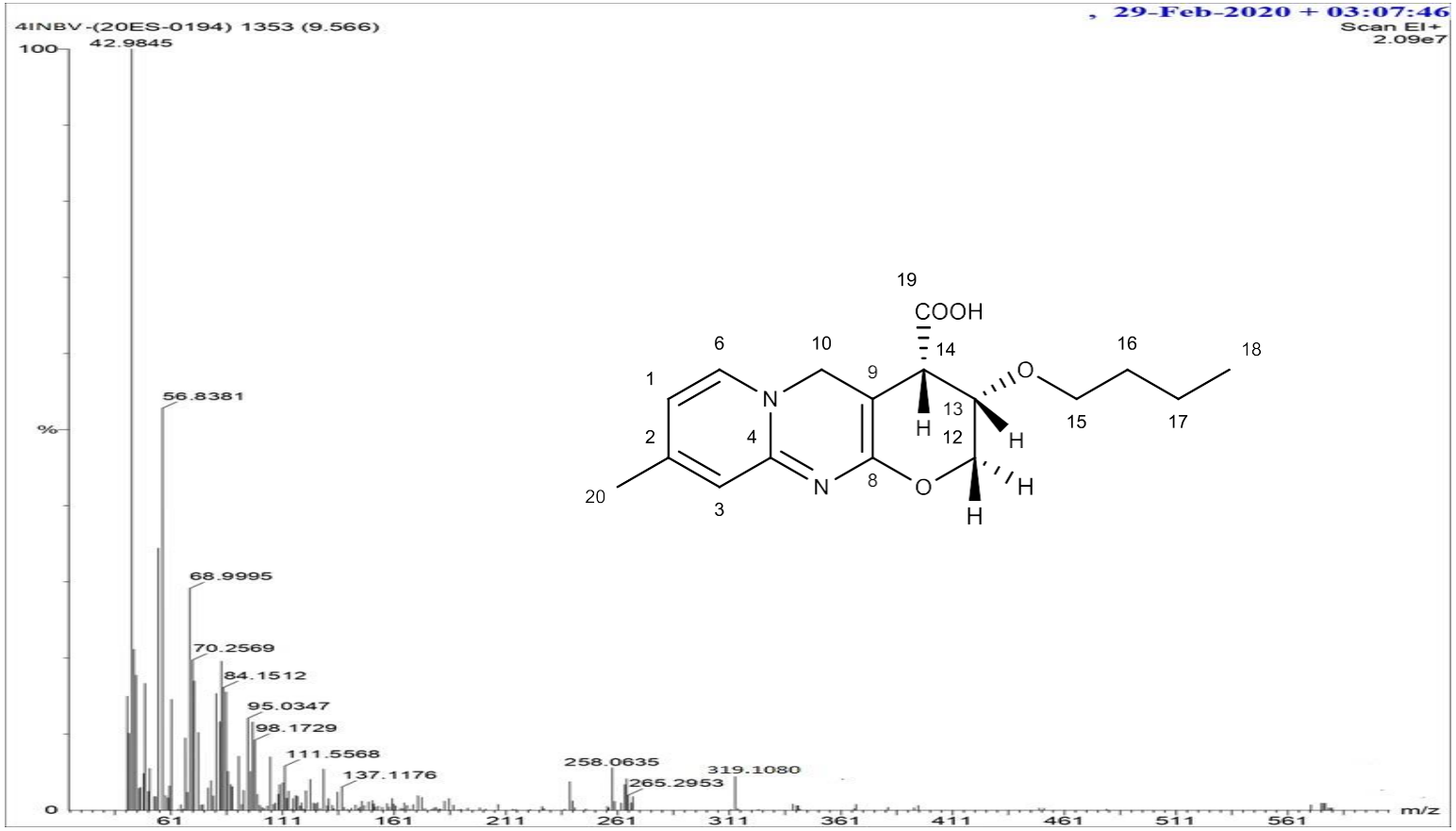

FIGURE 20 : Mass Spectrum of 3-Butoxy-9-Methyl-2,3,4,5-Tetrahydropyrano[2,3-*d*]Pyrido[1,2-*a*]Pyrimidine-4-Carboxylic Acid (5b)

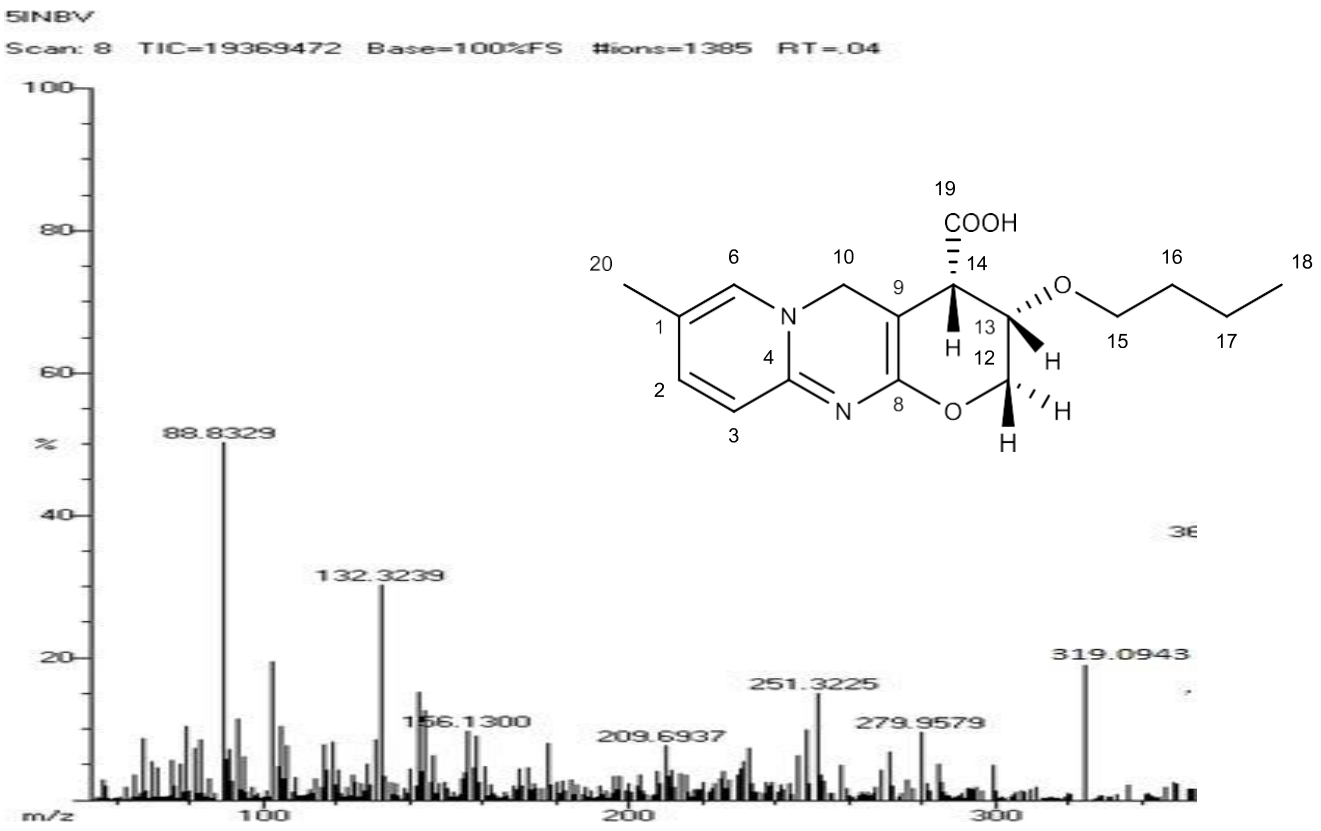

FIGURE 21 : MASS Spectrum of 3-Butoxy-8-Methyl-2,3,4,5-Tetrahydropyrano[2,3-*d*]Pyrido[1,2-*a*]Pyrimidine-4-Carboxylic Acid (5c)

4.3 SYNTHESIS OF METHYL-2-OXO-1-PHENYL-1,2,3,3*a*,4,5-HEXAHYDROPYRAZOLO[1,5-*b*]PYRIDO[1',2':1,2]PYRIMIDO[5,4-*e*][1,2] OXAZINE-4-CARBOXYLIC ACID DERIVATIVES

Under the optimized conditions with indium (III) chloride in DMF solvent diene 2-oxo-2*H*-pyrido [1, 2-*a*] pyrimidin-3(4*H*)-ylidiene acetic acid **(3)** and the dienophile 3-methyl-1-phenyl-1H-pyrazol-5(4*H*)-one **(6)** were refluxed under air at 90^{o}C for 4h. Similar to that with butyl vinyl ether dienophile, 3-methyl-1-phenyl-1*H*-pyrazol-5(4*H*)-one **(6)** also showed complete consumption of the starting materials after 4 h in TLC with one primary spot. After 4 ½ h of refluxing the reaction mixture afforded a purple precipitate. As mentioned for the adducts formed from diene **(3)** and dienophile **(4) Scheme -12**, purificationof the product by column chromatography failed hence recrystallized product, Methyl-2- oxo-1-phenyl-1,2,3,3*a*,4,5-hexahydropyrazolo[1,5-*b*]pyrido[1',2':1,2]pyrimido[5,4-*e*][1,2]oxazine-4-carboxylic acid **(7a)** was used for further characterization.

Under similar conditions the 7-methyl and 8-methyl substituted 2-oxo-*2H*-pyrido [1, 2-*a*] pyrimidin-3(4*H*)-ylidiene acetic acid **(3)** diene were refluxed with the dienophile 3-methyl-1-phenyl-1*H*-pyrazol-5(4*H*)-one **(6)**. The resulted products **7b** and **7c** were recrystallised **Scheme 13**. The time period required for the complete consumption of the starting materials differed and were found to be 5 ½ h and 6 h for **7b** and **7c** respectively. The details of yield and melting point of the synthesized adducts are tabulated in**Table 11.**

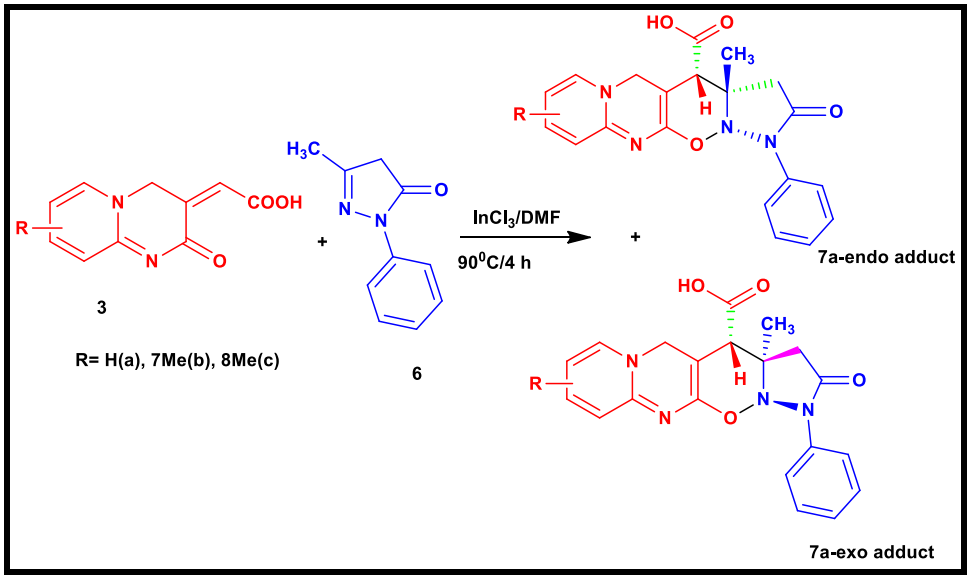

Scheme 13: Synthesis of Methyl-2-Oxo-1-Phenyl-1,2,3,3*a*,4,5-Hexahydro pyrazolo [1,5-*b*]Pyrido[1',2':1,2]Pyrimido[5,4-*e*][1,2]Oxazine-4-Carboxylic Acids

TABLE 11: Melting Point and Yield of Methyl-2-Oxo-1-Phenyl-1,2,3,3*a*,4,5-Hexahydropyrazolo[1,5-*b*] Pyrido[1',2':1,2]Pyrimido[5,4-*e*][1,2]Oxazine-4-Carboxylic Acid Derivatives

Diene	Dienophile	Temp./Time	Product	Yield/M.P
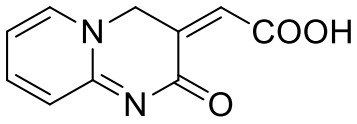		90˚C/4	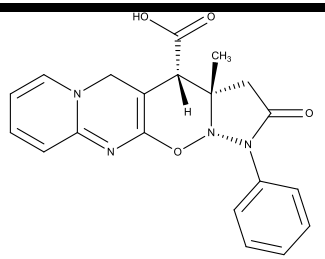	61% /284-294˚C
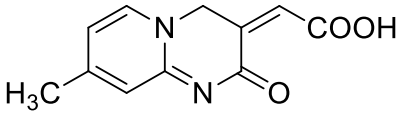	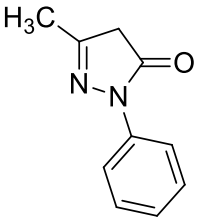	90˚C/5 ½	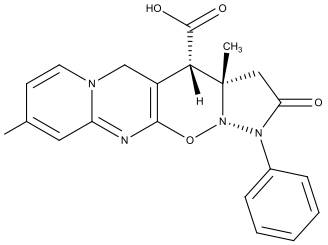	63% /300˚C above
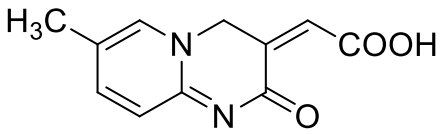		90˚C/6	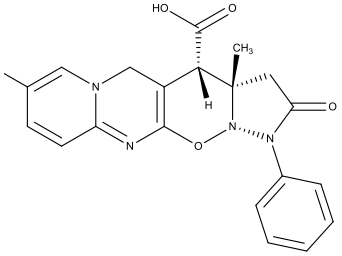	68%/ 300˚C above

4.3.1 SPECTRAL CHARACTERIZATION OF SYNTHESIZED ADDUCT (7a)

4.3.1.1 FT-IR SPECTRUM

The FTIR spectrum of compound **7a** showed the expected absorption bands of C=N at 1499 cm^{-1}corresponding to the pyridopyrimidine nucleus. A broad intense O-H stretching band centered at 3417 cm^{-1} was an overriding spectral feature of the carboxylic acid. This was also confirmed by the presence of strong intense O-H in plane bend at 1368 cm-^{1}along with medium intense O-H out of plane bend at 906cm^{-1}.

The strong and medium intense bands at 1598 cm^{-1} and 1273 cm^{-1} were attributed to the -C=O and -C-O stretch of the carboxylic acid moiety respectively. The absence of strong absorption band at 1680-1700 cm^{-1} confirmed the formation of the product **(Figure 22).**

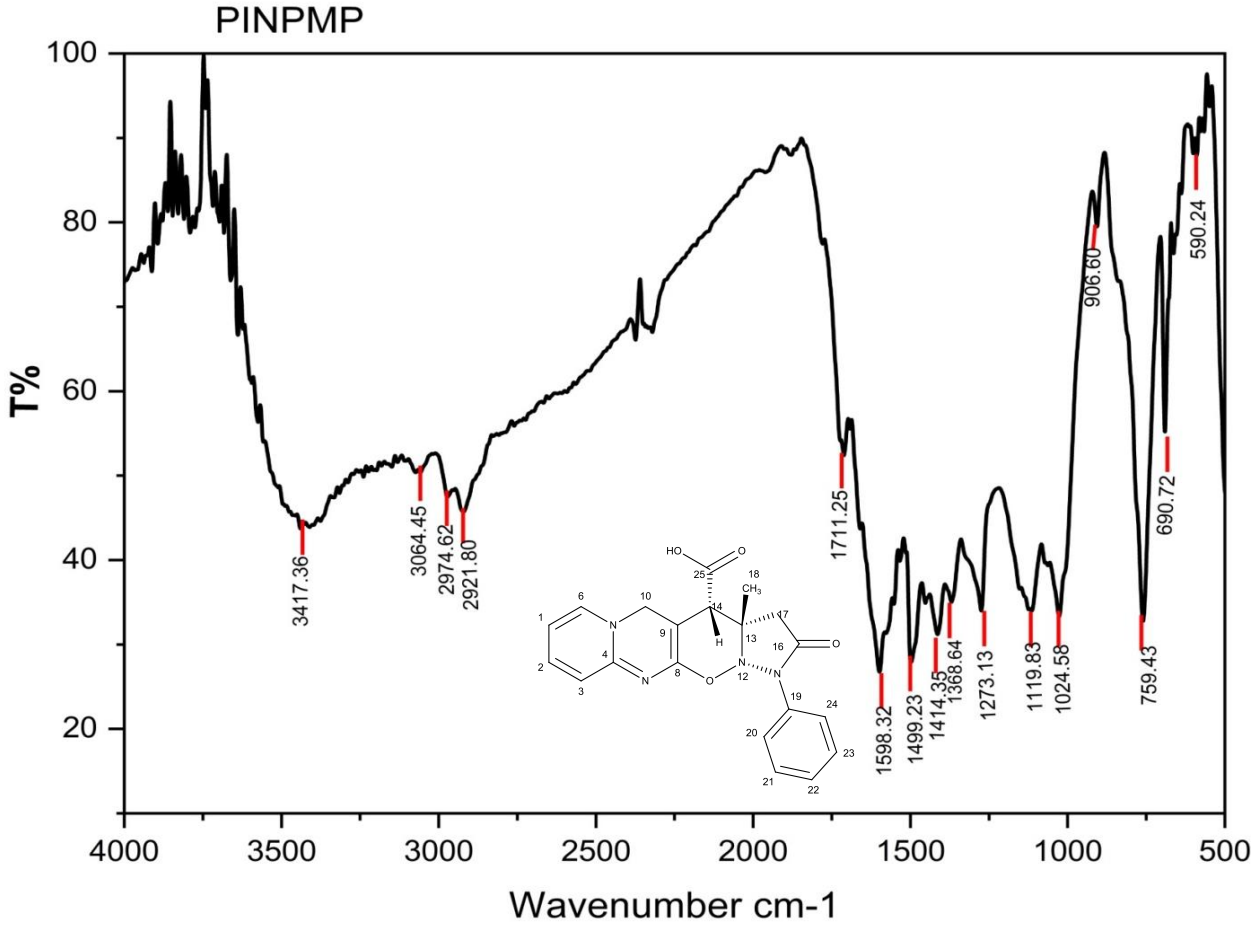

FIGURE 22 : FTIR Spectrum of Methyl-2-Oxo-1-Phenyl-1,2,3,3*a*,4,5-hexa hydropyrazolo[1,5-*b*]Pyrido[1',2':1,2]Pyrimido[5,4-*e*][1,2]Oxazine-4-Carboxylic Acid (7a)

4.3.1.2 ^{1}H NMR SPECTRUM

The inspection of ^{1}H NMR **(Figure 23)** spectrum of compound **7a** showed 14 sets of protons and the chemical shifts are presented in **Table 12**. The signal of proton C_{14}-H appeared as singlet at δ2.73 was diagnostic of *endo* isomer and the singlet at δ2.79 was indicative of the *exo* isomer. The intensity ratio was found to be 6:4. This confirmed the formation of *endo* and *exo* diastereoisomers in the ratio of **6:4.** The carboxylic acid proton peak was registered at δ 10.42. Other aromatic ring protons appeared as expected δ 7.9-7.0. The peaks at δ 7.7 (d, 2H, J-12.0), δ 7.4 (t, 2H, J-12.0) and δ 7.2 (t, 1H, J-12.0) corresponded to the two sets of chemically equivalent phenyl ring hydrogens. A positive singlet peak at δ 2.1 indicated the methyl group proton.

TABLE 12: ^{1}H NMR Assignments of Methyl-2-Oxo-1-Phenyl-1,2,3,3*a*,4,5-Hexahydro pyrazolo[1,5-*b*]Pyrido[1',2':1,2]Pyrimido[5,4-*e*][1,2] Oxazine-4-Carboxylic Acid (7a)

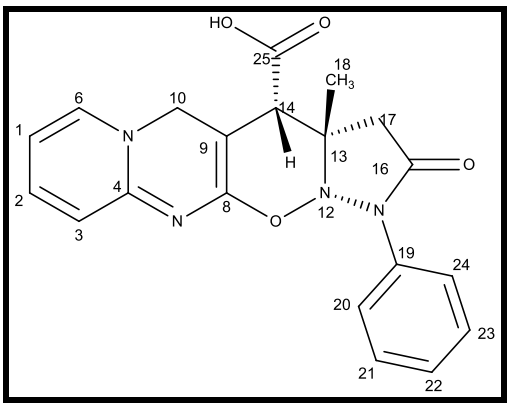

^{1}H Shift in ppm	No. of ^{1}H/ Multiplicity	J value (Hz)	^{1}H Shift in ppm	No. of ^{1}H/ Multiplicity	J value (Hz)
7.5	H^{1} /t	12.0,6.0	2.1	H^{18} /s	
7.3	H^{2} /t	12.0,12.0	7.7	H^{20} /d	12.0
7.8	H^{3} /d	12.0	7.4	H^{21} /t	12.0/12.0
7.9	H^{6} /d	6.0	7.2	H^{22} /t	12.0/12.0
2.86	H^{10} /s		7.4	H^{23} /t	12.0/12.0
2.79/2.72	H^{14} /s		7.7	H^{24} /d	12.0
2.3	H^{17} /s		10.42	H^{25} /s	

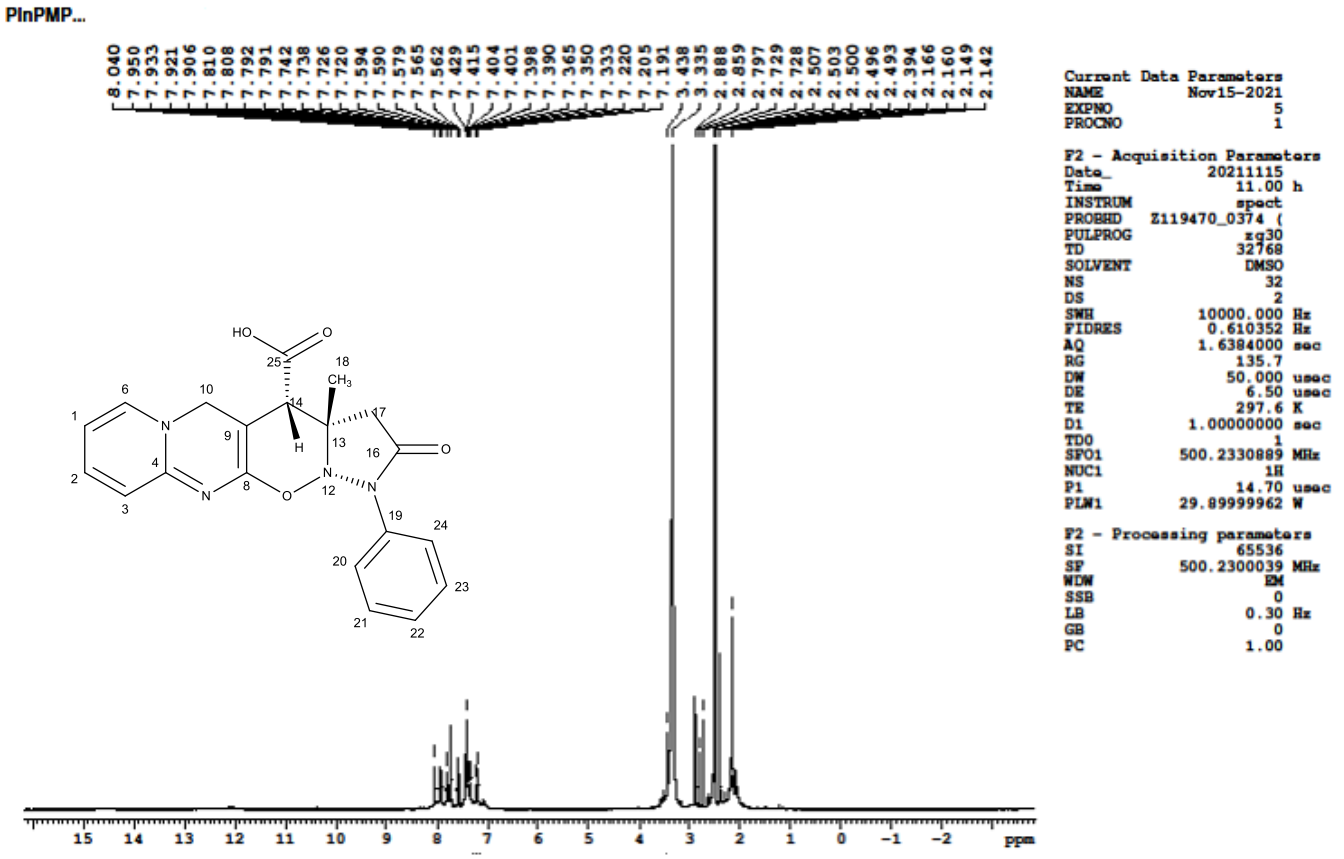

FIGURE 23 : ^{1}HNMR Spectrum of Methyl-2-Oxo-1-Phenyl-1,2,3,3*a*,4,5-Hexahydropyrazolo[1,5-*b*] Pyrido[1',2':1,2]Pyrimido[5,4-*e*][1,2]Oxazine-4-Carboxylic Acid (7a)

^{1}HNMR Spectrum of Methyl-2-Oxo-1-Phenyl-1,2,3,3*a*,4,5-Hexahydropyrazolo[1,5-*b*] Pyrido[1',2':1,2]Pyrimido[5,4-*e*][1,2]Oxazine-4-Carboxylic Acid (7a)

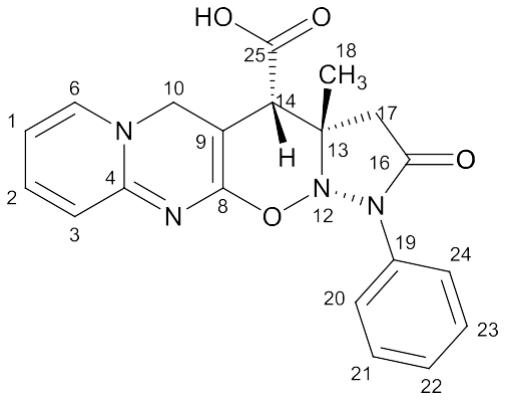

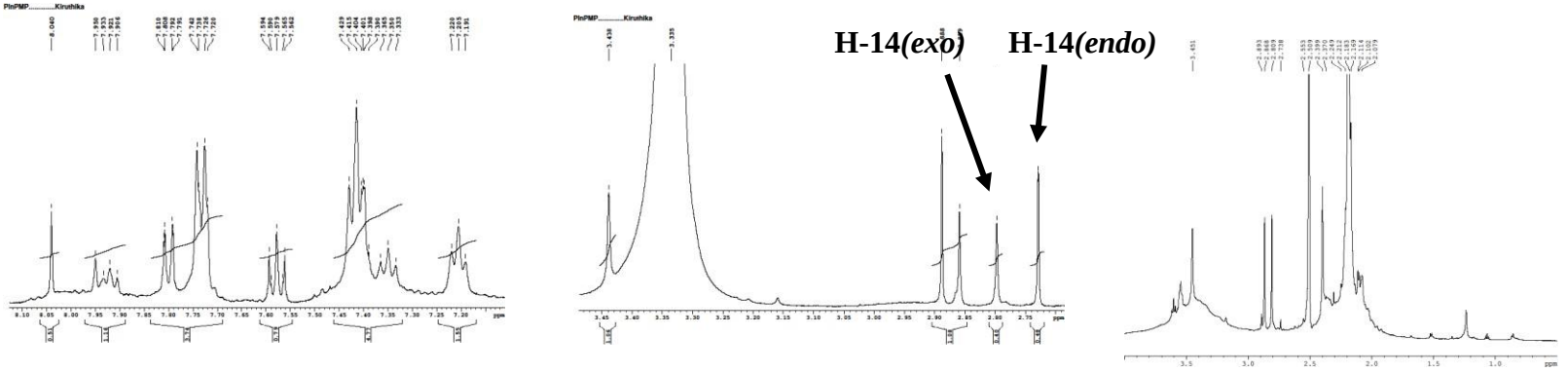

4.3.1.3 C^{13} NMR SPECTRUM

The C^{13} NMR analysis evidenced 13 peaks for the IEDDA adduct **7a (Figure 24)** and the values are tabulated in **Table 13**. The chemical shift observed at δ 11 was due to the methyl group**.** The peaks at δ 149, 144, 138, 137, 136, 127, 125, 101 and 32 corresponded to pyridopyrimidine ring. The peak at δ 174 represented the carboxylic acid group. The C-13 and C-19 appeared considerably further downfield at δ101 and δ 129 most probably due to the additional deshielding caused by the adjacent ring nitrogen atoms. The peak at δ145 was attributed to the carbonyl carbon C-16 bonded to oxygen. The peaks at δ 129, 120, 128.7 and 128 were indicative of carbons of benzene ring attached to the pyrazolone ring. The overall spectral data taken together confirmed the formation of the desired adducts **7a**.

TABLE 13: C^{13} NMR Assignments of Methyl-2-Oxo-1-Phenyl-1,2,3,3*a*,4,5-Hexahydro pyrazolo[1,5-*b*]Pyrido[1',2':1,2]Pyrimido[5,4-*e*][1,2]Oxazine-4-Carboxylic Acid (7a)

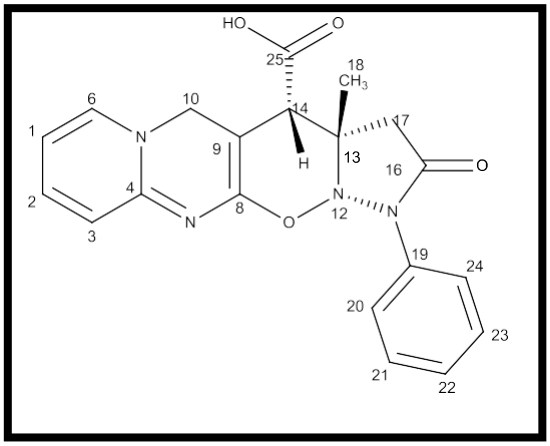

C^{13} shift in ppm	Carbon	C^{13} shift in ppm	Carbon	C^{13} shift in ppm	Carbon
127	C^{1}	32	C^{10}	120	C^{20}
137	C^{2}	101	C^{13}	128.7	C^{21}
136	C^{3}	36	C^{14}	128	C^{22}
149	C^{4}	145	C^{16}	128.7	C^{23}
138	C^{6}	27	C^{17}	120	C^{24}
144	C^{8}	11	C^{18}	174	C^{25}
125	C^{9}	129	C^{19}		

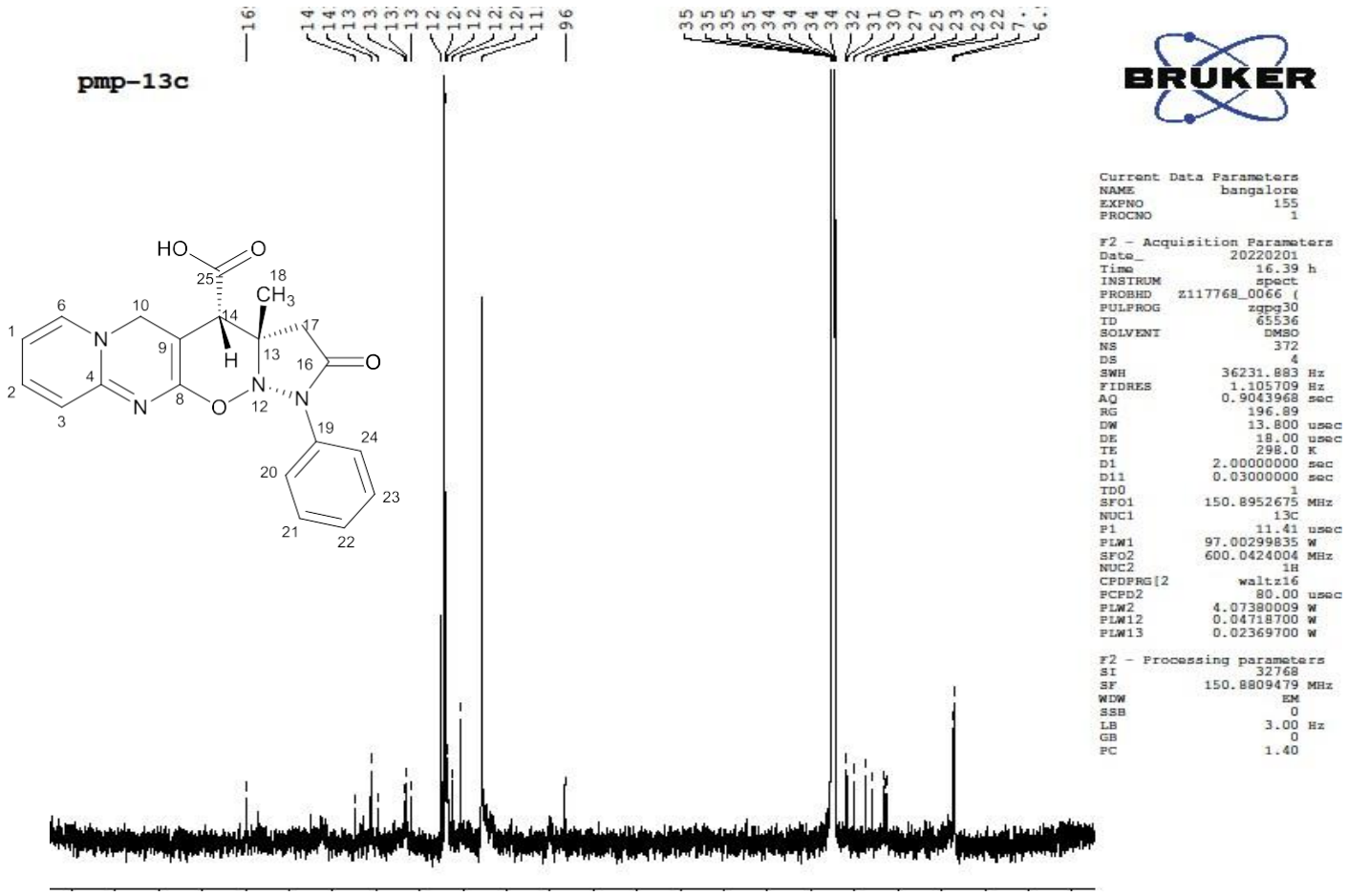

FIGURE 24 : ^{13}C Spectrum of 3*a*-Methyl-2-Oxo-1-Phenyl-1,2,3,3*a*,4,5-Hexahydropyrazolo[1,5-*b*]Pyrido[1',2':1,2]Pyrimido [5,4-*e*] [1,2]Oxazine-4-Carboxylic Acid (7a)

4.3.1.4 MASS SPECTRUM

Mass spectral analysis of the adduct **7a (Figure 25)** showed M+1 peak at *m/z* value of 379.85 indicated the formation of protonated molecular ion. The major fragments showed peaks at *m/z* values 352.44, 309.75 and 179.71 which confirmed the proposed structure for the adduct **7a**.

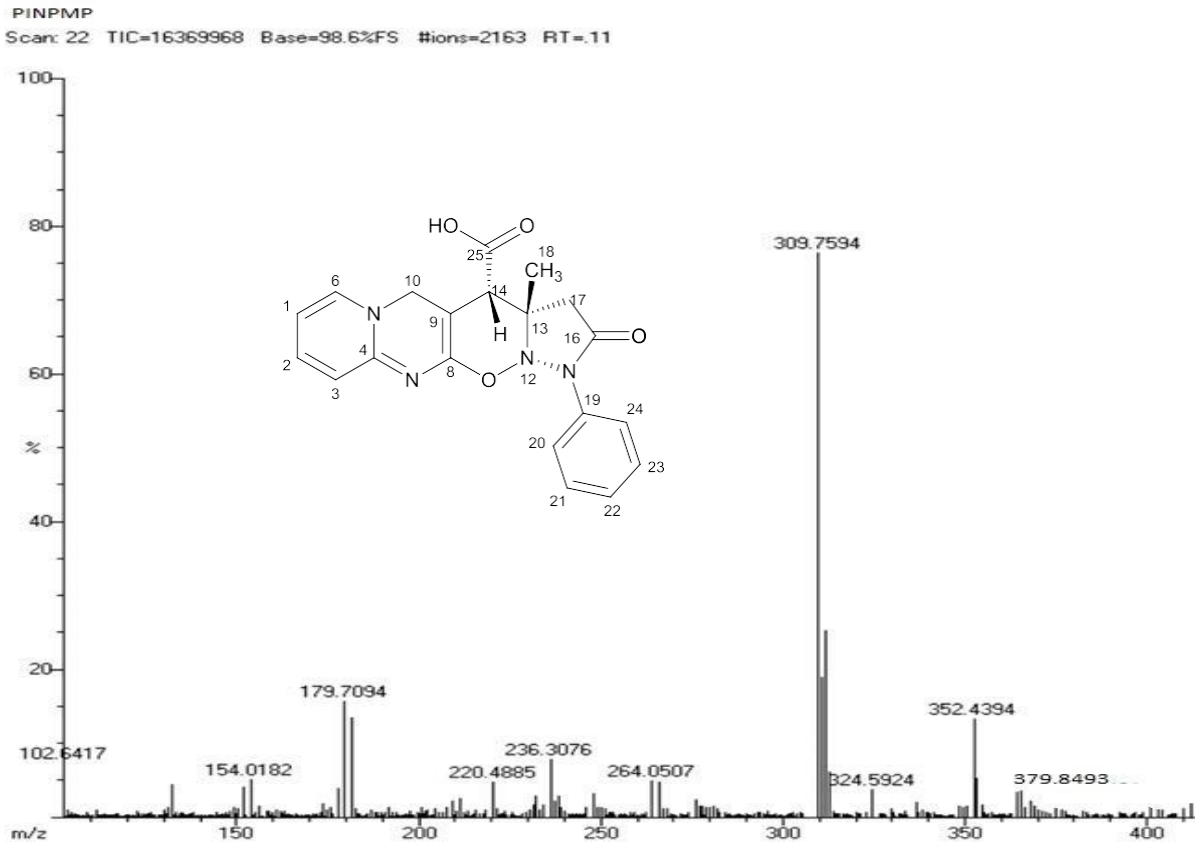

FIGURE 25 : Mass Spectrum of Methyl-2-Oxo-1-Phenyl-1,2,3,3*a*,4,5-Hexahydropyrazolo[1,5-*b*]Pyrido[1',2':1,2]Pyrimido[5,4-*e*][1,2]Oxazine-4-Carboxylic Acid (7a)

4.3.2 SPECTRAL CHARACTERIZATION OF SYNTHESIZED CYCLIC ADDUCTS (7b & 7c)

The IEDDA adducts formed from 7-methyl and 8-methyl substituted 2-oxo-2*H*-pyrido [1, 2-*a*] pyrimidin-3(4*H*)-ylidiene acetic acid **(3a and 3c)** diene with the dienophile 3-methyl-1-phenyl-1*H*-pyrazol-5(4*H*)-one **(6)** provided the products **7b** and **7c** respectively. The spectral analysis of these adducts showed similarities with that of **7a**. The FTIR, ^{1}H NMR and ^{13}C NMR spectra are presented in **Figures 26 to 31** and their respective data are provided in the **Tables 14 to 16.**

The mass spectra of the adducts **(Figures 32 and 33)** showed molecular ion peaks at m/z values 392 for **7b** and 393.5for **7c**, respectively which confirmed the proposed structures.

TABLE 14: FTIR Assignments of Compounds 7b & 7c

Functional group	Types of vibration	Wave number cm^{-1}	Intensity
7b	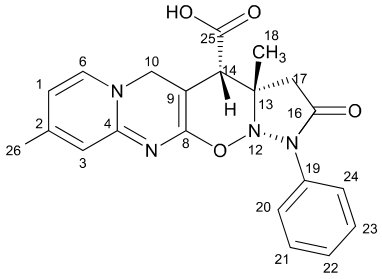		
C=O	Stretch	1605	Strong
C=N	Bending	1498	Medium
O-H	Stretch	3412	Very broad
O-H	Stretch	1408	Strong
O-H	Stretch	1020	Medium
C-O	Stretch	1270	Strong
7c	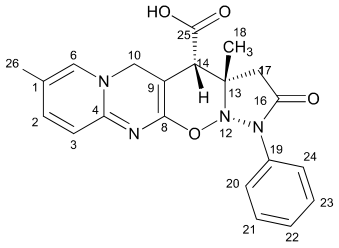		
C=O	Stretch	1606	Strong
C=N	Bending	1487	Medium
O-H	Stretch	3441	Very broad
O-H	Stretch	1411	Strong
C-O	Stretch	1274	Strong

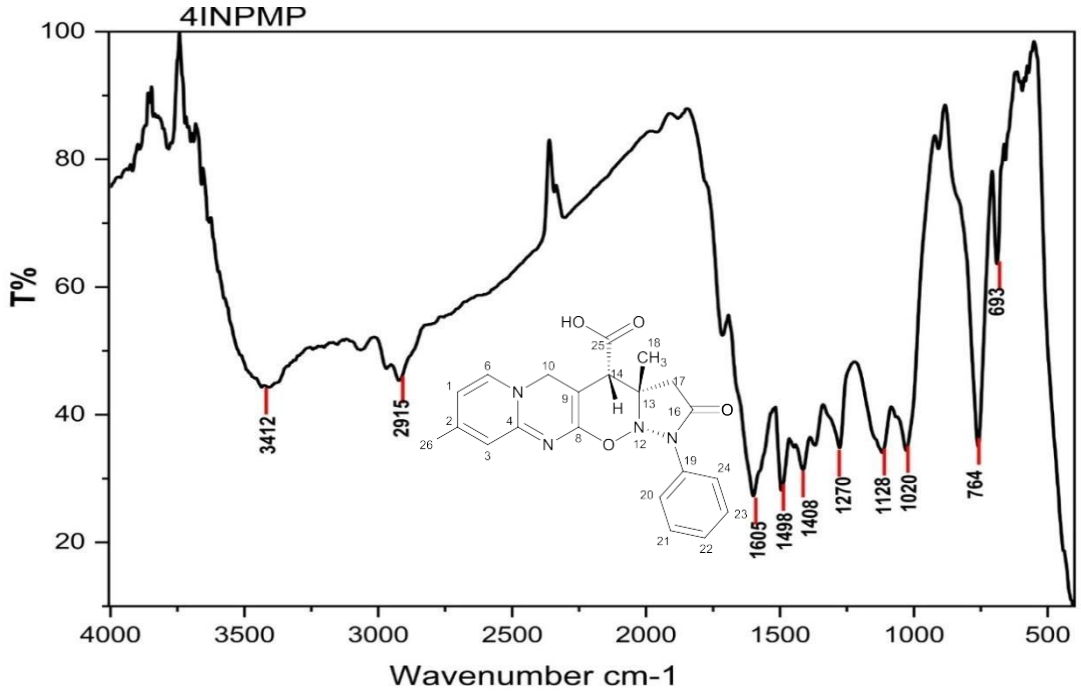

FIGURE 26: FTIR Spectrum of 9-Dimethyl-2-Oxo-1-Phenyl-1,2,3,3*a*,4,5-Hexa hydropyrazolo[1,5-*b*]Pyrido[1',2':1,2]Pyrimido[5,4-*e*][1,2]Oxazine-4-Carboxylic Acid (7b)

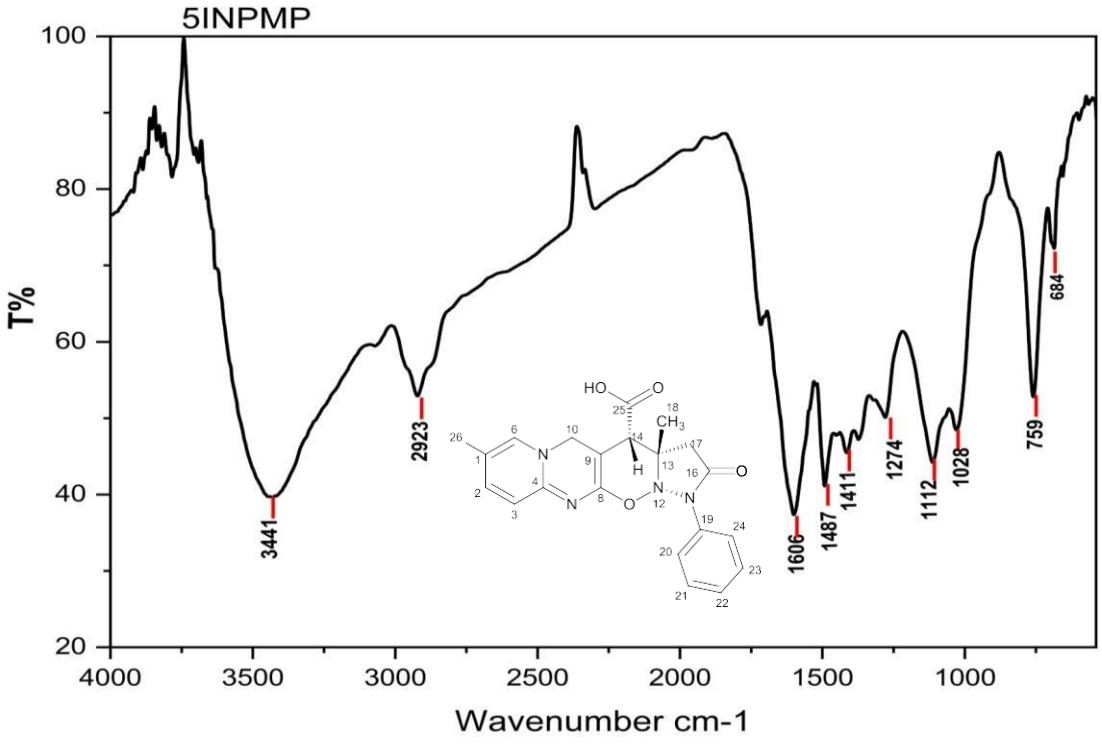

FIGURE 27: FTIR Spectrum of 9-Dimethyl-2-Oxo-1-Phenyl-1,2,3,3*a*,4,5-Hexa hydropyrazolo[1,5-*b*] Pyrido[1',2':1,2]Pyrimido[5,4-*e*][1,2]Oxazine-4-Carboxylic Acid (7c)

TABLE 15: ^{1}H NMR Assignments of Compounds 7b and 7c

(7b) 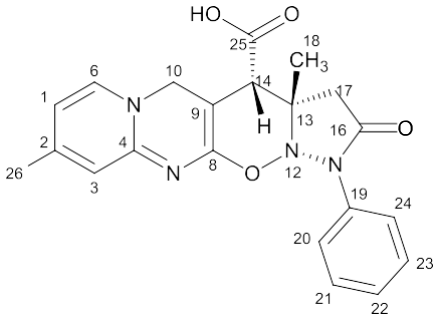			**(7c)** 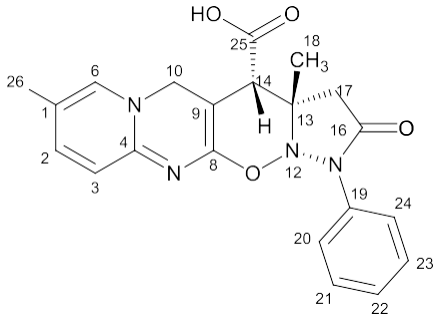		
^{1}H Shift in ppm	**No. of ^{1}H/ Multiplicity**	**J value (Hz)**	**^{1}H Shift in ppm**	**No. of ^{1}H/ Multiplicity**	**J value (Hz)**
7.8	^{1}H /d	12.0	7.6	^{2}H /d	6.0
7.1	^{3}H /s		7.8	^{3}H /d	6.0
7.5	^{6}H /d	12.0	7.29	^{6}H /s	
2.8	^{10}H /s		2.87	^{10}H /s	
2.72/2.78	^{14}H /s		2.71/2.77	^{14}H /s	
2.3	^{17}H /s		2.3	^{17}H /s	
2.1	^{18}H /s		2.1	^{18}H /s	
7.68	^{20}H /d	12.0	7.66	^{20}H /d	6.0
7.4	^{21}H /t	12.0/6.0	7.4	^{21}H /t	6.0/6.0
7.2	^{22}H /t	12.0/6.0	7.2	^{22}H /t	6.0/6.0
7.4	^{23}H /t	12.0/6.0	7.4	^{23}H /t	6.0/6.0
7.68	^{24}H /d	12.0	7.66	^{24}H /d	6.0
9.02	^{25}H /s		9.64	^{25}H /s	
1.9	^{26}H /s		1.9	^{26}H /s	

TABLE 16: ^{13}C NMR Assignments for Compounds 7b and 7c

7b 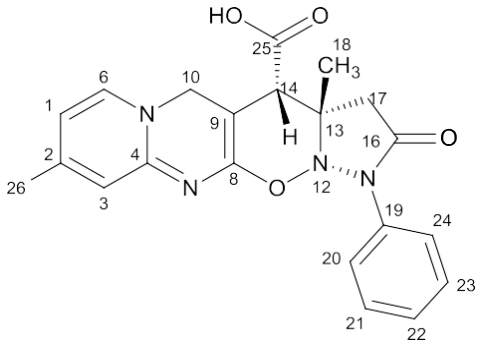				**7c** 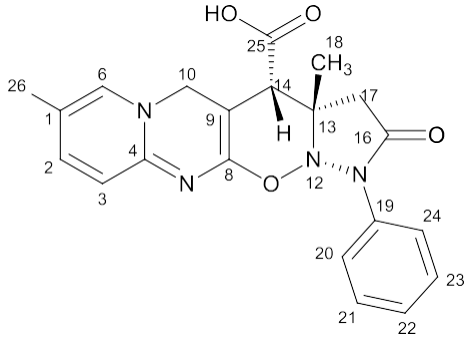			
C^{13} shift in ppm (7b)	**Carbon(7b)**	**C^{13} shift in ppm (7b)**	**Carbon(7b)**	**C^{13} shift in ppm (7c)**	**Carbon (7c)**	**C^{13} shift in ppm (7c)**	**Carbon (7c)**
120.5	C^{1}	28	C^{17}	119	C^{1}	31	C^{17}
125.2	C^{2}	11	C^{18}	120	C^{2}	11	C^{18}
126	C^{3}	125	C^{19}	128	C^{3}	121.5	C^{19}
146	C^{4}	121	C^{20}	146	C^{4}	121	C^{20}
125.7	C^{6}	129.4	C^{21}	125.5	C^{6}	129.41	C^{21}
137	C^{8}	129	C^{22}	137	C^{8}	129	C^{22}
120	C^{9}	129.4	C^{23}	118	C^{9}	129.41	C^{23}
34	C^{10}	121	C^{24}	34	C^{10}	121	C^{24}
118	C^{13}	163	C^{25}	109	C^{13}	163	C^{25}
36	C^{14}	17	C^{26}	36	C^{14}	14	C^{26}
129.5	C^{16}			129.5	C^{16}		

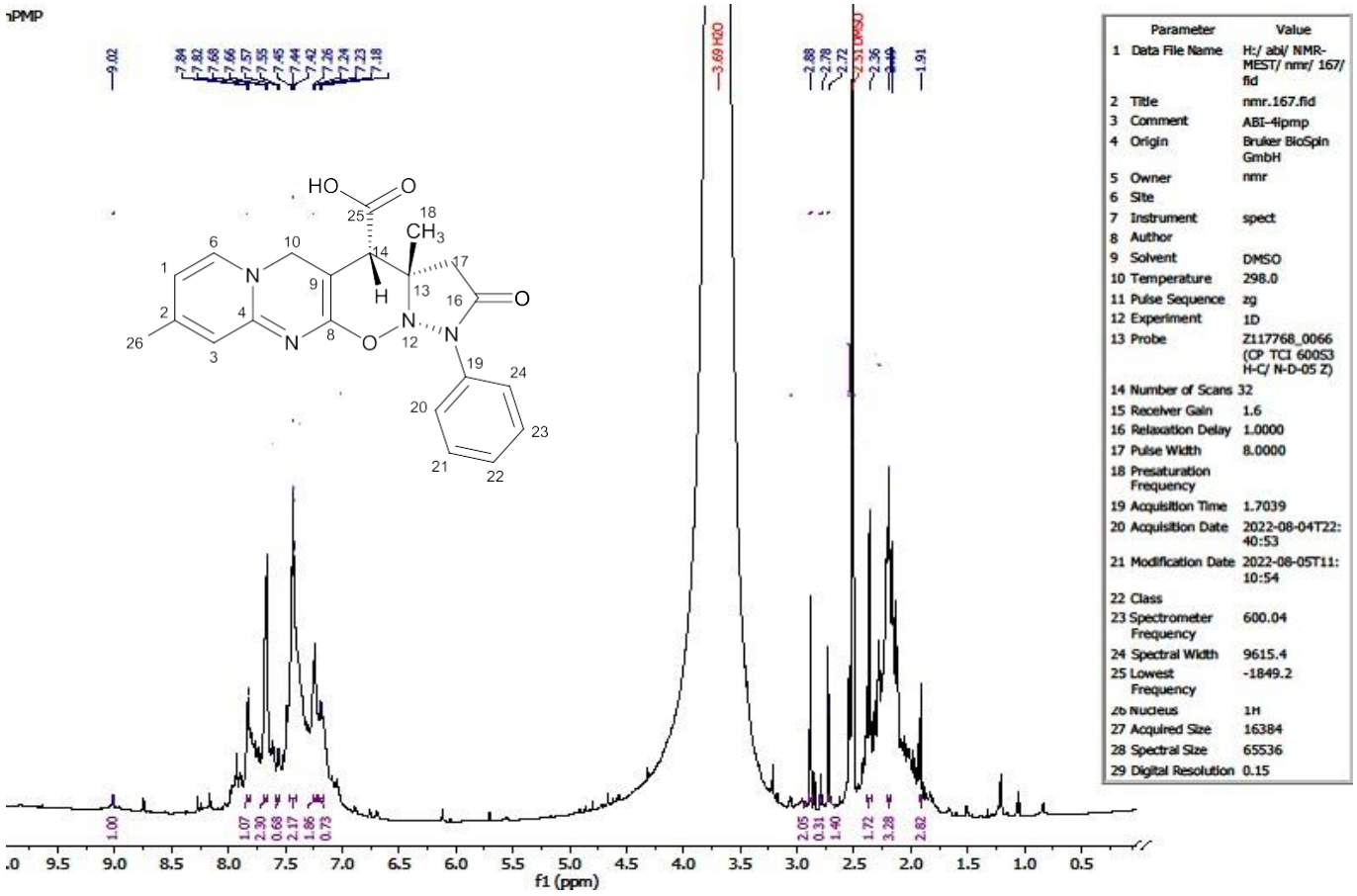

FIGURE 28 : ^{1}HNMR Spectrum of 3*a*,9-Dimethyl-2-Oxo-1-Phenyl-1,2,3,3*a*,4,5-Hexahydropyrazolo[1,5-*b*] Pyrido[1',2':1,2]Pyrimido [5,4-*e*][1,2]Oxazine-4-Carboxylic Acid (7b)

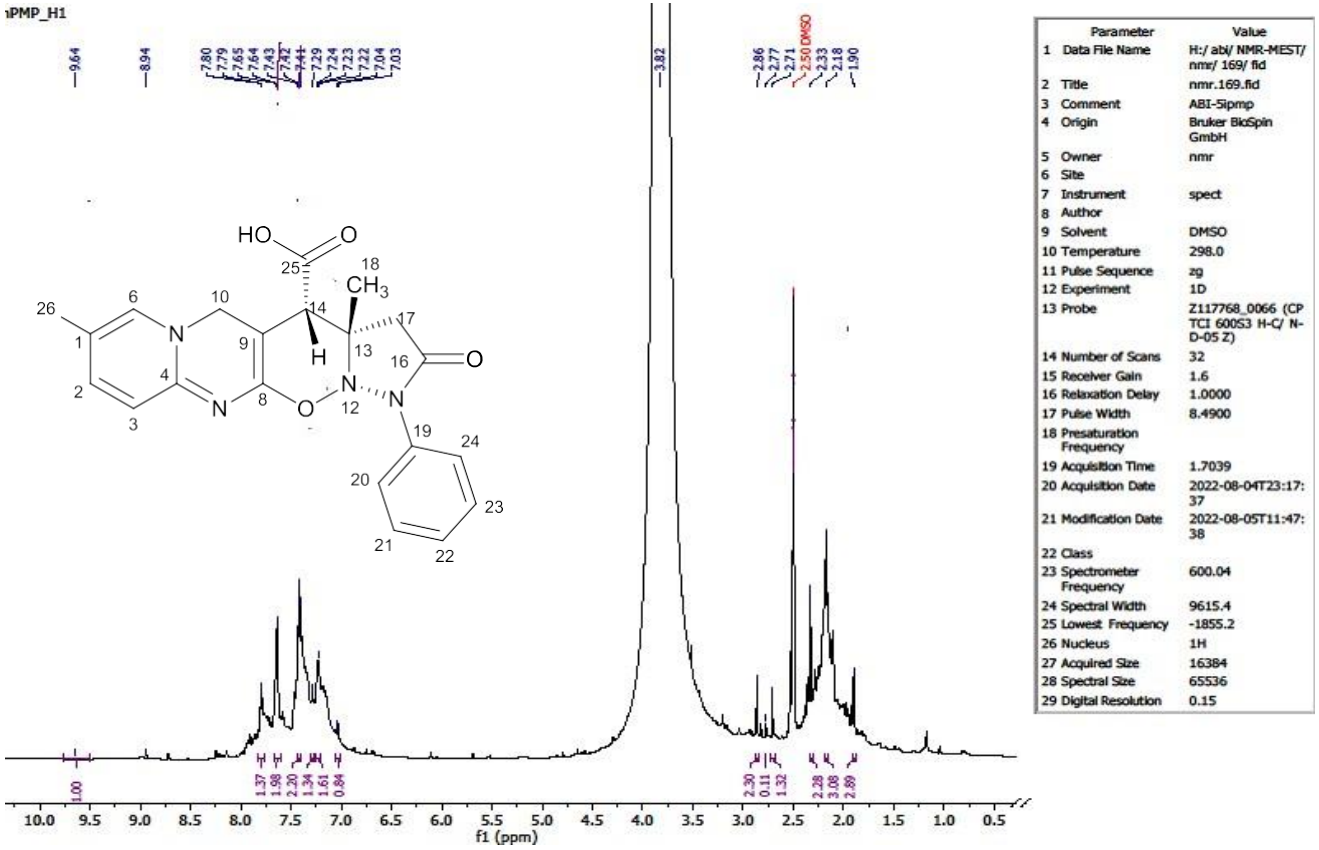

FIGURE 29 : ^{1}HNMR Spectrum of 9-Dimethyl-2-Oxo-1-Phenyl-1,2,3,3*a*,4,5-Hexahydropyrazolo[1,5-*b*] Pyrido[1',2':1,2]Pyrimido [5,4-*e*] [1,2]Oxazine-4-Carboxylic Acid (7c)

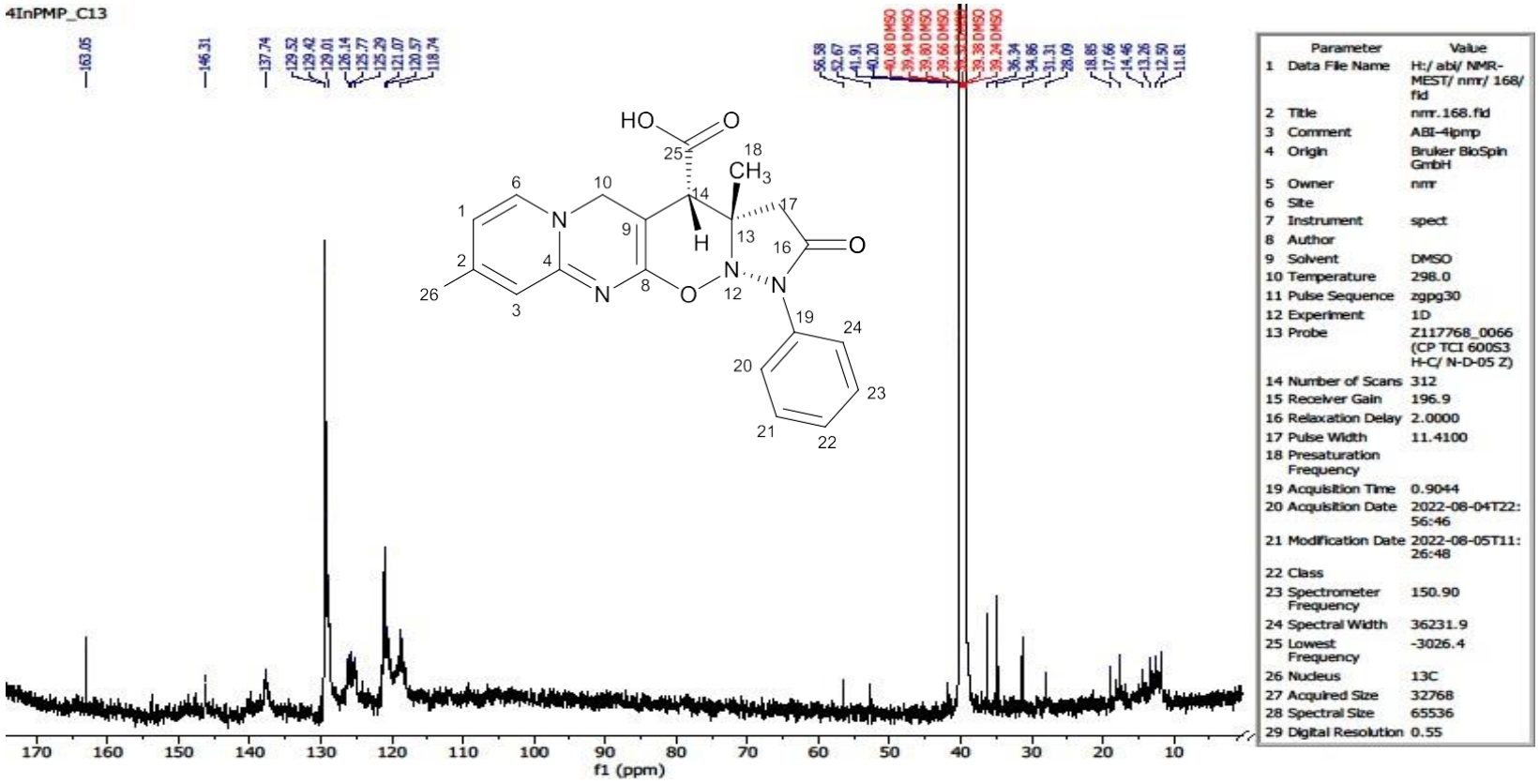

	Parameter	Value
1	Data File Name	H:/ abi/ NMR-MEST/ nmr/ 168/ fid
2	Title	nmr.168.fid
3	Comment	ABI-4ipmp
4	Origin	Bruker BioSpin GmbH
5	Owner	nmr
6	Site	
7	Instrument	spect
8	Author	
9	Solvent	DMSO
10	Temperature	298.0
11	Pulse Sequence	zgpg30
12	Experiment	1D
13	Probe	Z117768_0066 (CP TCI 600S3 H-C/ N-D-05 Z)
14	Number of Scans	312
15	Receiver Gain	196.9
16	Relaxation Delay	2.0000
17	Pulse Width	11.4100
18	Presaturation Frequency	
19	Acquisition Time	0.9044
20	Acquisition Date	2022-08-04T22:56:46
21	Modification Date	2022-08-05T11:26:48
22	Class	
23	Spectrometer Frequency	150.90
24	Spectral Width	36231.9
25	Lowest Frequency	-3026.4
26	Nucleus	13C
27	Acquired Size	32768
28	Spectral Size	65536
29	Digital Resolution	0.55

FIGURE 30 : ^{13}C Spectrum of 9-Dimethyl-2-Oxo-1-Phenyl-1,2,3,3*a*,4,5-Hexahydropyrazolo[1,5-*b*] Pyrido[1',2':1,2]Pyrimido [5,4-*e*][1,2]Oxazine-4-Carboxylic Acid (7b)

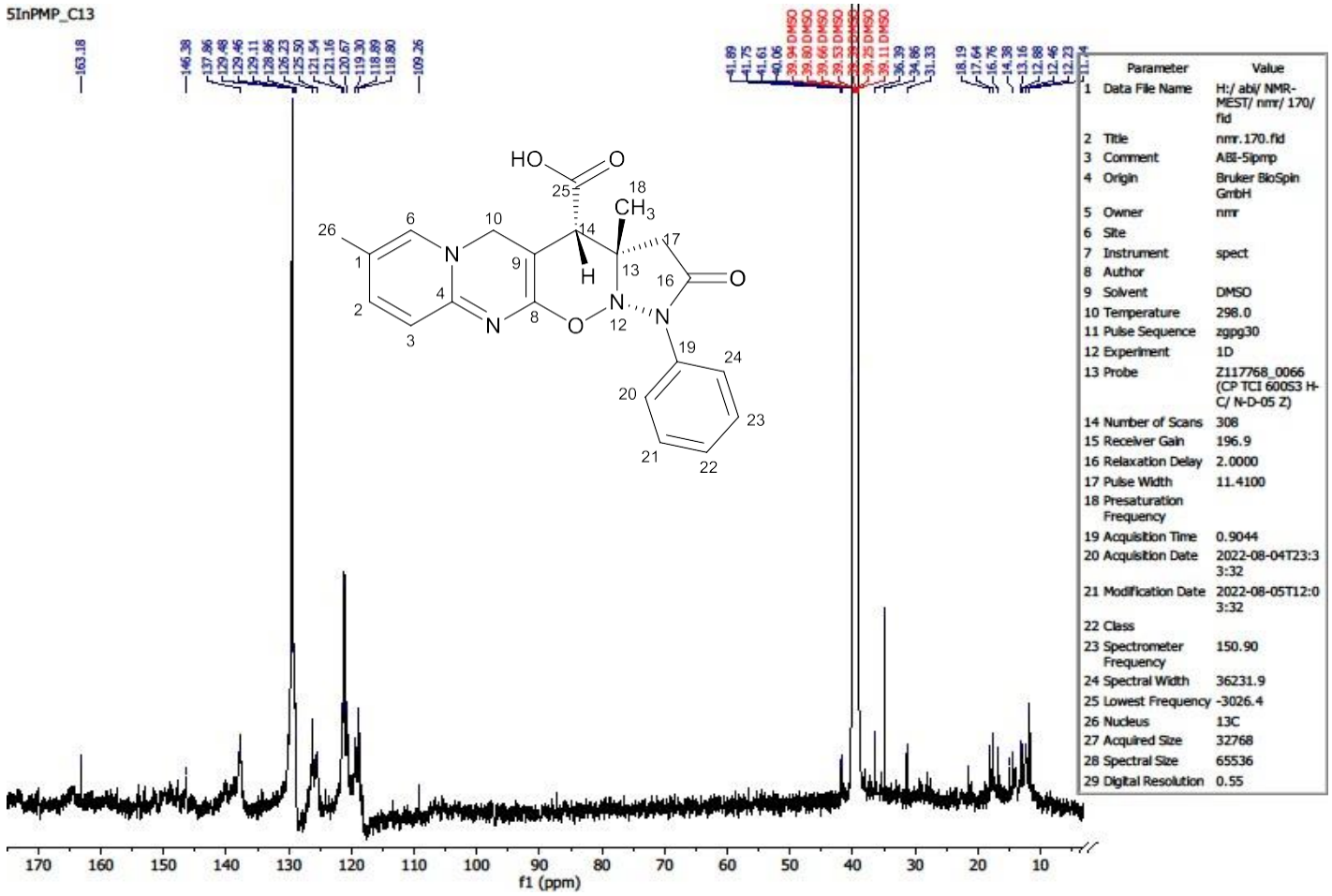

FIGURE 31 : ^{13}C Spectrum of 9-Dimethyl-2-Oxo-1-Phenyl-1,2,3,3*a*,4,5-Hexahydropyrazolo[1,5-*b*] Pyrido[1',2':1,2]Pyrimido [5,4-*e*][1,2]Oxazine-4-Carboxylic Acid (7c)

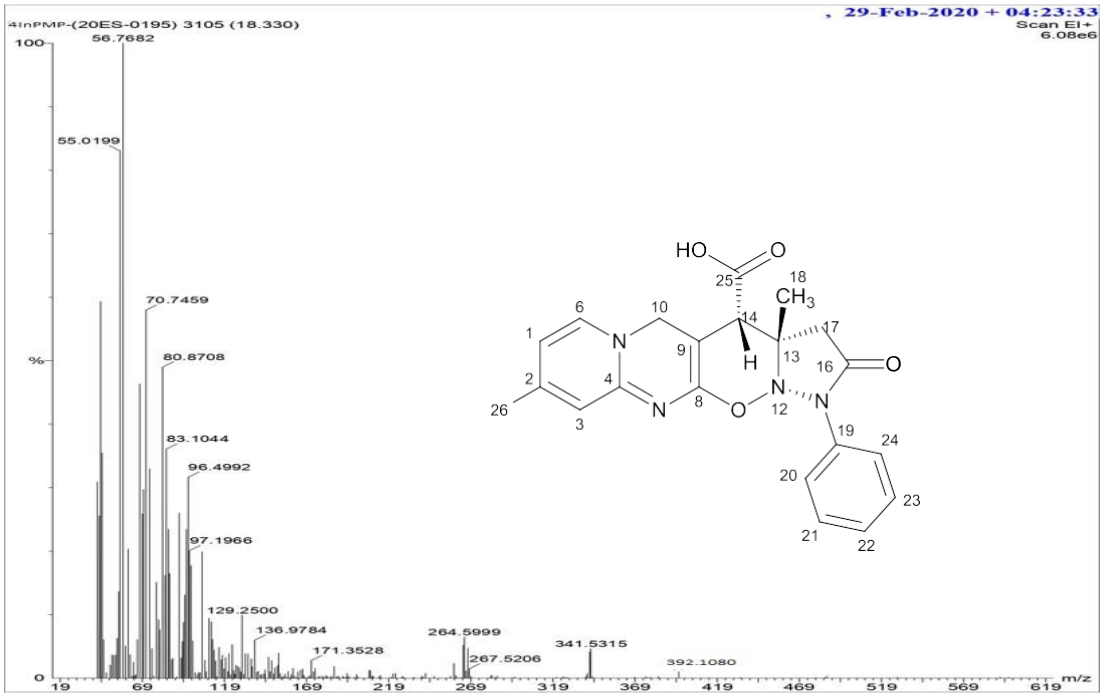

FIGURE 32 : Mass Spectrum of 9-Dimethyl-2-Oxo-1-Phenyl-1,2,3,3*a*,4,5-Hexahydropyrazolo[1,5-*b*] Pyrido[1',2':1,2]Pyrimido [5,4-*e*][1,2]Oxazine-4-Carboxylic Acid (7b)

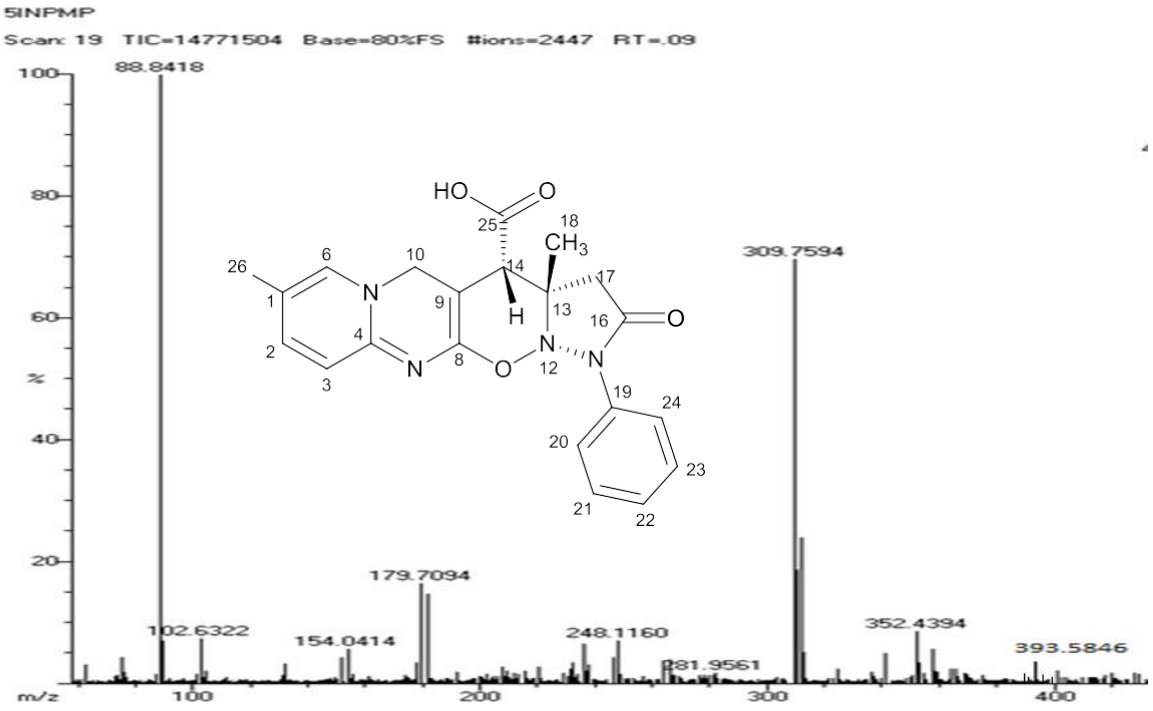

FIGURE 33 : Mass Spectrum of 9-Dimethyl-2-Oxo-1-Phenyl-1,2,3,3*a*,4,5-Hexahydropyrazolo[1,5-*b*] Pyrido[1',2':1,2]Pyrimido [5,4-*e*] [1,2]Oxazine-4-Carboxylic Acid (7c)

4.4 SYNTHESIS OF 13*a*-METHYL-1,2,3,4,4*a*,12,13,13*a*-OCTAHYDROCHROMENO [2,3-*d*]PYRIDO[1,2-*a*]PYRIMIDINE-13-CARBOXYLIC ACID DERIVATIVES

The reaction between 2-oxo-2*H*-pyrido [1, 2-*a*] pyrimidin-3(4*H*)-ylidiene acetic acid **(3)** and dienophile 1-methyl-1-cyclohexene **(8)** in presence of indium (III) chloride catalyst and DMF solvent at 90^{o}C, proceeded smoothly under the optimized conditions. The reaction mixture showed 6 h of time period for the completion of the reaction. Formation of the adduct **9a** was confirmed by TLC, which showed no remaining starting material and a single major spot. The reaction provided corresponding adduct **9a** with good yields. The obtained precipitate was purified by recrystallisation without separation of diastereoisomers and used for further analysis.

Similarly, 7-methyl and 8-methyl substituted 2-oxo-2*H*-pyrido [1, 2-*a*] pyrimidin-3(4*H*)-ylidiene acetic acid **(3b and 3c)** were refluxed with the selected dienophile 1-methyl-1-cyclohexene **(8).** The reaction mixture after refluxing yielded adducts **9b and 9c** respectively. The reaction between 2-oxo-2*H*-pyrido [1, 2-*a*] pyrimidin-3(4*H*)-ylidiene acetic acid **(3)** & its methyl derivatives and dienophile 1-methyl-1-cyclohexene **(8)** is represented in the **Scheme 14**. Melting point and yields of the adducts **9a, 9b and 9c** are given in **Table 17**.

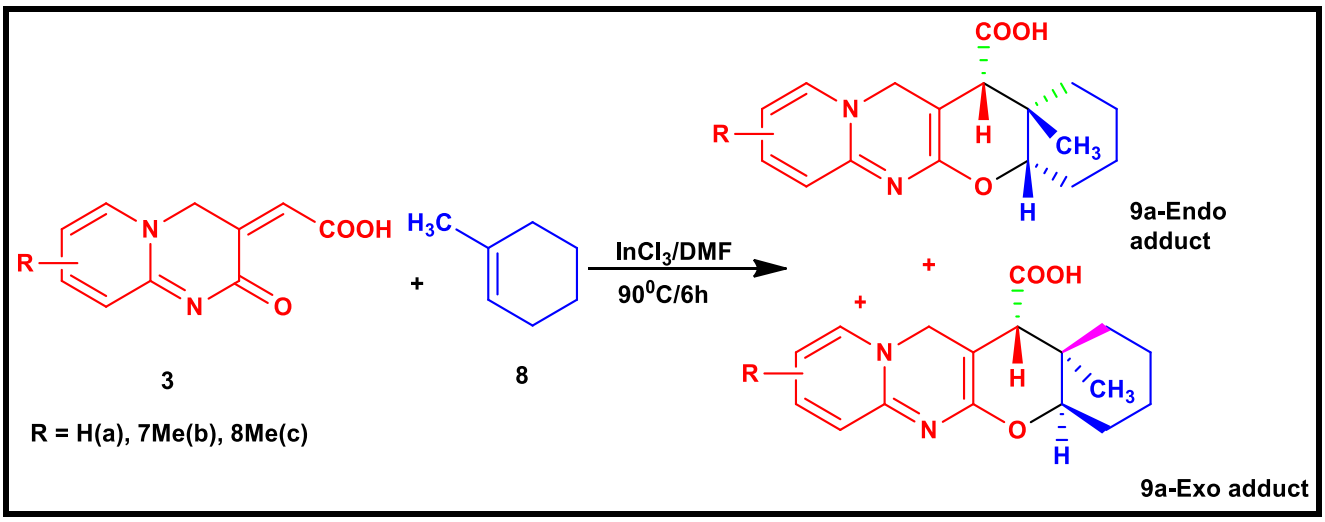

Scheme 14: Synthesis of 13*a*-Methyl-1,2,3,4,4*a*,12,13,13*a*-Octahydro chromeno[2,3-*d*]Pyrido[1,2-*a*]Pyrimidine-13-Carboxylic Acid Derivatives

TABLE 17 : Melting Point and Yield of 13*a*-Methyl-1,2,3,4,4*a*,12,13,13*a*-Octahydrochromeno[2,3-*d*]Pyrido [1,2-*a*] Pyrimidine-13-Carboxylic Acid Derivatives

Diene	Dienophile	Temp./Time	Product	Yield/M.P
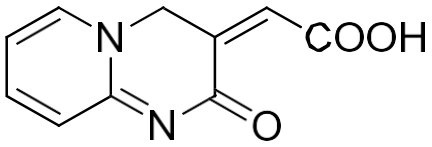	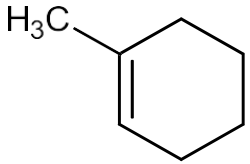	90˚C/6	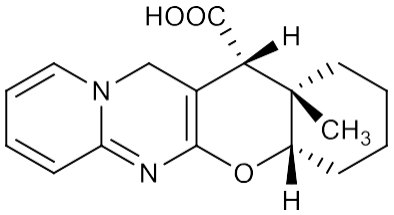	57% /257-268˚C
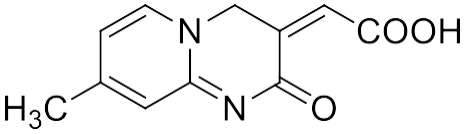		90˚C/7	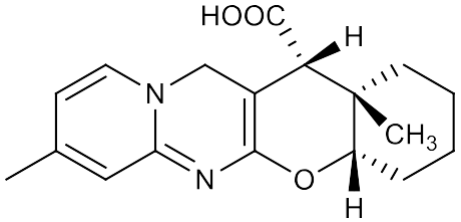	58% /278-290˚C
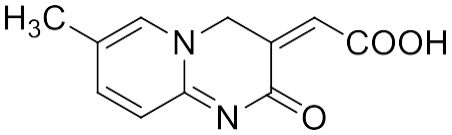		90˚C/7 ½	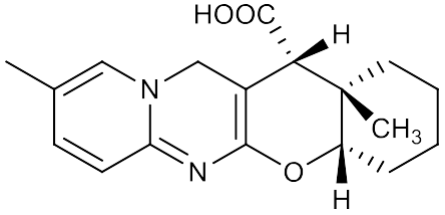	59%/ 272-286˚C

4.4.1 SPECTRAL CHARACTERIZATION OF THE SYNTHESIZED CYCLO ADDUCT(9a)

4.4.1.1 FT-IR SPECTRUM

The IR spectrum of compound **9a** product showed the expected absorption bands of C=N at 1496 cm^{-1}corresponding to the pyridopyrimidine nucleus. A broad intense O-H stretching band centered at 3394 cm^{-1} was also observed which is overriding spectral feature of the carboxylic acid. This was also confirmed by the presence of strong intense O-H in plane bend at 1388 cm^{-1}.

The strong and medium intense bands at 1651 cm^{-1} and 1249 cm^{-1} were attributed to the -C=O and -C-O stretch of the carboxylic acid moiety respectively. The absence of strong absorption band at 1680-1700 cm^{-1} confirmed the formation of the product. **(Figure 34).**

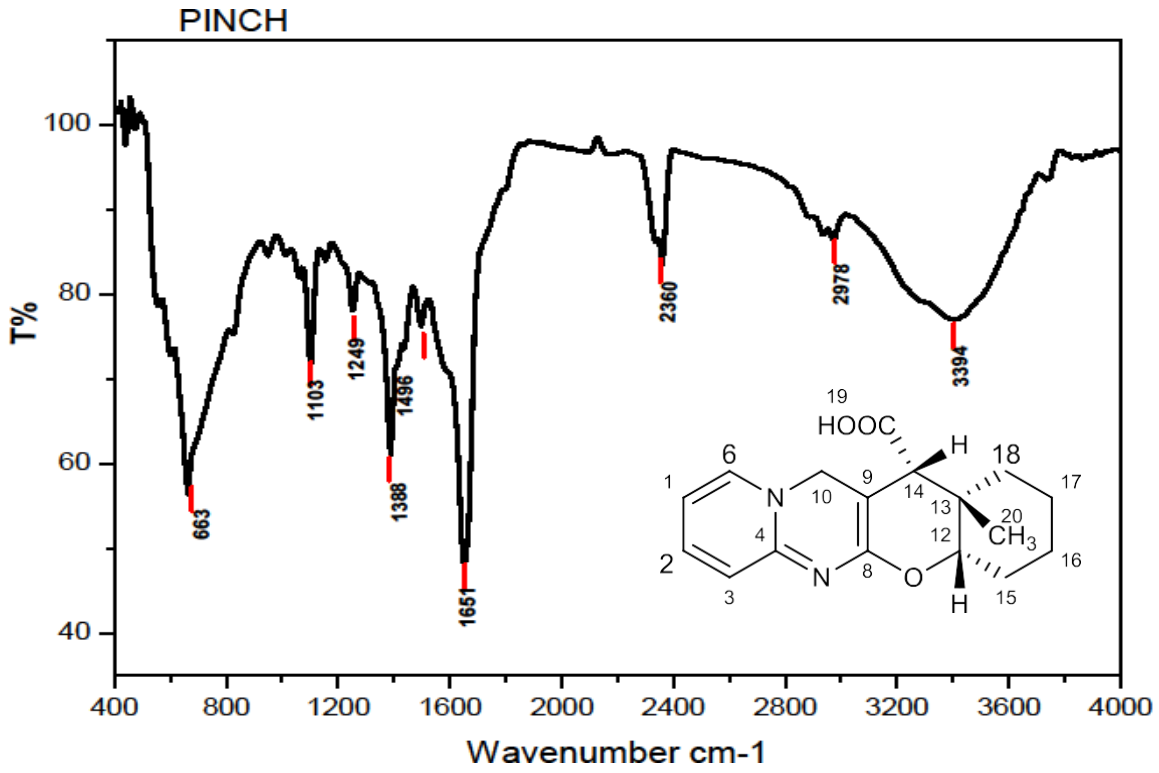

FIGURE 34: FTIR Spectrum of 13*a*-Methyl-1,2,3,4,4*a*,12,13,13*a*-Octahydro chromeno[2,3-*d*]Pyrido[1,2-*a*]Pyrimidine-13-Carboxylic Acid (9a)

4.4.1.2 ^{1}H NMR SPECTRUM

The proton NMR **(Figure 35)** spectrum of compound **9a** presented 13 sets of protons. The two signals of C_{20} methyl proton appeared as singlet at δ 4.8 and at δ 4.92 was indicative of *endo* and *exo* diastereoisomers with the intensity ratio of **6:1**. Hence the diastereoselectivity of the reaction was validated. C_{12}-H proton appeared as triplet at δ 6.3 (J=18Hz, 6Hz) considerably downfield probably due to the additional deshielding of adjacent oxygen atom. -C_{15}-H, C_{16}-H, C_{17}-H and C_{18} -H appeared in the range of δ 5.0-5.5 with J value 6.0Hz and 12.0Hz respectively. Carboxylic acid proton C_{19}-H appeared at δ 12.6. Other aromatic ring protons appeared in more downfield region of δ 10.6-9.6.

TABLE 18: ^{1}H NMR Assignments of 13*a*-Methyl-1,2,3,4,4*a*,12,13,13*a*-Octahydrochromeno[2,3-*d*] Pyrido[1,2-*a*]Pyrimidine-13-Carboxylic Acid (9a)

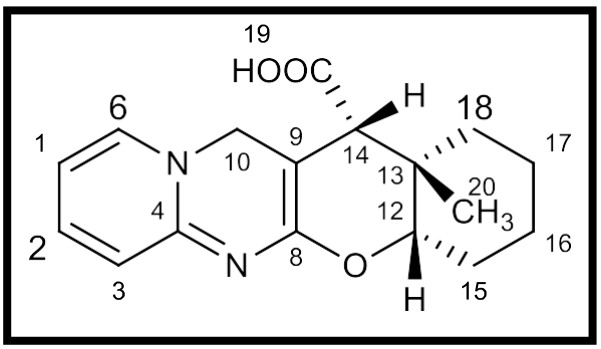

^{1}H Shift in ppm	No. of ^{1}H/ Multiplicity	J value (Hz)	^{1}H Shift in ppm	No. of ^{1}H/ Multiplicity	J value (Hz)
9.5	H^{1} /t	6.0,6.0	5.5	H^{15} /q	6.0/6.0/12.0
10.5	H^{2} /t	6.0,6.0	5.0	H^{16} /q	6.0/6.0/6.0/12.0
10.6	H^{3} /d	6.0	5.4	H^{17} /q	6.0/6.0/12.0/6.0
9.6	H^{6} /d	6.0	5.6	H^{18} /t	6.0/6 .0
6.1	H^{10} /s		12.6	H^{19} /s	
6.3	H^{12} /t	18.0,6.0	4.8/4.92	H^{20} /s	
5.9	H^{14} /s				

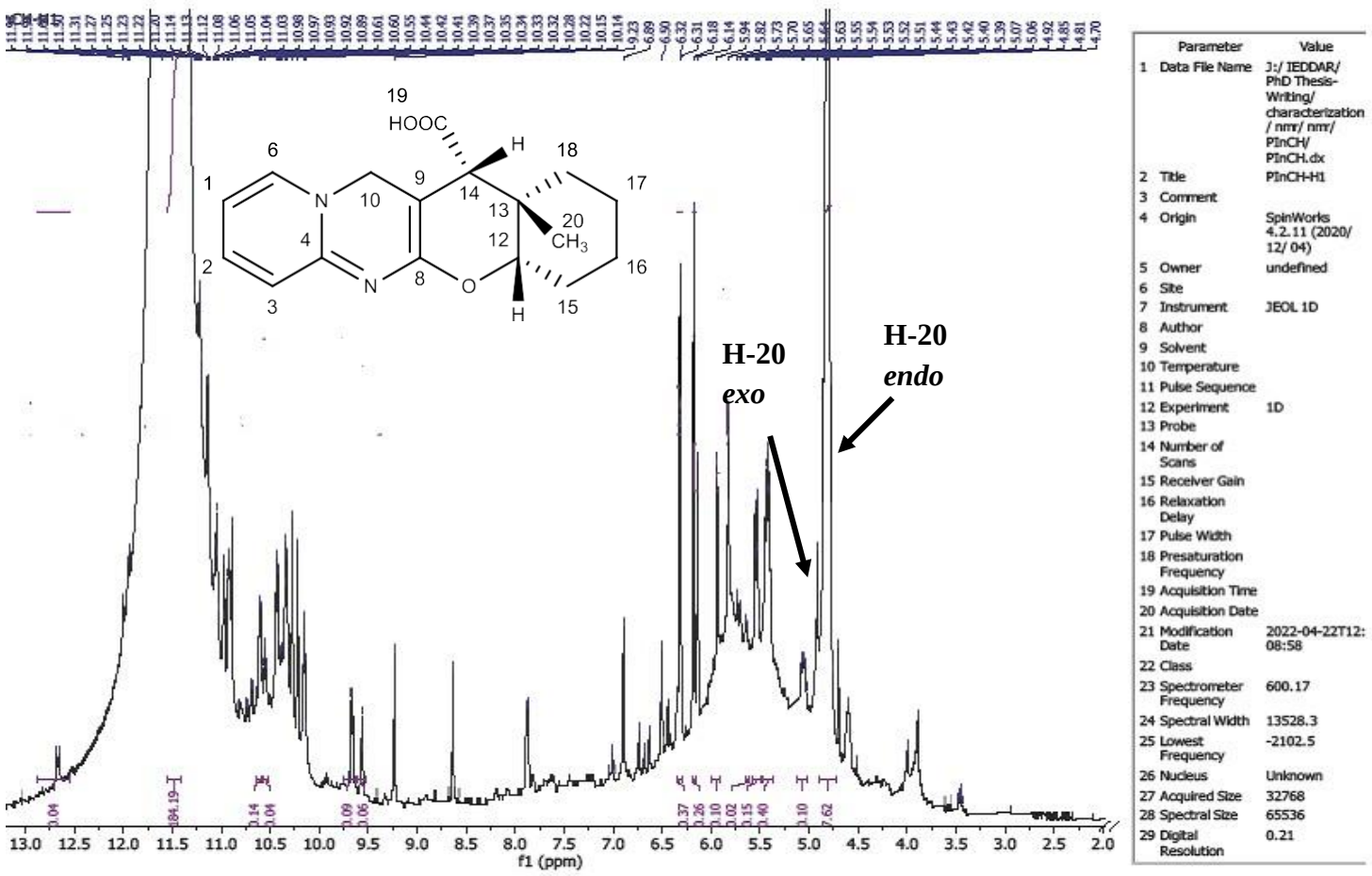

FIGURE 35 : ^{1}HNMR Spectrum of 13*a*-Methyl-1,2,3,4,4*a*,12,13,13*a*-Octahydrochromeno[2,3-*d*]Pyrido[1,2-a]Pyrimidine-13-Carboxylic Acid (9a)

^{1}HNMR Spectrum of 13*a*-Methyl-1,2,3,4,4*a*,12,13,13*a*-Octahydrochromeno[2,3-*d*]Pyrido[1,2-a]Pyrimidine-13-Carboxylic Acid (9a)

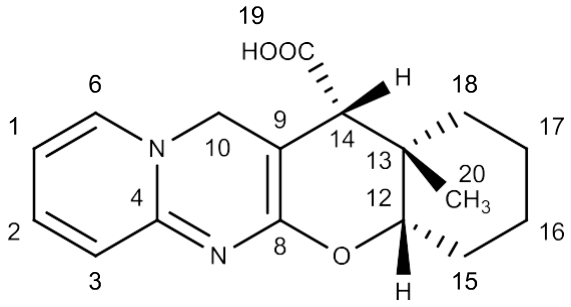

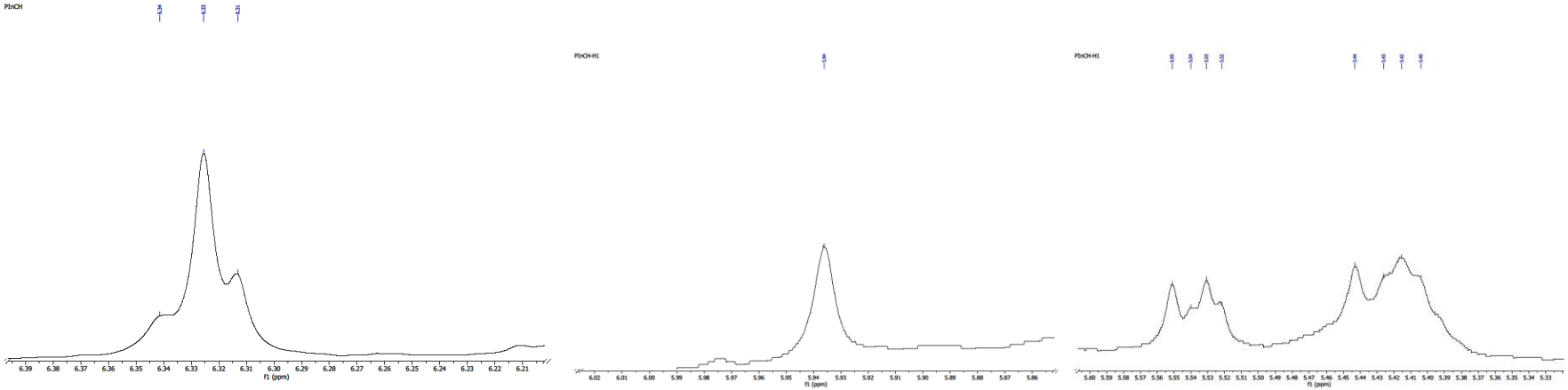

4.4.1.3 C^{13} NMR SPECTRUM

Further confirmation of the product **9a** was established through C^{13} NMR analysis. Seventeen distinct carbons were seen in the spectrum. Six peaks, up field at δ 29, 30, 33, 36, and 39 were believed to correspond to C-17, C-16, C-15, C-13 and C-14 respectively. Chemical shifts at δ 17, was typical for the methyl group carbon C-20. The C-12 carbon was noticed at δ 121 owing to the deshielding influence of the adjacent oxygen atom. The characteristic signals at δ 179, 161, 151, 152, 148, 141, 124,121 and 37 corresponded to the pyridopyrimidine ring system. The carboxylic carbon C-19 peak was seen near δ 183. The spectral data confirmed the expected product **(Figure 36).**

TABLE 19 : C^{13} NMR Assignments of 13*a*-Methyl-1,2,3,4,4*a*,12,13,13*a*-Octahydrochromeno[2,3-*d*]Pyrido[1,2-*a*]Pyrimidine-13-Carboxylic Acid (9a)

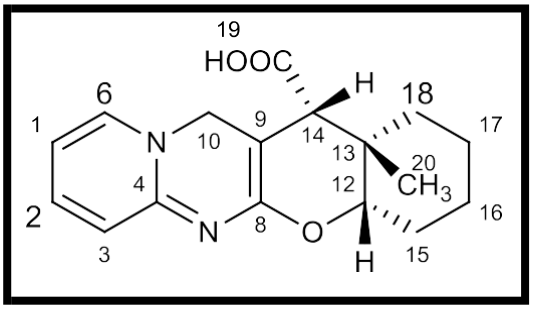

C^{13} shift in ppm	Carbon	C^{13} shift in ppm	Carbon
141	C^{1}	36	C^{13}
151	C^{2}	39	C^{14}
148	C^{3}	33	C^{15}
179	C^{4}	30	C^{16}
152	C^{6}	29	C^{17}
161	C^{8}	35	C^{18}
124	C^{9}	183	C^{19}
37	C^{10}	21	C^{20}
121	C^{12}		

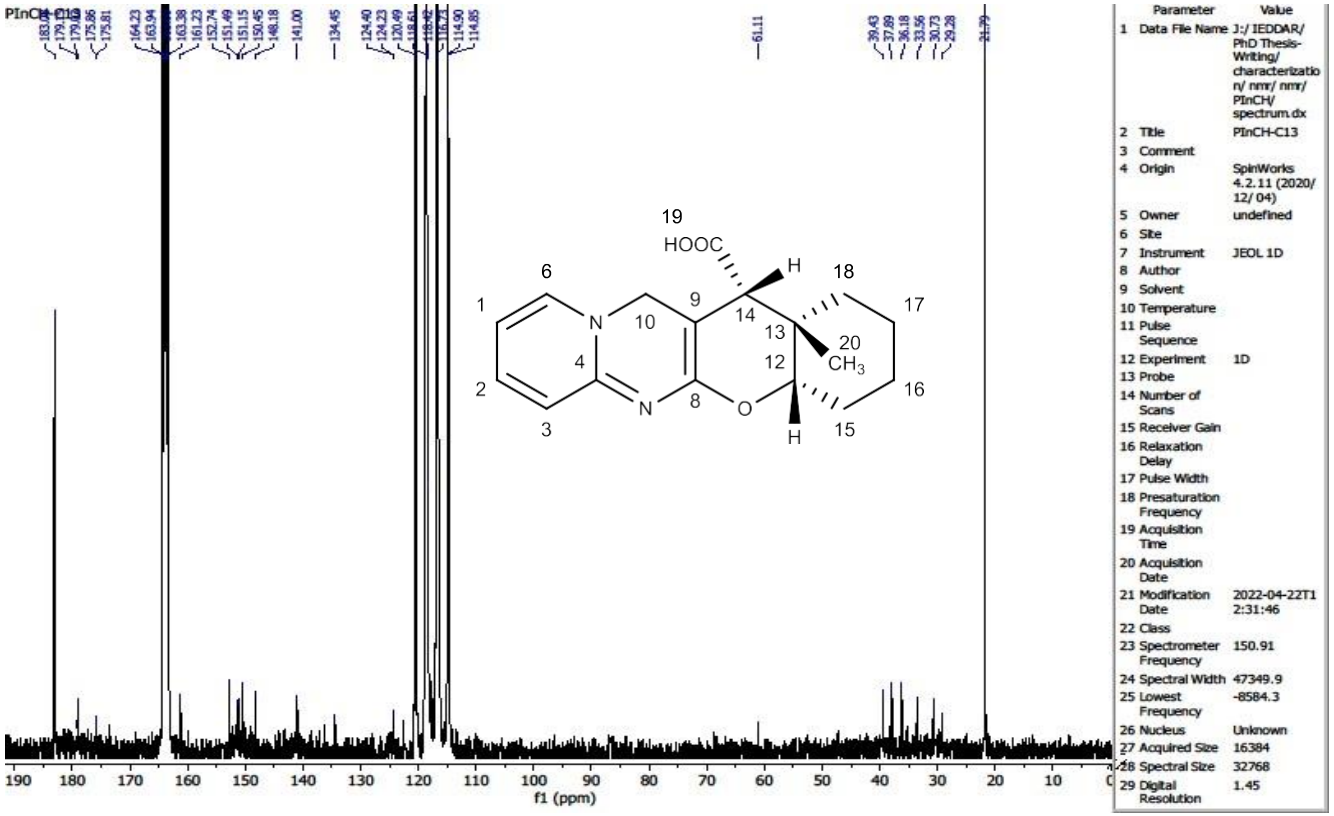

FIGURE 36 : ^{13}C Spectrum of 13*a*-Methyl-1,2,3,4,4*a*,12,13,13*a*-Octahydrochromeno[2,3-*d*]Pyrido[1,2-*a*]Pyrimidine-13-Carboxylic Acid (9a)

4.4.1.4 MASS SPECTRUM

Further evidence for the structure was obtained from the mass spectrum of the adduct which showed M+1 peak at m/z 301.64 **Figure-37**. The important mass fragment signals were observed at m/z values 280.87, 211.33, 184.84, 173.78, 171.83, 144.91. Hence the assigned structure of adduct **(9a)** was confirmed.

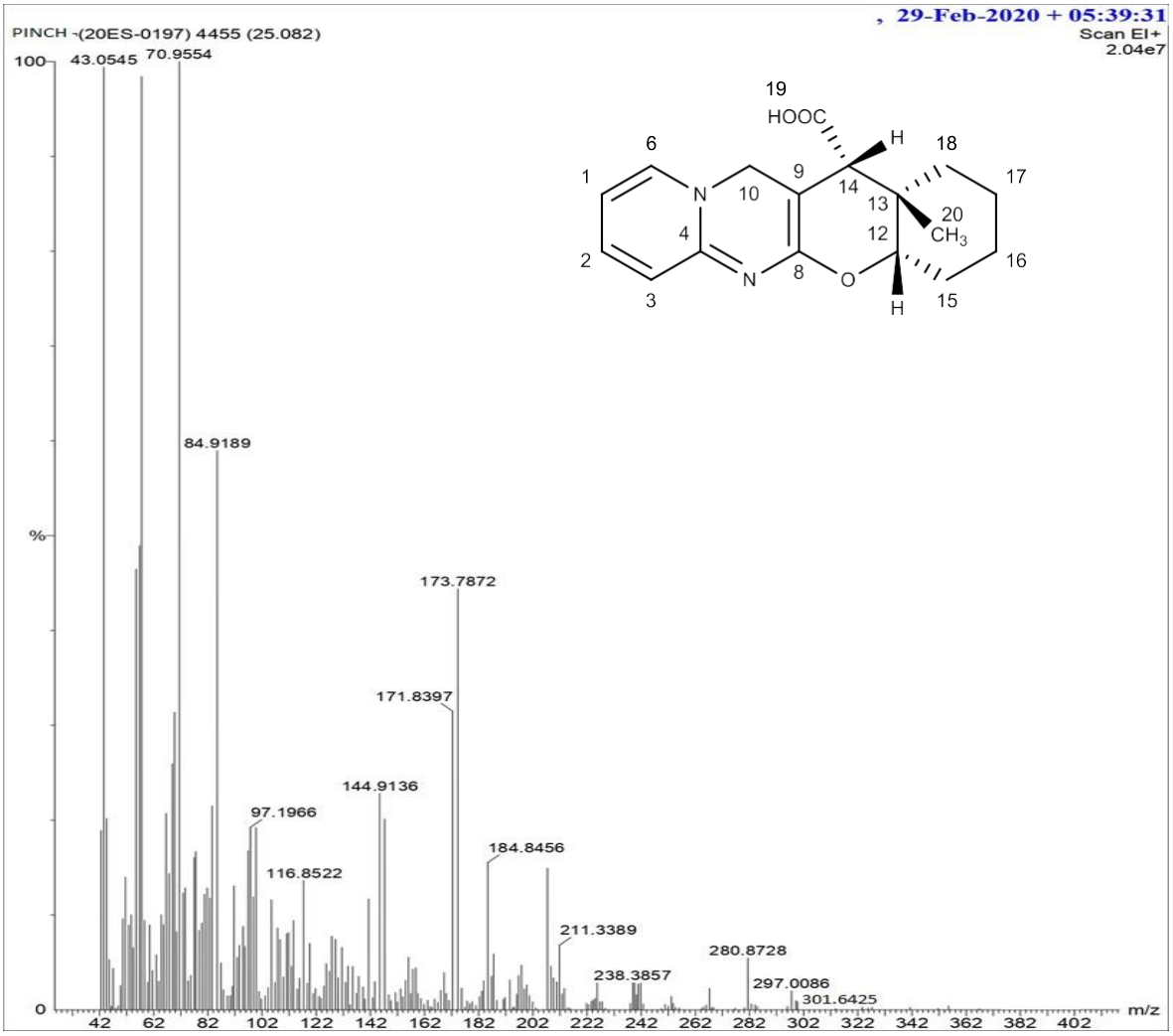

Figure 37 : Mass Spectrum of 13*a*-Methyl-1,2,3,4,4*a*,12,13,13*a*-Octahydrochromeno[2,3-*d*] Pyrido[1,2-*a*]Pyrimidine-13-Carboxylic Acid (9a)

4.4.2 SPECTRAL CHARACTERIZATION OF SYNTHESIZED CYCLO ADDUCTS (9b& 9c)

FT-IR, ^{1}H NMR, C^{13} NMR and Mass spectrum of the adducts **9b** and **9c** given in **Figures - 38, 39, 40, 41, 42, 43, 44, 45** and the assignments are tabulated in **Tables- 20, 21, 22.**

TABLE 20: FTIR Assignments of Compounds 9b & 9c

Functional group	Types of vibration	Wave number cm^{-1}	Intensity
(9b)	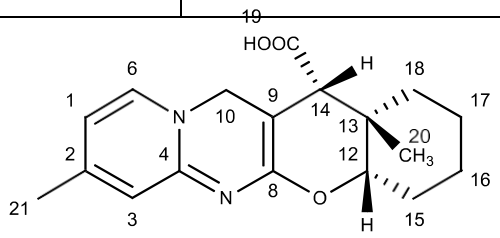		
C=O	Stretch	1696	strong
C=N	Bending	1559	medium
O-H	Stretch	3333	Very broad
O-H	Stretch	1390	strong
O-H	Stretch	807	medium
C-O	Stretch	1291	strong
(9c)	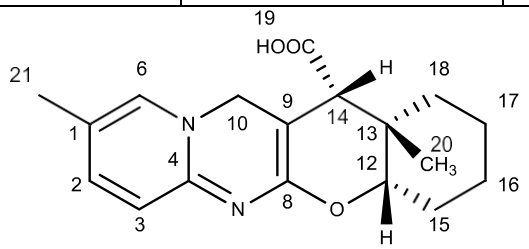		
C=O	Stretch	1697	strong
C=N	Bending	1567	medium
O-H	Stretch	3354	Very broad
O-H	Stretch	1480	strong
O-H	Stretch	1028	medium
C-O	Stretch	1296	Strong

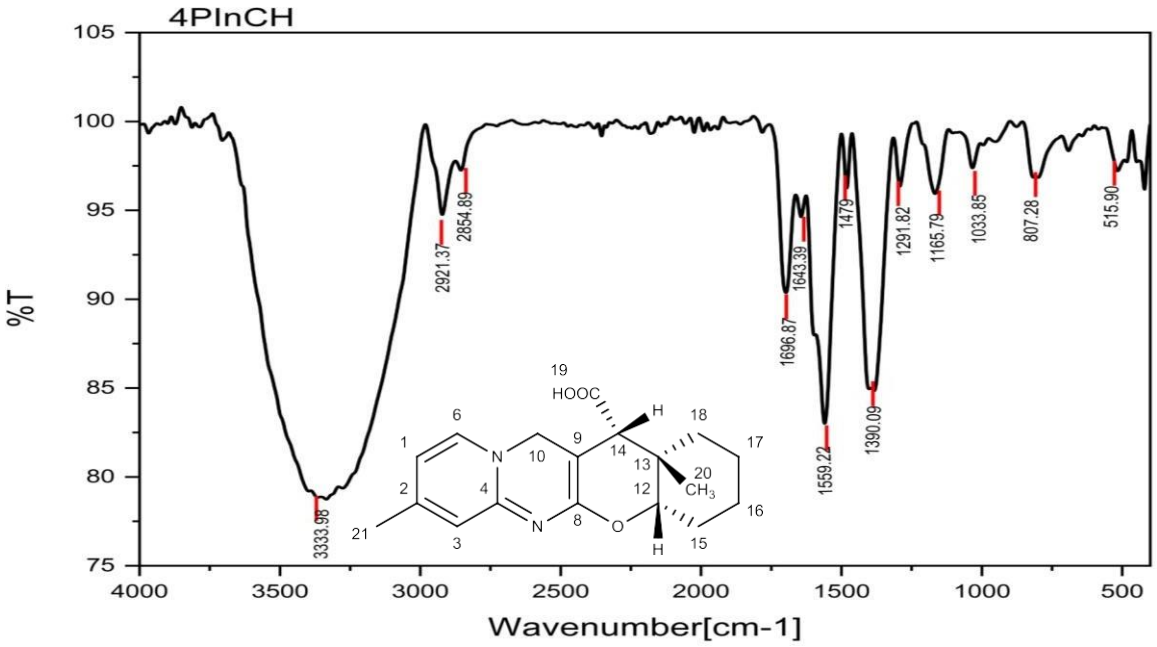

FIGURE 38: FTIR Spectrum of 8,13*a*-Dimethyl-1,2,3,4,4*a*,12,13,13*a*-Octahydrochromeno[2,3-*d*]Pyrido[1,2-*a*]Pyrimidine-13-Carboxylic Acid (9b)

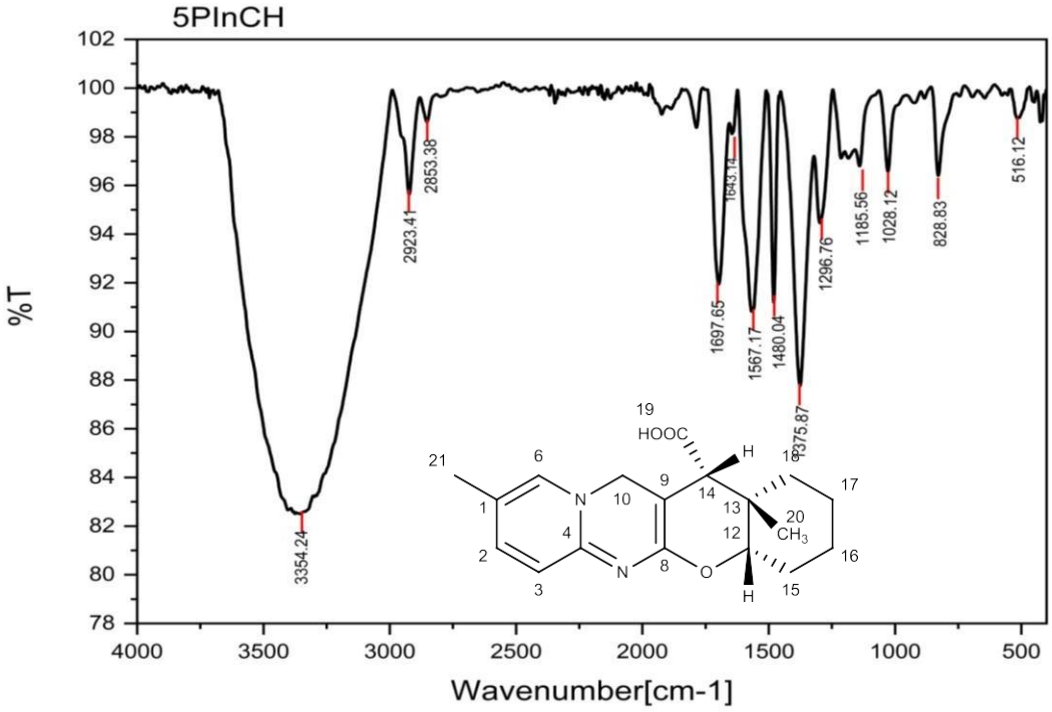

FIGURE 39:FTIR Spectrum of 9,13*a*-Dimethyl-1,2,3,4,4*a*,12,13,13*a*-Octahydrochromeno[2,3-*d*]Pyrido[1,2-*a*]Pyrimidine-13-Carboxylic Acid (9c)

TABLE 21: ^{1}H NMR Assignments of Compounds 9b & 9c

(9b) 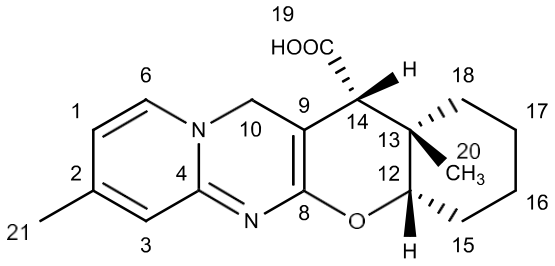			**(9c)** 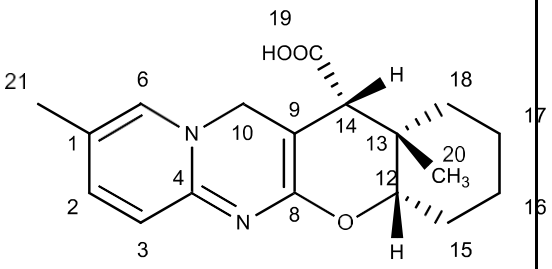		
^{1}H Shift in Ppm	**No. of ^{1}H/ Multiplicity**	**J value (Hz)**	**^{1}H Shift in ppm**	**No. of ^{1}H/ Multiplicity**	**J value (Hz)**
10.26	H^{1} /d	12.0	10.6	H^{2} /d	6.0
9.45	H^{3} /s		10.5	H^{3} /d	6.0
10.21	H^{6} /d	12.0	10.1	H^{6} /s	
6.1	H^{10} /s		6.1	H^{10} /s	
6.3	H^{12} /t	12.0/6.0	6.3	H^{12} /t	12.0/6.0
5.9	H^{14} /s		5.9	H^{14} /s	
5.5	H^{15} /dd	6.0/6.0/6.0	5.5	H^{15} /dd	6.0/6.0/6.0
5.28	H^{16} ,$H^{17,}$, H^{18} /m	6.0/6.0/6.0/12.0	5.0	H^{16} ,H^{17} /m	
12.4	H^{19} /s		5.4	H^{18} /t	6.6
4.8/4.92	H^{20} /s		12.6	H^{19} /s	
5.03	H^{21} /s		4.8/4.92	H^{20} /s	
			4.88	H^{21} /s	

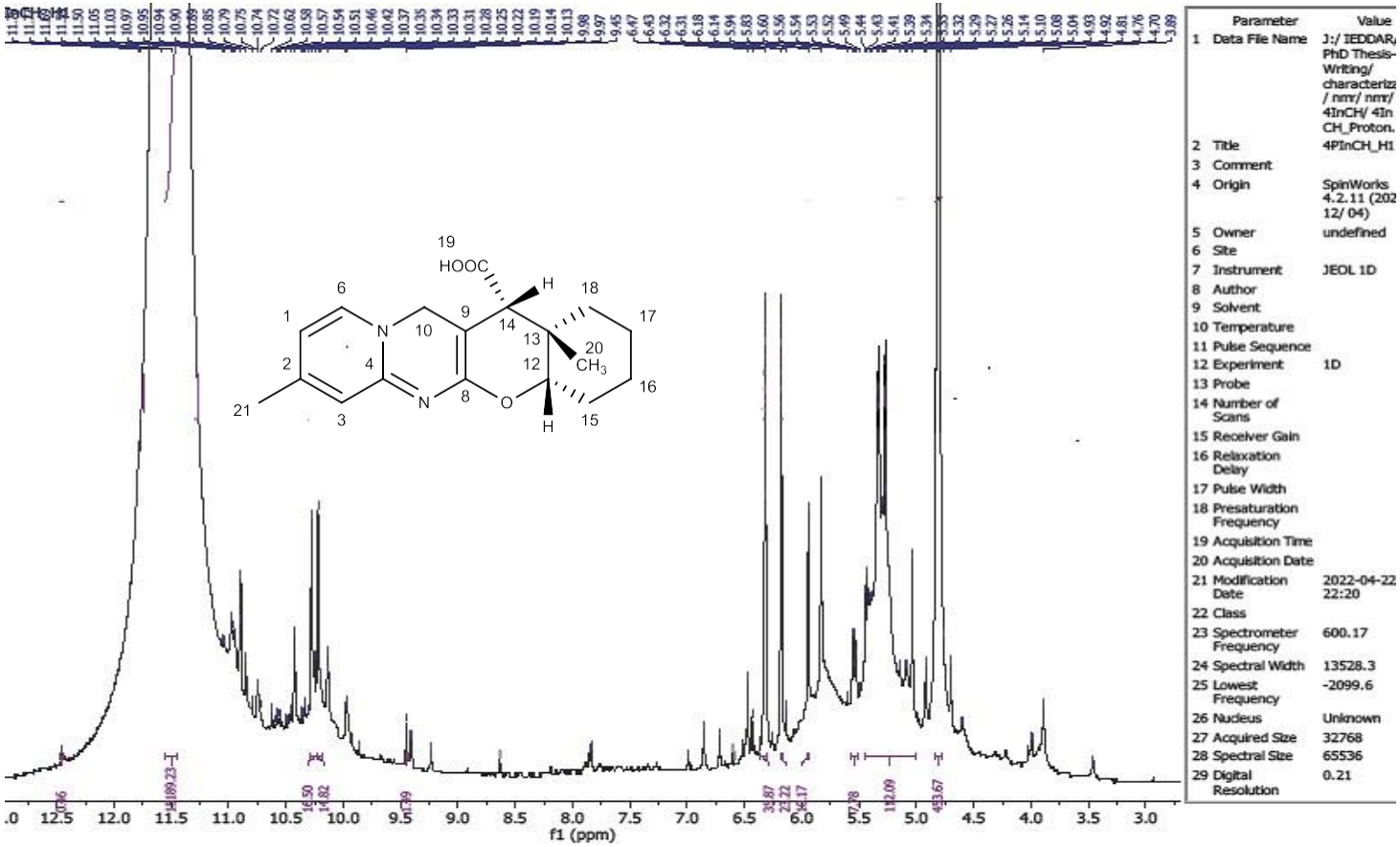

FIGURE 40 : ^{1}HNMR Spectrum of 8,13*a*-Dimethyl-1,2,3,4,4*a*,12,13,13*a*-Octahydrochromeno[2,3-*d*]Pyrido[1,2-*a*] Pyrimidine-13-Carboxylic Acid (9b)

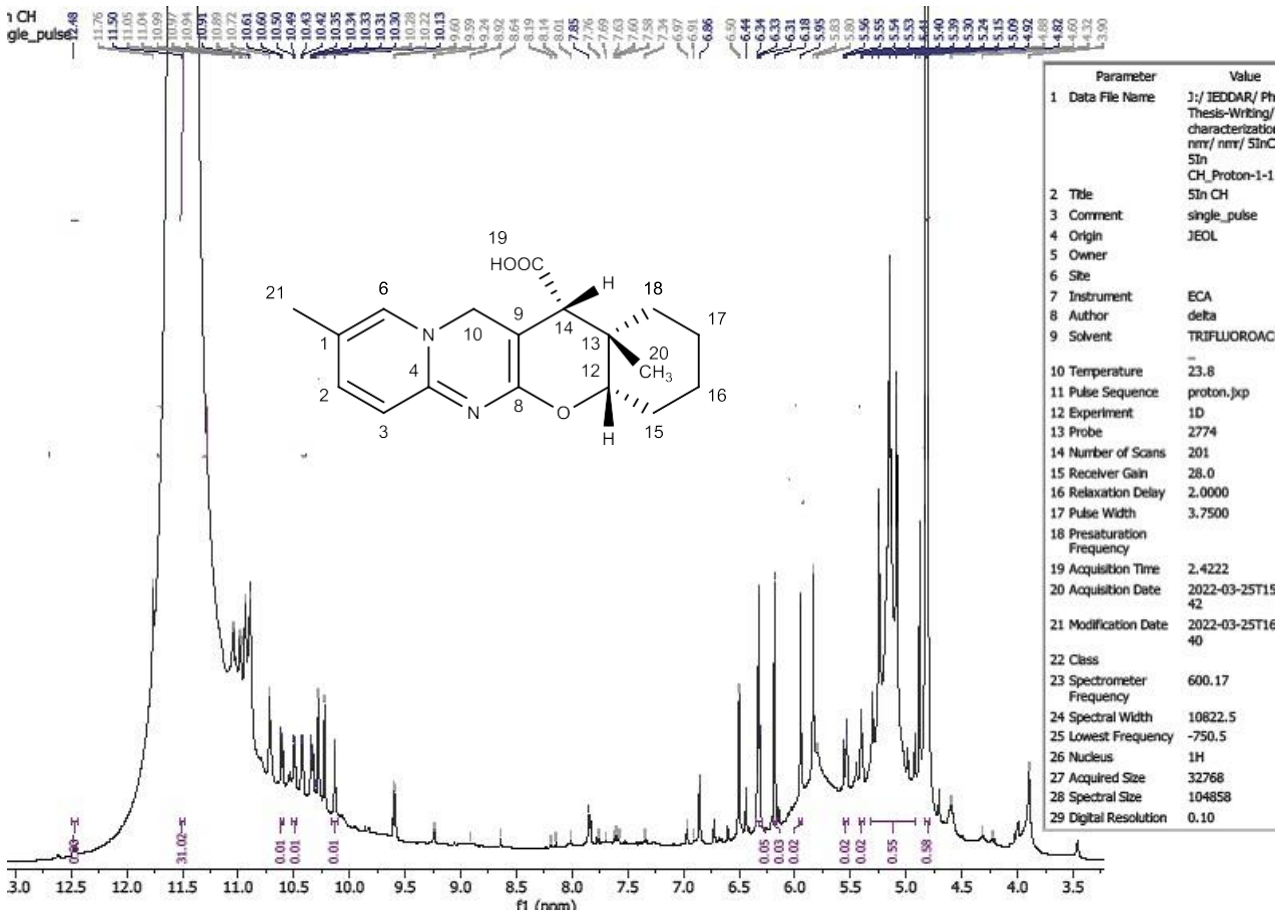

FIGURE 41 : ^{1}HNMR Spectrum of 9,13*a*-Dimethyl-1,2,3,4,4*a*,12,13,13*a*-Octahydrochromeno[2,3-*d*]Pyrido[1,2-*a*]Pyrimidine-13-Carboxylic Acid (9c)

TABLE 22: ^{13}C NMR Assignments of Compounds 9b & 9c

(9b)	**(9c)**
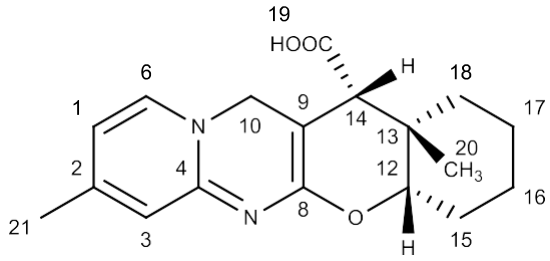	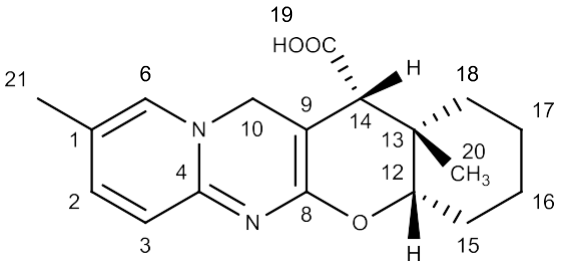

C^{13} shift in ppm (9b)	**Carbon (9b)**	**C^{13} shift in ppm (9b)**	**Carbon (9b)**	**C^{13} shift in ppm (9c)**	**Carbon (9c)**	**C^{13} shift in ppm (9c)**	**Carbon (9c)**
144	C^{1}	36	C^{13}	134	C^{1}	35	C^{13}
150	C^{2}	38	C^{14}	130	C^{2}	37	C^{14}
131	C^{3}	30	C^{15}	147	C^{3}	30	C^{15}
179	C^{4}	24.3	C^{16}	155	C^{4}	19	C^{16}
152	C^{6}	24	C^{17}	150	C^{6}	18	C^{17}
161	C^{8}	33	C^{18}	152	C^{8}	33	C^{18}
120	C^{9}	183	C^{19}	124	C^{9}	183	C^{19}
37	C^{10}	21	C^{20}	36	C^{10}	21	C^{20}
124	C^{12}	23	C^{21}	127	C^{12}	17	C^{21}

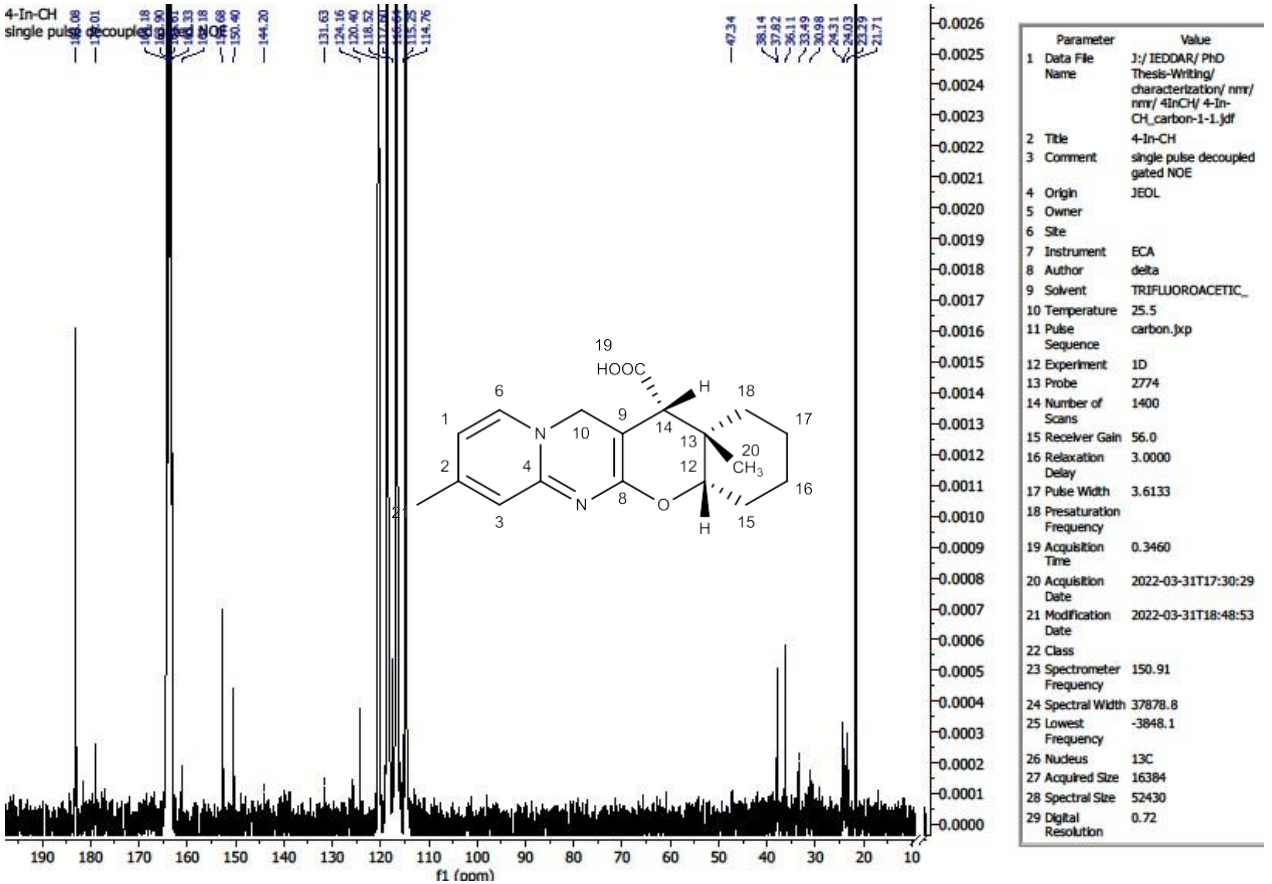

FIGURE 42 : ^{13}C Spectrum of 8,13*a*-Dimethyl-1,2,3,4,4*a*,12,13,13*a*-Octahydrochromeno[2,3-*d*]Pyrido[1,2-*a*] Pyrimidine-13-Carboxylic Acid (9b)

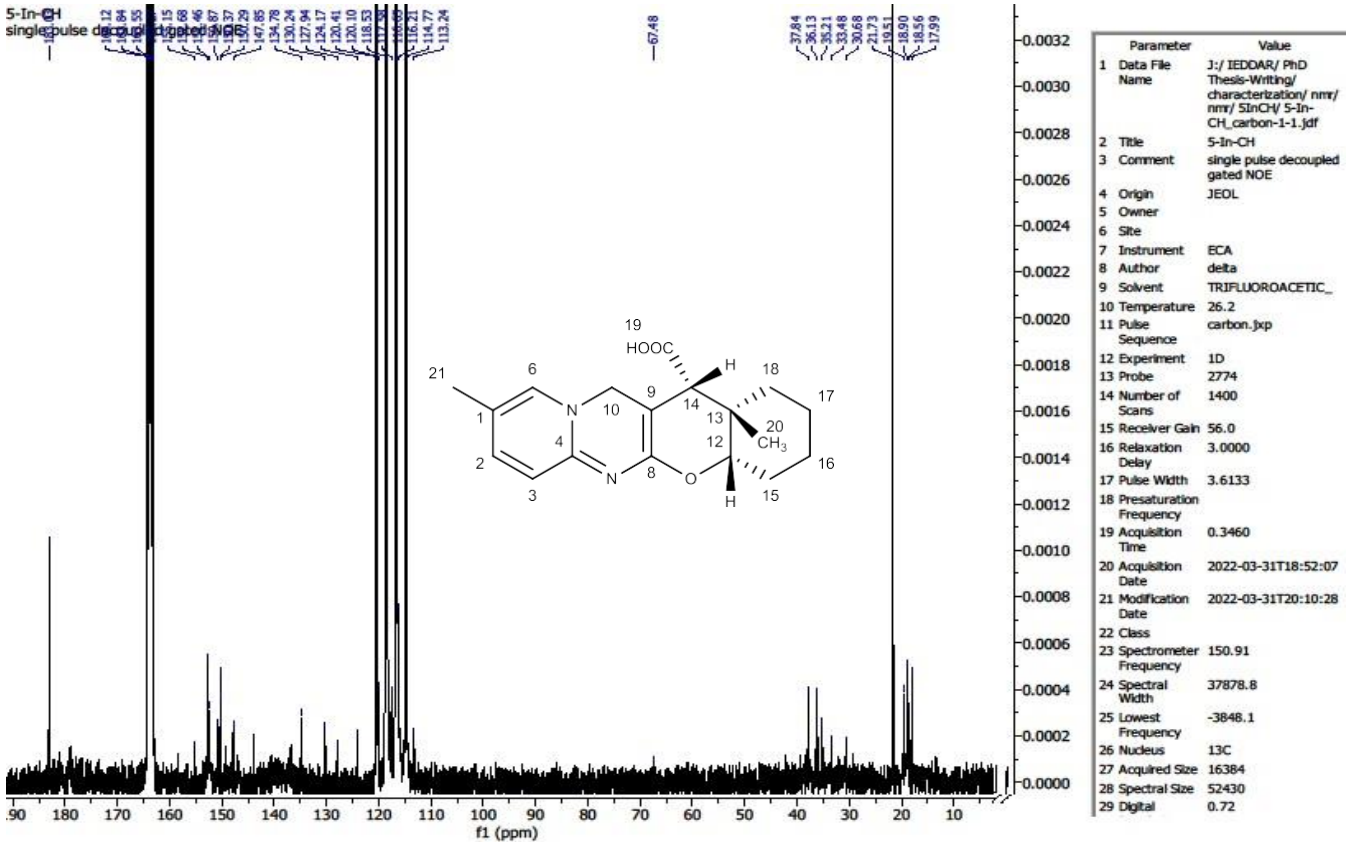

FIGURE 43 : ^{13}C Spectrum of 9,13*a*-Dimethyl-1,2,3,4,4*a*,12,13,13*a*-Octahydrochromeno[2,3-*d*]Pyrido[1,2-*a*] Pyrimidine-13-Carboxylic Acid (9c)

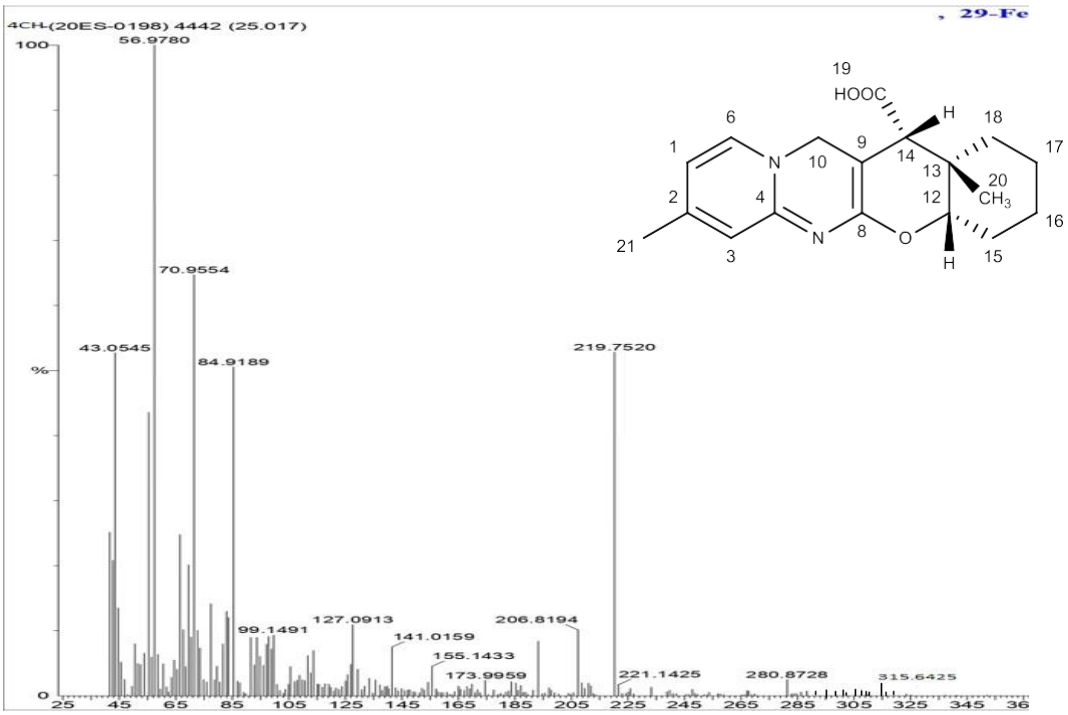

FIGURE 44 : Mass Spectrum 8,13*a*-Dimethyl-1,2,3,4,4*a*,12,13,13*a*-Octahydrochromeno[2,3-*d*]Pyrido[1,2-*a*]Pyrimidine-13-Carboxylic Acid (9b)

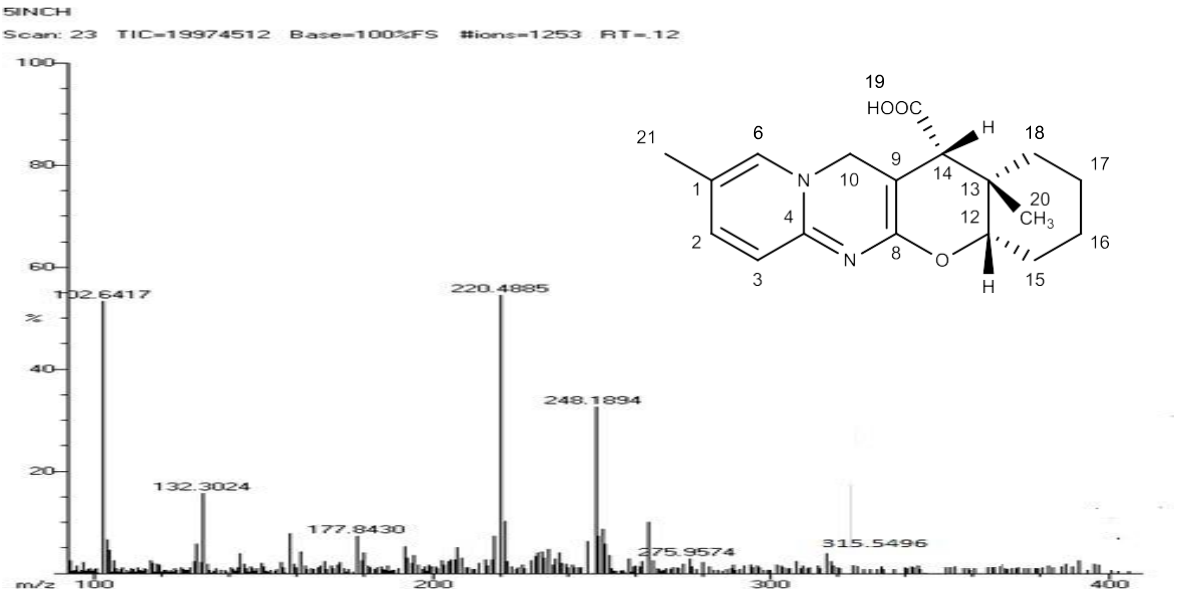

FIGURE 45 : Mass Spectrum of 9,13*a*-Dimethyl-1,2,3,4,4*a*,12,13,13*a*-Octahydrochromeno[2,3-*d*]Pyrido[1,2-*a*] Pyrimidine-13-Carboxylic Acid (9c)

4.5 SYNTHESIS OF 3,4,4*a*,12,13,13*a*-HEXAHYDRO-2*H*-PYRANO[2',3':5,6]PYRANO [2,3-*d*]PYRIDO[1,2-*a*]PYRIMIDINE-13-CARBOXYLIC ACID DERIVATIVES

The reaction between 2-oxo-2*H*-pyrido [1, 2-*a*] pyrimidin-3(4*H*)-ylidiene acetic acid **(3)** and dienophile 3,4-Dihydro-2*H*-pyran **(10)** in presence of indium (III) chloride catalyst and DMF solvent at 90^{o}C afforded brown precipitate. The reaction mixture showed 4 ½ hof time period for the completion of the reaction. Formation of the adduct **11a** was confirmed by TLC, which showed no spot for the starting materials and a single major spot. The reaction provided corresponding product **9a** with good yields. The obtained precipitate was purified by recrystallisation without the separation of diastereoisomers and used for further analysis.

Similarly, 7-methyl and 8-methyl substituted 2-oxo-2*H*-pyrido [1, 2-*a*] pyrimidin-3(4*H*)-ylidiene acetic acid **(3b and 3c)** were refluxed with the selected dienophile 3,4-Dihydro-2*H*-pyran **(10)**. The reaction mixtures after refluxing yielded adduct products **11b** and **11c** respectively. The reaction between 2-oxo-2*H*-pyrido [1, 2-*a*] pyrimidin-3(4*H*)-ylidiene acetic acid **(3)** & its methyl derivatives and dienophile is represented in the **Scheme 15**. Melting point and yields of the adducts compounds **11a, 11b** and **11c** are presented in **Table 23.**

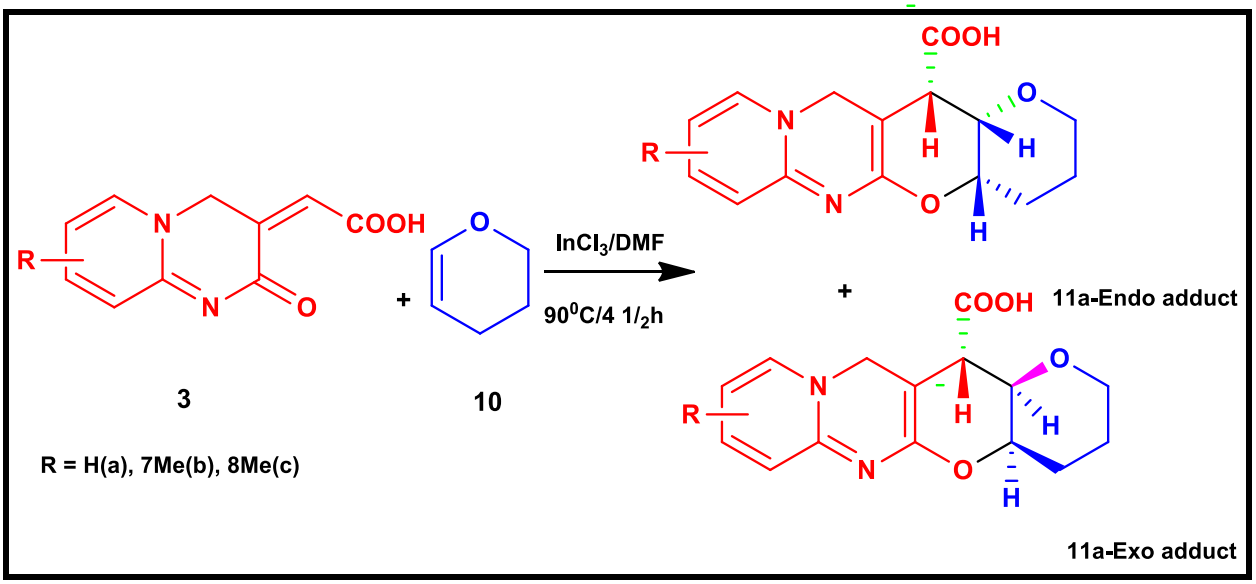

Scheme 15: Synthesis of 3,4,4*a*,12,13,13*a*-Hexahydro-2H-Pyrano[2',3':5,6]Pyrano[2,3-*d*] Pyrido[1,2-*a*]Pyrimidine-13-Carboxylic Acid Derivatives

TABLE 23: Melting Point and Yield of 3,4,4*a*,12,13,13*a*-Hexahydro-2*H*-Pyrano[2',3':5,6]Pyrano[2,3-*d*]Pyrido[1,2-*a*] Pyrimidine-13-Carboxylic Acid Derivatives

Diene	Dienophile	Temp./Time	Product	Yield/M.P
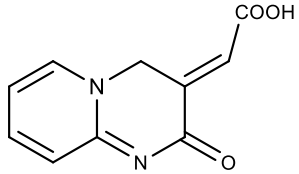	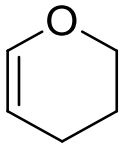	90˚C/4½	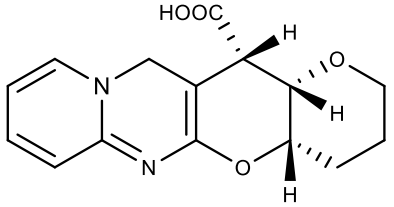	62% /260-270˚C
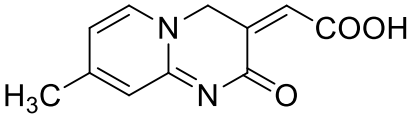		90˚C/6	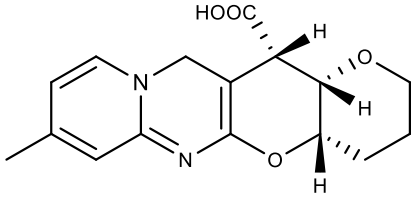	61% /290-300˚C
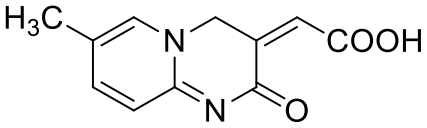		90˚C/6½	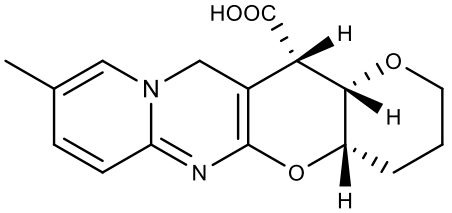	65%/ 288-296˚C

4.5.1 SPECTRAL CHARACTERIZATION OF SYNTHESIZED CYCLO ADDUCT COMPOUND (11c)

4.5.1.1 FT-IR SPECTRUM

The IR spectrum of cycloadduct **11c** showed the expected absorption bands of C=N at 1573 cm^{-1}corresponding to the pyrido pyrimidine nucleus. A broad intense O-H stretching band centered at 3370 cm^{-1} was also observed which is overriding spectral feature of the carboxylic acid. This was also confirmed by the presence of strong intense O-H in plane bend at 1378 cm^{-1} along with medium intense O-H out of plane bend at 828 cm^{-1}.

The strong and medium intense bands at 1691 cm^{-1} and 1295 cm^{-1} were attributed to the -C=O and -C-O stretch of the carboxylic acid moiety respectively. The absence of strong absorption band at 1680-1700 cm^{-1} confirmed the formation of the product. **(Figure 46)**

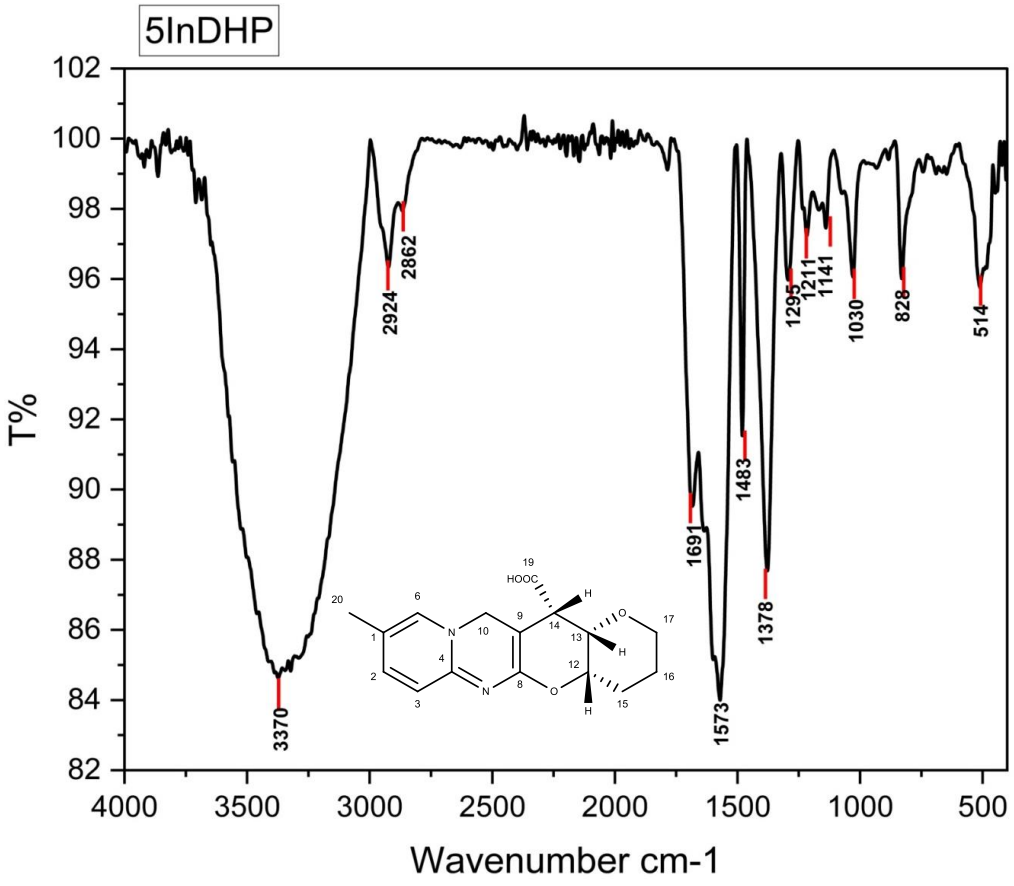

FIGURE 46 : FTIR Spectrum of Methyl-1,2,3,4,4*a*,12,13,13*a*-Octahydrochromeno[2,3-*d*]Pyrido[1,2-*a*]Pyrimidine-13-Carboxylic Acid (11c)

4.5.1.2 ^{1}H NMR SPECTRUM

The proton NMR **(Figure 47)** spectrum of cycloadduct **11c** demonstrated 11 distinct signals in agreement with the proposed structure. The signal of proton C_{14}-H appeared as doublet with J=12 at δ 6.3 for *endo* isomer for *exo* isomer C_{14}-H was registered as doublet with J=12 at δ 4.9**.** Hence the formation of *endo* and *exo* isomers in the ratio **6:1** was confirmed. The reaction was found to be diastereoselective. The proton attached to C-14 gave doublet with coupling constant J=12 due to coupling with C-13 carbon. The proton attached to C-13 was registered as a triplet at δ 6.4 with coupling constant J=12, 18 due to coupling with proton attached to C-14 and C-12 carbons respectively. The proton attached to C_{-12}–H resonated at δ 5.5 as quartet with coupling constant J=12, 6, 18 due to coupling with C_{-13}–H and C_{-15}-H carbons respectively. The COOH proton resonated at δ 12.46. The peaks resonating at δ 10.4-10.2 were assigned for aromatic ring protons. The more downfield shift may be due to the recording of NMR in trifluoroacetic acid **Hirday n. Jha et al., 1982**. In the DA reaction between 1-oxo-1,3-butadiene and 3,4-Dihydro-2*H*-pyran. **Aleksandra palasz *et al.*, 2013** reported the formation of diastereoisomers in the ratio of 1:1.

TABLE 24 : ^{1}H NMR Assignments of 9-methyl-3,4,4*a*,12,13,13*a*-hexahydro-2*H*-pyrano[2',3':5,6]pyrano[2,3-d]pyrido[1,2-*a*]pyrimidine-13-carboxylic acid (11c)

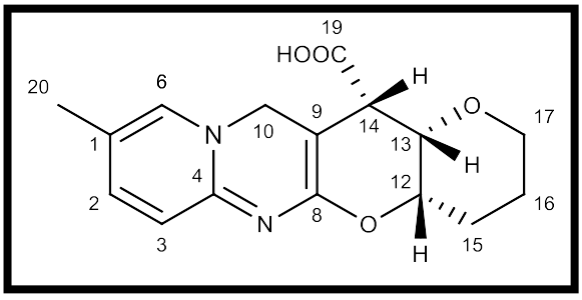

^{1}H Shift in ppm	No. of ^{1}H/ Multiplicity	J value (Hz)	^{1}H Shift in ppm	No. of ^{1}H/ Multiplicity	J value (Hz)
10.4	H^{2}/d	12.0	6.3/4.9	H^{14}/d	12.0
10.32	H^{3}/d	12.0	5.4	H^{15}/dd	6.0/6.0/6.0
10.27	H^{6}/s	-	5.2-4.9	H^{16}, H^{17}/m	-
5.8	H^{10}/s	-	12.46	H^{19}/s	
5.5	H^{12}/q	6.0/12.0/18.0	4.8	H^{20}/s	
6.4	H^{13}/t	12.0/18.0			

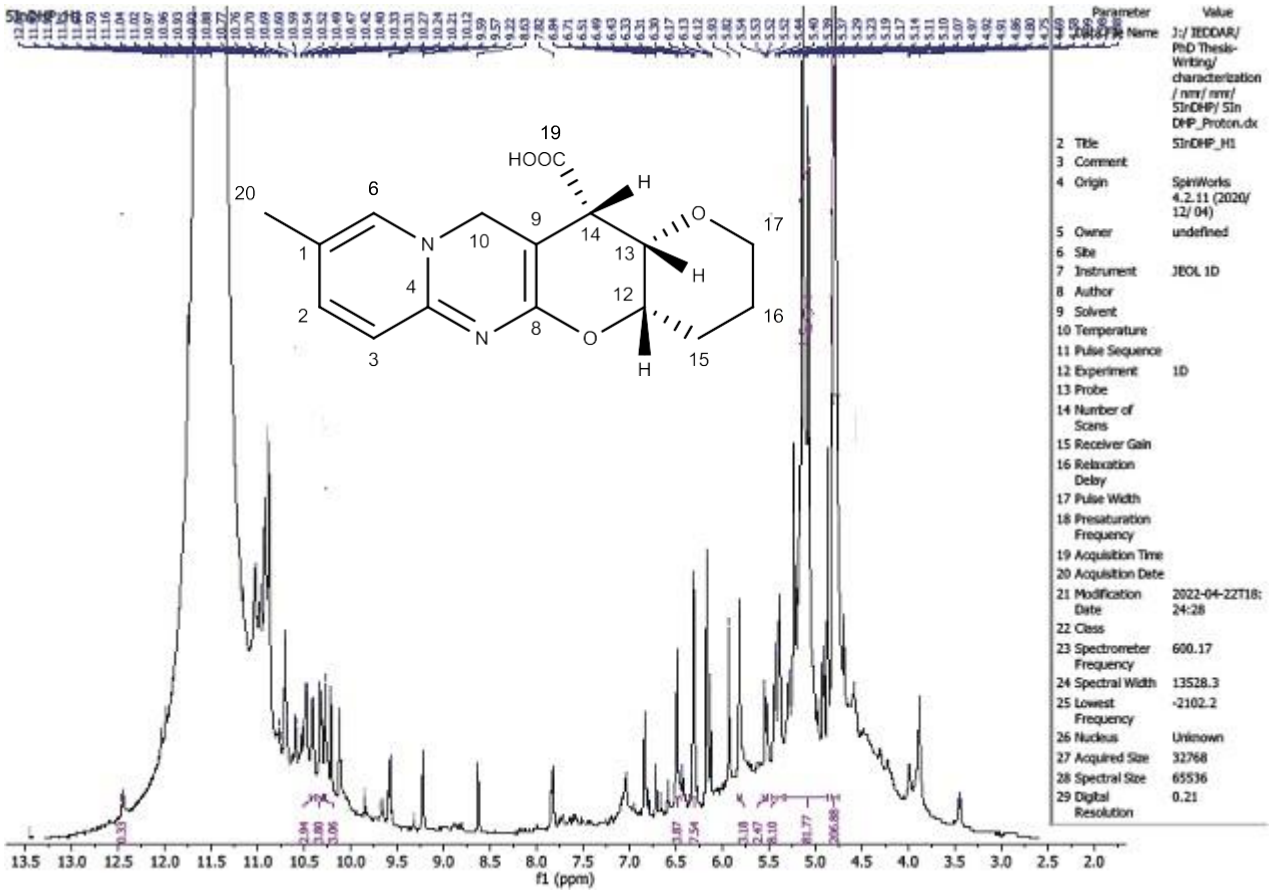

FIGURE 47 : ^{1}HNMR Spectrum of 13*a*-Methyl-1,2,3,4,4*a*,12,13,13*a*-Octahydrochromeno[2,3-*d*]Pyrido[1,2-*a*] Pyrimidine-13-Carboxylic Acid (11c)

^{1}HNMR Spectrum of 13*a*-Methyl-1,2,3,4,4*a*,12,13,13*a*-Octahydrochromeno[2,3-*d*]Pyrido[1,2-*a*]Pyrimidine-13-Carboxylic Acid (11c)

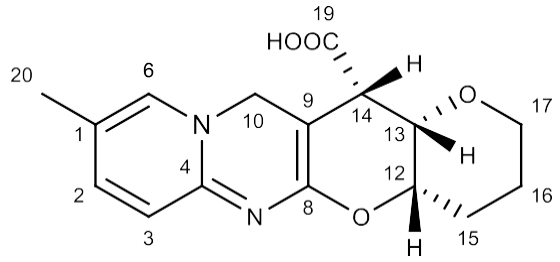

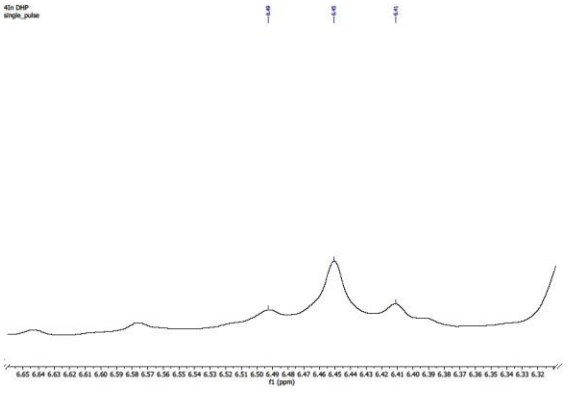

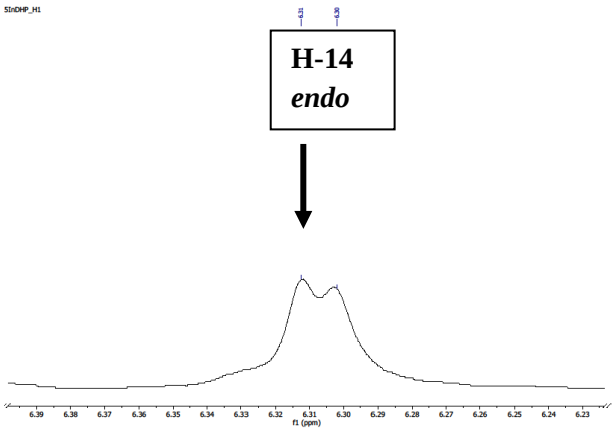

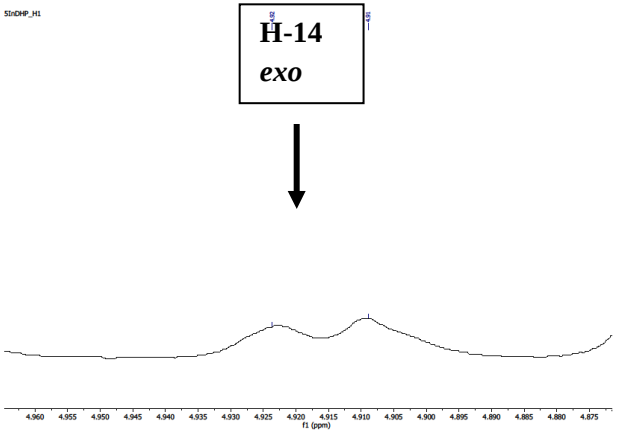

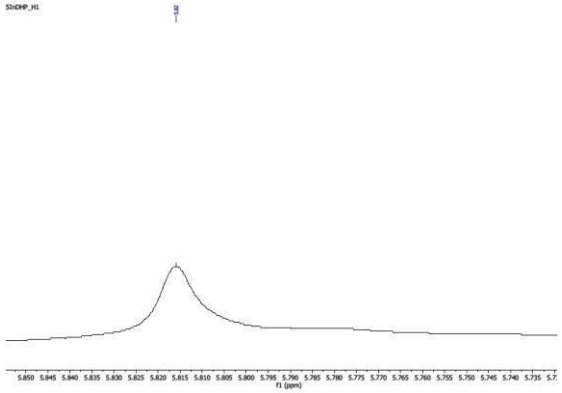

4.5.1.3 C^{13} NMR SPECTRUM

The C^{13} NMR spectrum for adduct **11c** displayed 16 distinct carbons corresponding to the 16 chemically non-equivalent carbons found in the compound. The chemical shifts at δ 18.8 were due to the methyl groups attached to pyridopyrimidine ring. The peaks resonating at δ 181, 162, 161, 152.4, 152, 150, 134 and 36 were assigned for pyridopyrimidine ring carbons. Three peaks downfield at δ 58, 70, and 78 were expected to belong to C-17, C-12, and C-13, most likely because of the existence of oxygen within the ring. The registered signals at δ 21 and 22 corresponded to the C-15 and C-16 in the pyran ring. The carboxylic acid group was depicted by the peak at δ 183. **(Figure 48)**

TABLE 25: C^{13} NMR Assignments of 13*a*-Methyl-1,2,3,4,4*a*,12,13,13*a*-Octahydrochromeno[2,3-*d*] Pyrido[1,2-*a*]Pyrimidine-13-Carboxylic Acid (11c)

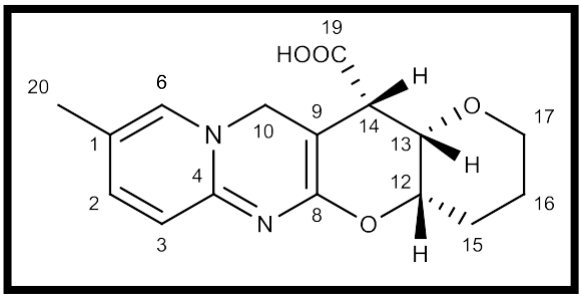

C^{13} shift in ppm	Carbon	C^{13} shift in ppm	Carbon
152.4	C^{1}	70	C^{12}
152	C^{2}	78	C^{13}
150	C^{3}	25	C^{14}
181	C^{4}	21	C^{15}
161	C^{6}	22	C^{16}
162	C^{8}	58	C^{17}
134	C^{9}	183	C^{19}
36	C^{10}	18.8	C^{20}

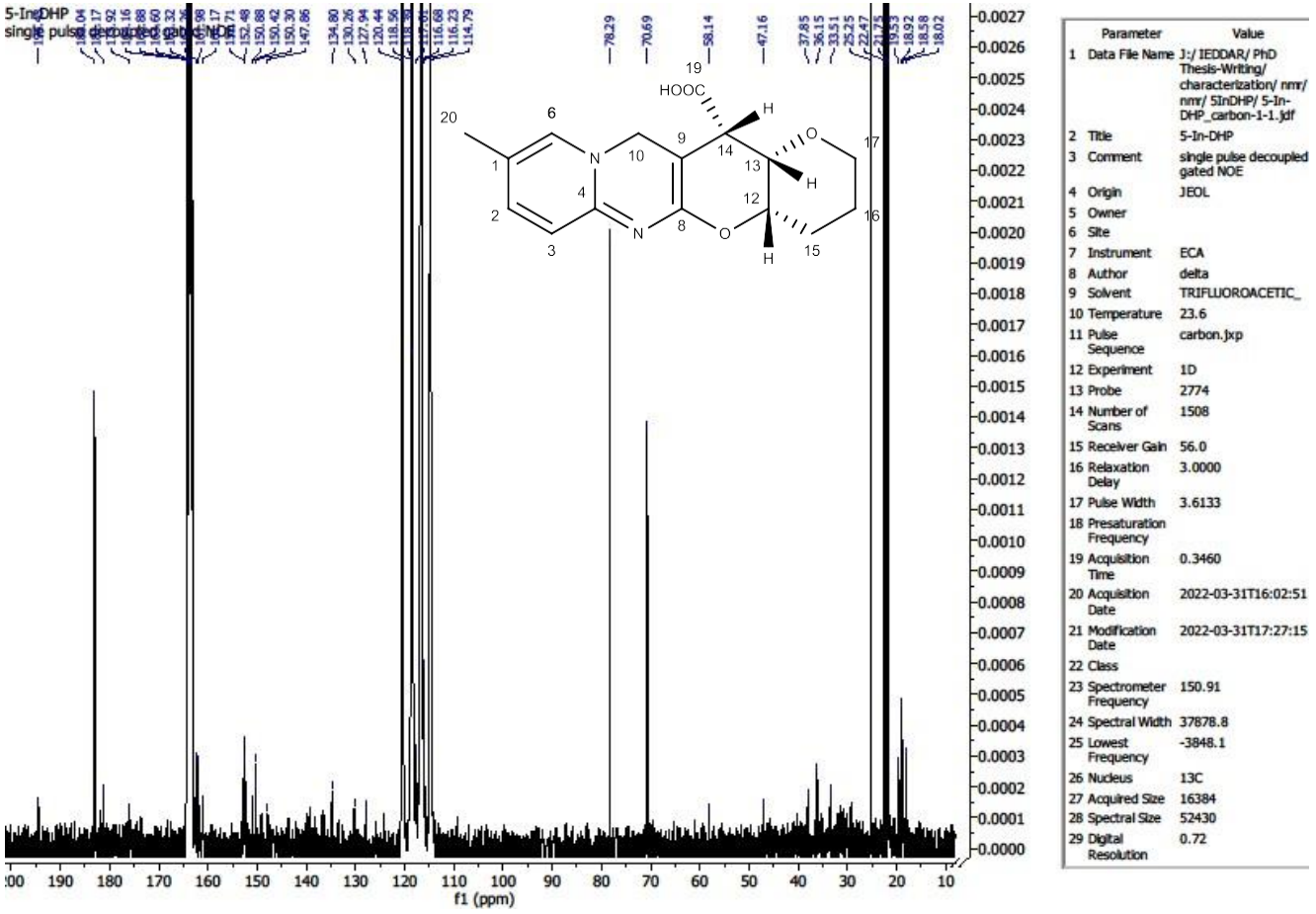

FIGURE 48 : ^{13}C Spectrum 13*a*-Methyl-1,2,3,4,4*a*,12,13,13*a*-Octahydrochromeno[2,3-*d*]Pyrido[1,2-*a*]Pyrimidine-13-Carboxylic Acid (11c)

4.5.1.4 MASS SPECTRUM

Further evidence for the structure was obtained from the mass spectrum which showed M+1peak at m/z 303.84 **Figure-49**. Hence the assigned structure of the cycloadduct **(11c)** was confirmed.

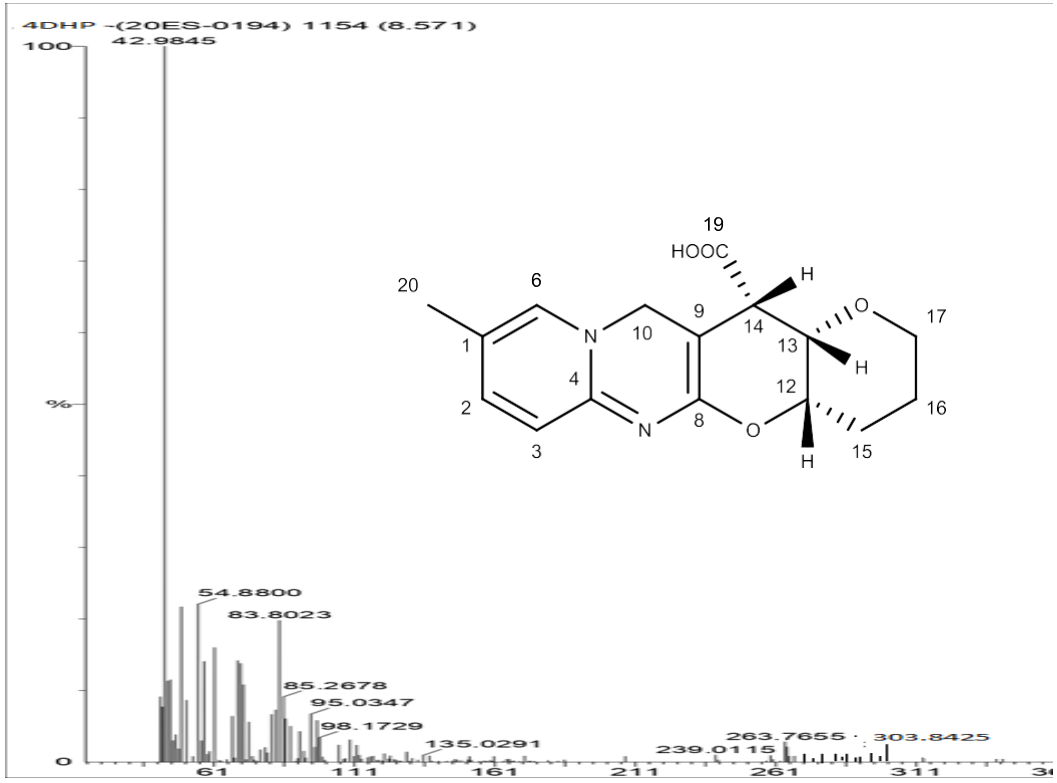

FIGURE 49 : Mass Spectrum of 13*a*-Methyl-1,2,3,4,4*a*,12,13,13*a*-Octahydro chromeno[2,3-*d*]Pyrido[1,2-*a*]Pyrimidine-13-Carboxylic Acid (11c)

4.5.2 SPECTRAL CHARACTERIZATION OF SYNTHESIZED CYCLOADDUCTS (11a&11b).

FT-IR, ^{1}H NMR, C^{13} NMR and Mass spectrum of the adducts **11a** and **11b** given in **Figures – 50, 51 , 53, 54, 55, 56, 57** and the assignments are tabulated in **Tables- 26, 27, 28.**

TABLE 26 : FTIR Assignments of Cyclic Adducts 11a & 11b

Functional group	Types of vibration	Wave number $^{19}cm^{-1}$	Intensity
11a	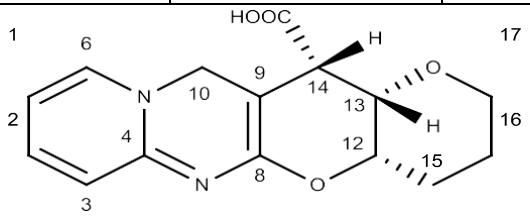		
C=O	Stretch	1699	Strong
C=N	Bending	1581	Medium
O-H	Stretch	3426	Very broad
O-H	Stretch	1378	Strong
O-H	Stretch	1044	Medium
C-O	Stretch	1295	Strong
11b	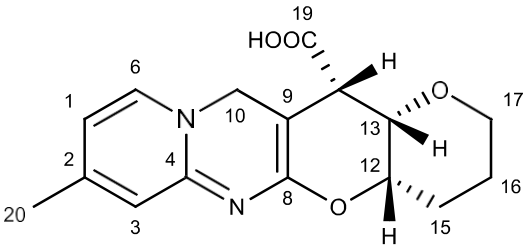		
C=O	Stretch	1610	Strong
C=N	Bending	1565	Medium
O-H	Stretch	3423	Very broad
O-H	Stretch	1390	Strong
O-H	Stretch	1041	Medium
C-O	Stretch	1270	Strong

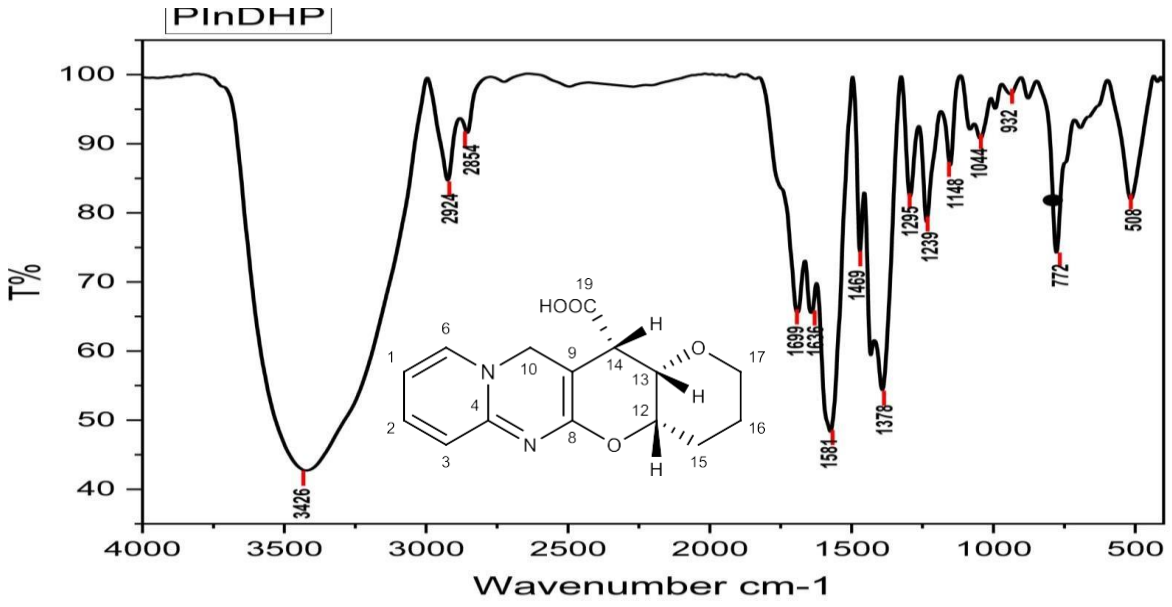

FIGURE 50 : FTIR Spectrum of 3,4,4*a*,12,13,13*a*-Hexahydro-2*H*-Pyrano[2',3':5,6]Pyrano[2,3-*d*]Pyrido[1,2-*a*]Pyrimidine-13-Carboxylic Acid (11a)

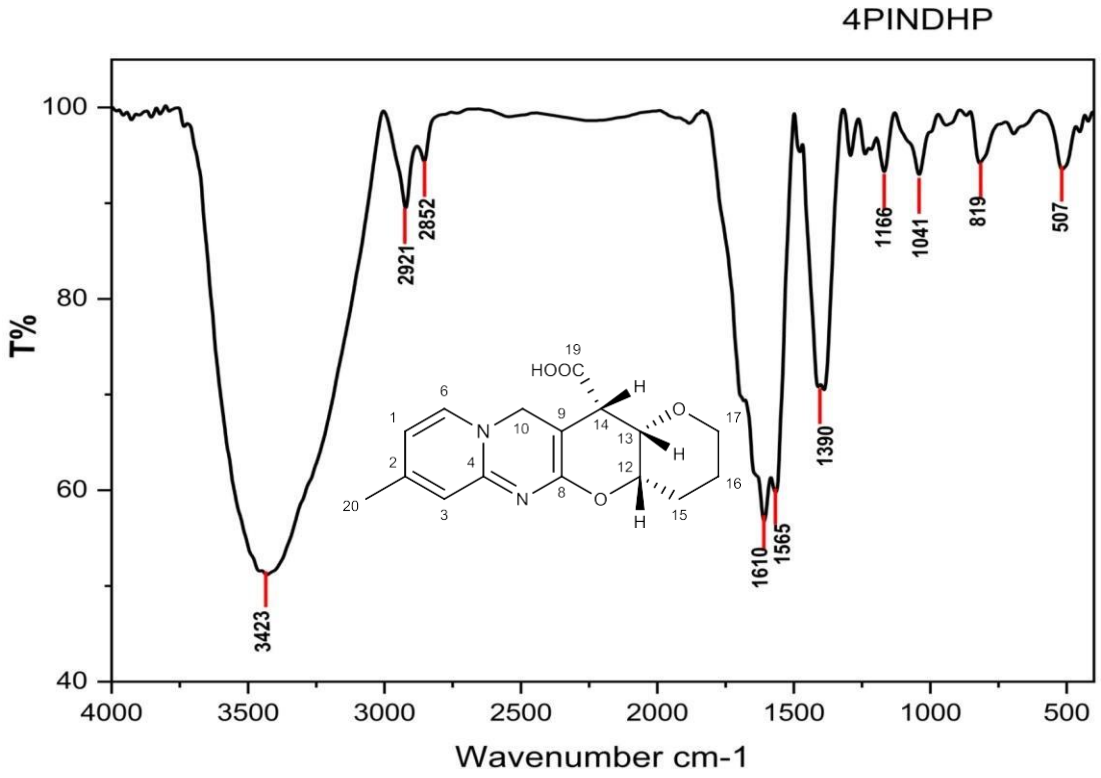

FIGURE 51 : FTIR Spectrum of 8-Methyl-3,4,4*a*,12,13,13*a*-Hexahydro-2*H*-Pyrano[2',3':5,6]Pyrano[2,3-*d*]Pyrido[1,2-*a*]Pyrimidine-13-Carboxylic Acid (11b)

4.5.2.2 ^{1}H NMR SPECTRUM

TABLE 27 : ^{1}H NMR Assignments of Compounds 11a & 11b

11a 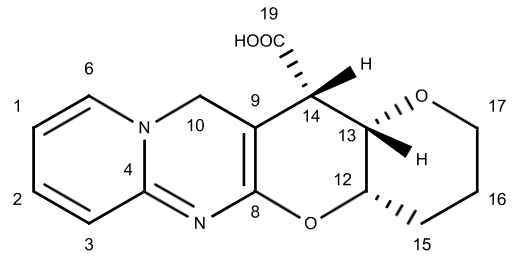			**11b** 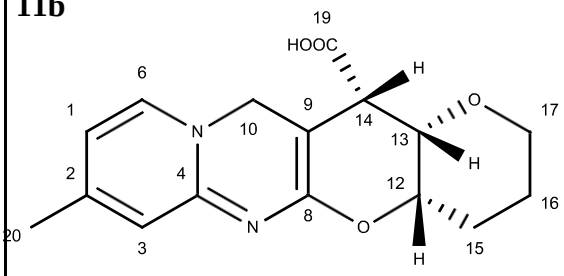		
^{1}H Shift in ppm	**No. of ^{1}H/ Multiplicity**	**J value (Hz)**	**^{1}H Shift in ppm**	**No. of ^{1}H/ Multiplicity**	**J value (Hz)**
10.1	H^{1} /t	6.0/6.0	10.2	H^{1} /d	12.0
10.3	H^{2} /t	6.0/6.0	9.4	H^{6} /d	12.0
10	H^{3} /d	6.0	9.21	H^{3} /s	-
9.8	H^{6} /d	6.0	5.8	H^{10} /s	-
5.1	H^{10} /s	-	5.39	H^{12} /dd	12.0/12.0/6.0
6.1	H^{12} /m		6.4	H^{13} /t	12.0/12.0
5.8/5.5	H^{14} /d	6.0	6.1/4.9	H^{14} /d	12.0
5.9	H^{13} /t	6.0/6.0	5.3	H^{15} , H^{16} , H^{17} /m	
5.4	H^{15} ,H^{16} , H^{17} /m		12.46	H^{19} /s	
12.4	H^{19} /s		4.79	H^{20} /s	

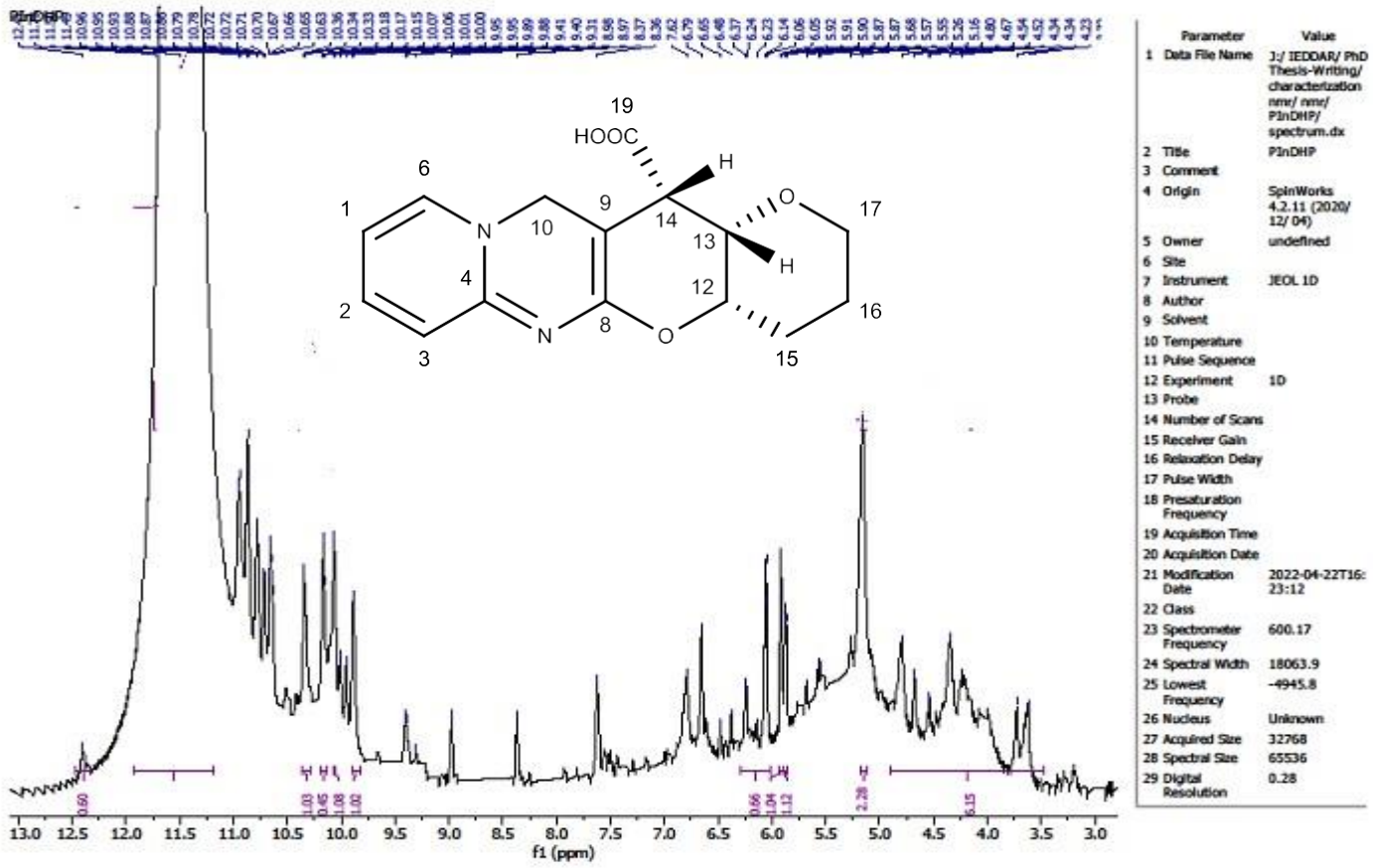

FIGURE 52 : ^{1}HNMR Spectrum of 3,4,4*a*,12,13,13*a*-Hexahydro-2*H*-Pyrano[2',3':5,6]Pyrano[2,3-*d*]Pyrido[1,2-*a*] Pyrimidine-13-Carboxylic Acid (11a)

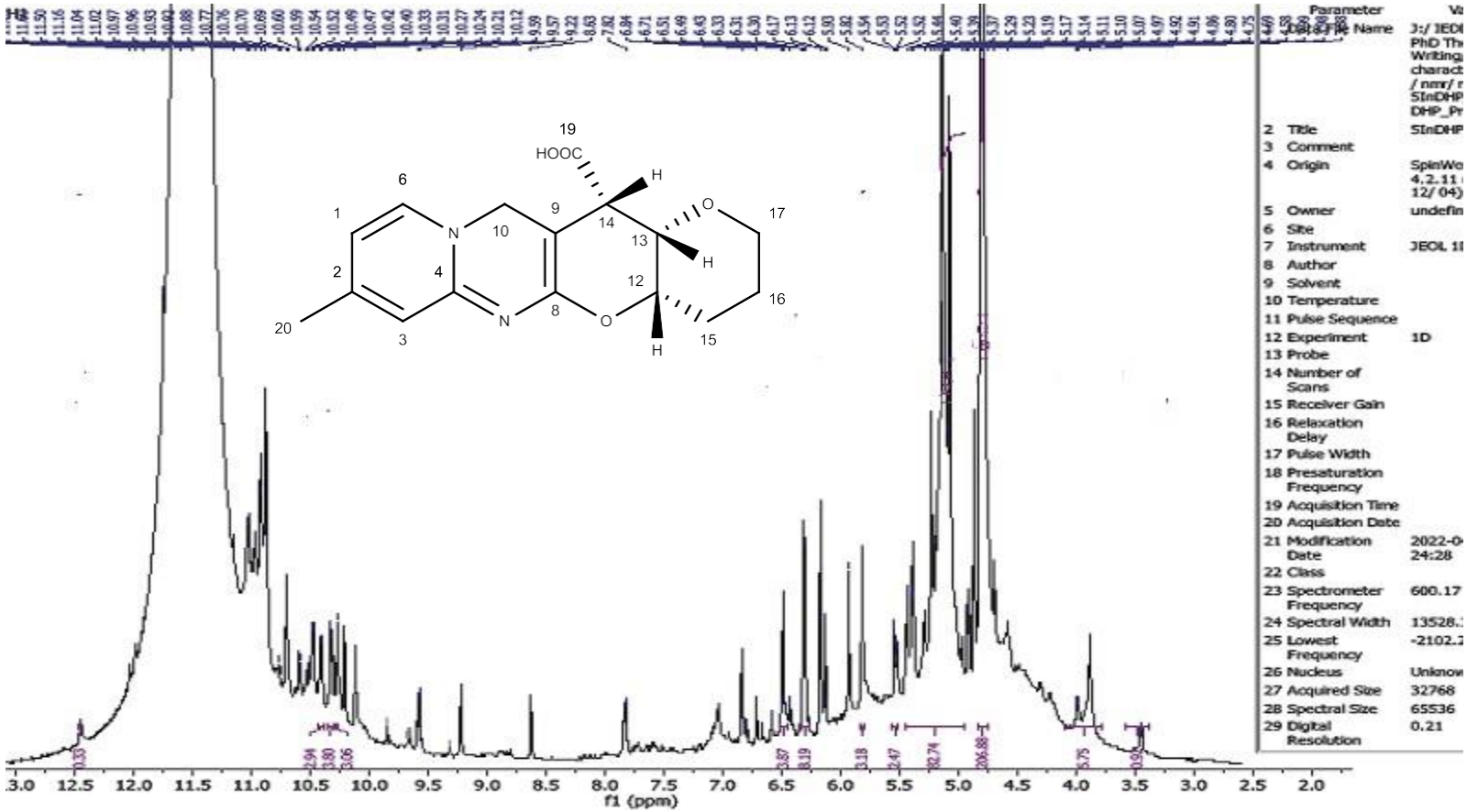

FIGURE 53 : ^{1}HNMR Spectrum of 8-Methyl-3,4,4*a*,12,13,13*a*-Hexahydro-2*H*-Pyrano[2',3':5,6]Pyrano[2,3-*d*] Pyrido[1,2-*a*]Pyrimidine-13-Carboxylic Acid (11b)

TABLE 28: ^{13}C NMR Assignments of Compounds 11a & 11b

(11a)				**(11b)**			
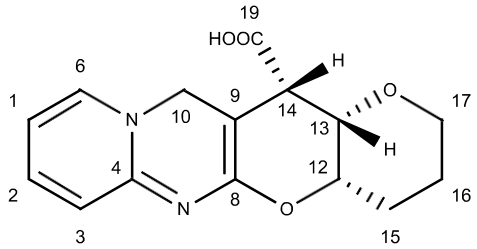				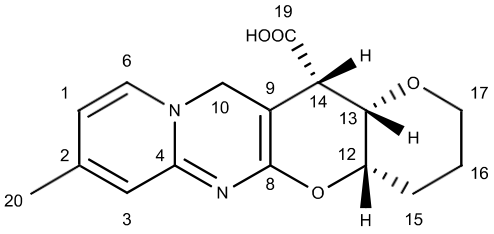			
C^{13} shift in ppm (11a)	**Carbon(11a)**	**C^{13} shift in ppm (11a)**	**Carbon(11a)**	**C^{13} shift in ppm (11b)**	**Carbon (11b)**	**C^{13} shift in ppm (11b)**	**Carbon (11b)**
120.7	C^{1}	104	C^{12}	130	C^{1}	39	C^{12}
138	C^{2}	63.4	C^{13}	150	C^{2}	45	C^{13}
129.4	C^{3}	44.7	C^{14}	136	C^{3}	33	C^{14}
167.7	C^{4}	28.2	C^{15}	173	C^{4}	23	C^{15}
138.1	C^{6}	25.2	C^{16}	152	C^{6}	24	C^{16}
157.6	C^{8}	63.4	C^{17}	162	C^{8}	37	C^{17}
112.4	C^{9}	176	C^{19}	94	C^{9}	183	C^{19}
35.3	C^{10}			36	C^{10}	21	C^{20}

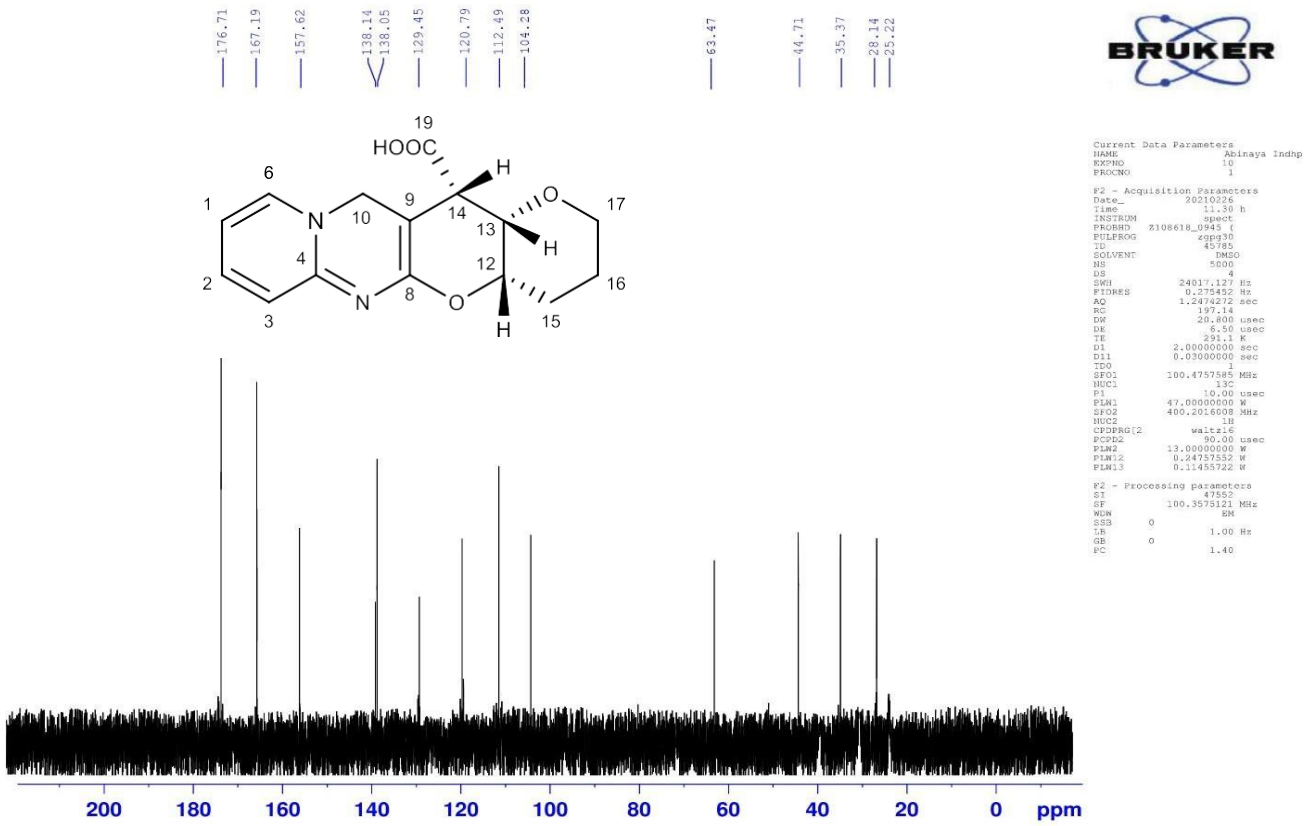

FIGURE 54 : ^{13}C NMR Spectrum of 3,4,4*a*,12,13,13*a*-Hexahydro-2*H*-Pyrano[2',3':5,6]Pyrano[2,3-*d*]Pyrido[1,2-*a*] Pyrimidine-13-Carboxylic Acid (11a)

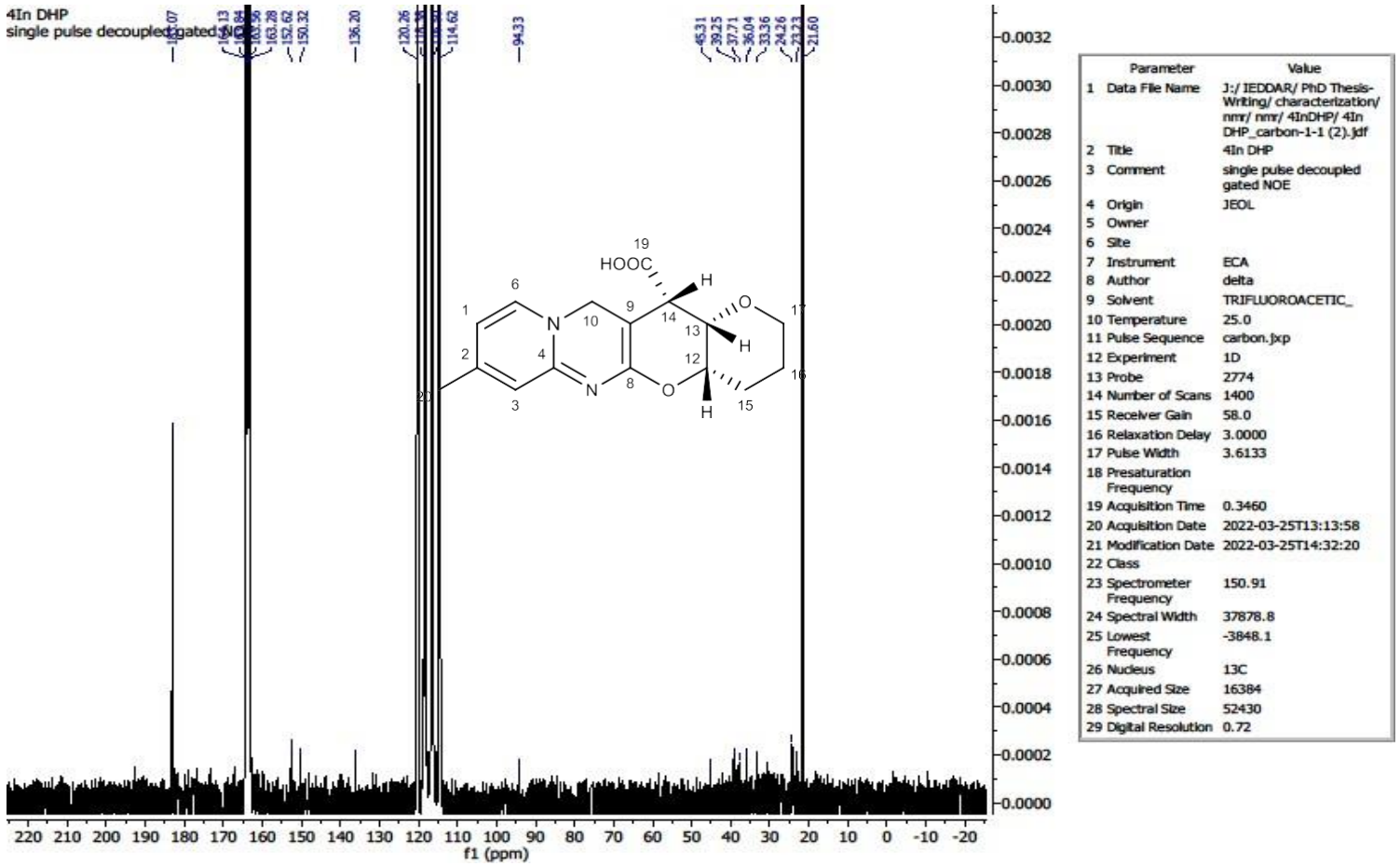

FIGURE 55 : ^{13}C Spectrum 8-Methyl-3,4,4*a*,12,13,13*a*-Hexahydro-2*H*-Pyrano[2',3':5,6]Pyrano[2,3-*d*]Pyrido[1,2-*a*] Pyrimidine-13-Carboxylic Acid (11b)

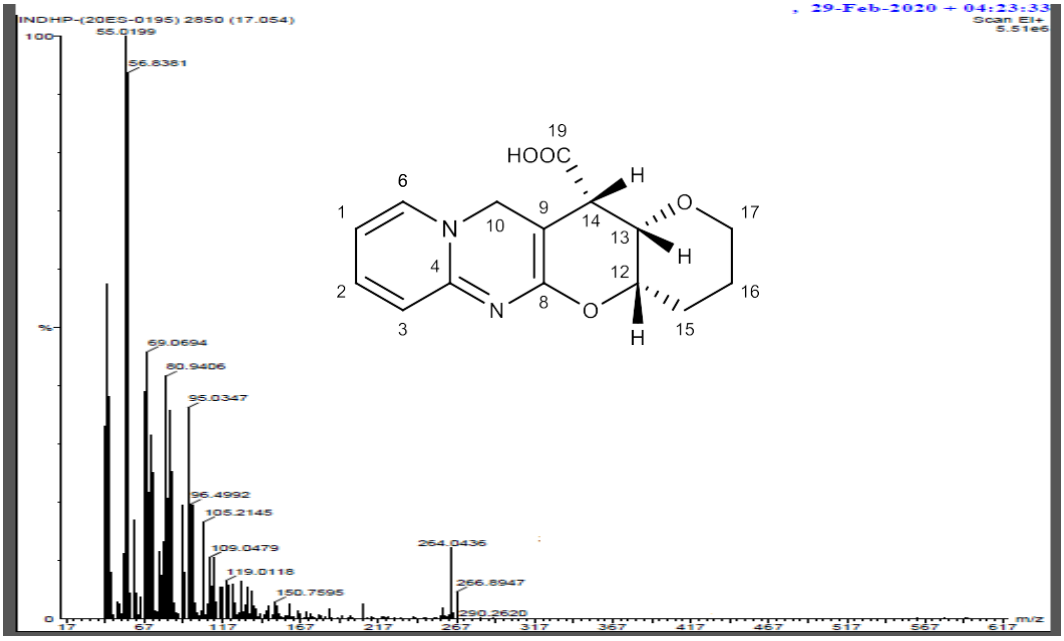

FIGURE 56 : Mass Spectrum of 3,4,4*a*,12,13,13*a*-Hexahydro-2*H*-Pyrano[2',3':5,6]Pyrano[2,3-*d*]Pyrido[1,2-*a*] Pyrimidine-13-Carboxylic Acid (11a)

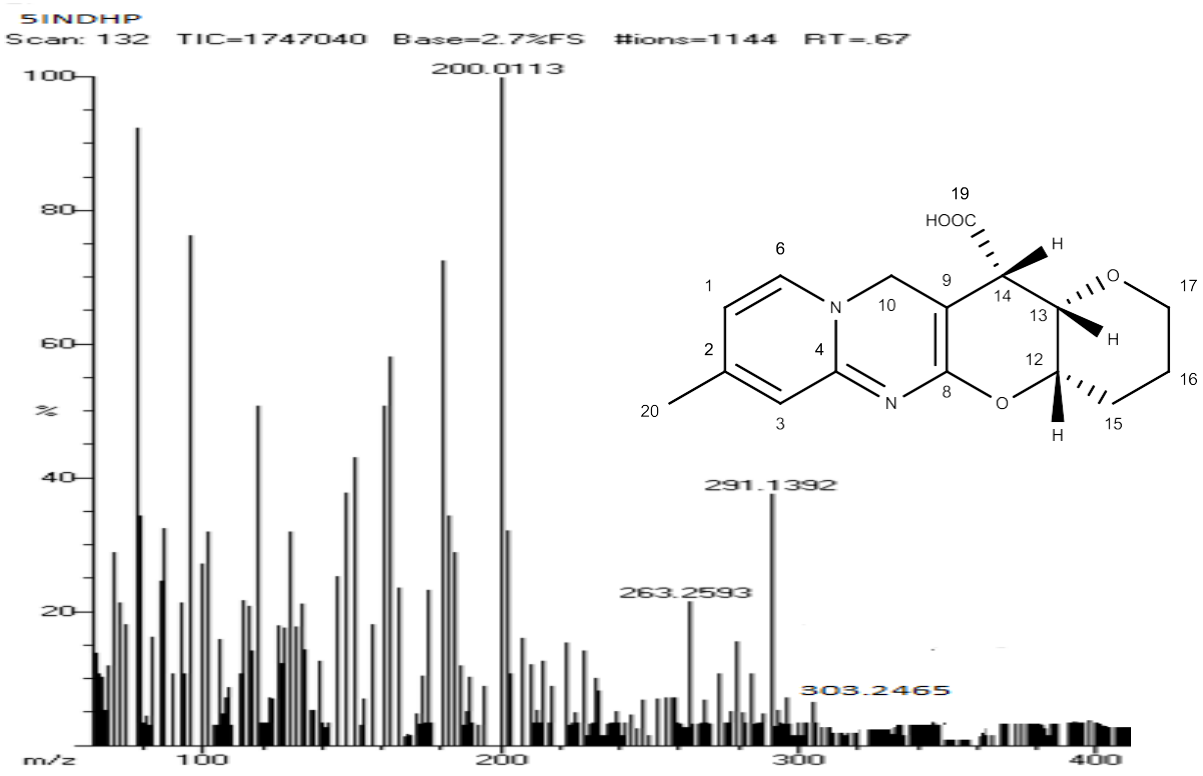

FIGURE 57 : Mass Spectrum of 8-Methyl-3,4,4*a*,12,13,13*a*-Hexahydro-2*H*-Pyrano[2',3':5,6]Pyrano[2,3-*d*] Pyrido[1,2-*a*]Pyrimidine-13-Carboxylic Acid (11b)

4.6 SYNTHESIS OF 9,13,13*a*-TRIMETHYL-4*a*-MORPHOLINO-1,2,3,4,4*a*,12,13,13*a*-OCTAHYDROCHROMENO[2,3-*d*]PYRIDO[1,2-*a*]PYRIMIDINE-13-CARBOXYLIC ACID DERIVATIVES

The reaction between 2-oxo-2*H*-pyrido [1, 2-*a*] pyrimidin-3(4*H*)-ylidiene acetic acid **(3)** and its 7-methyl **(3b)** and 8-methyl **(3c)** substituents with dienophile 1-morpholinocyclohexene **(12)** in presence of indium (III) chloride catalyst and DMF as solvent was carried out at 90^{o}C. The reaction gave the desired cycloadducts after 9 h of refluxing. **Scheme 16**. As the reaction proceed with very poor yield for **13a** and **13b** compared to **13c**. Hence further characterisation was done only for the cycloadduct **13c**. Because of less yields of the cycloadducts C^{13} NMR spectrum could not be recorded. Melting point and yield of the compound are given in **Table 29**:

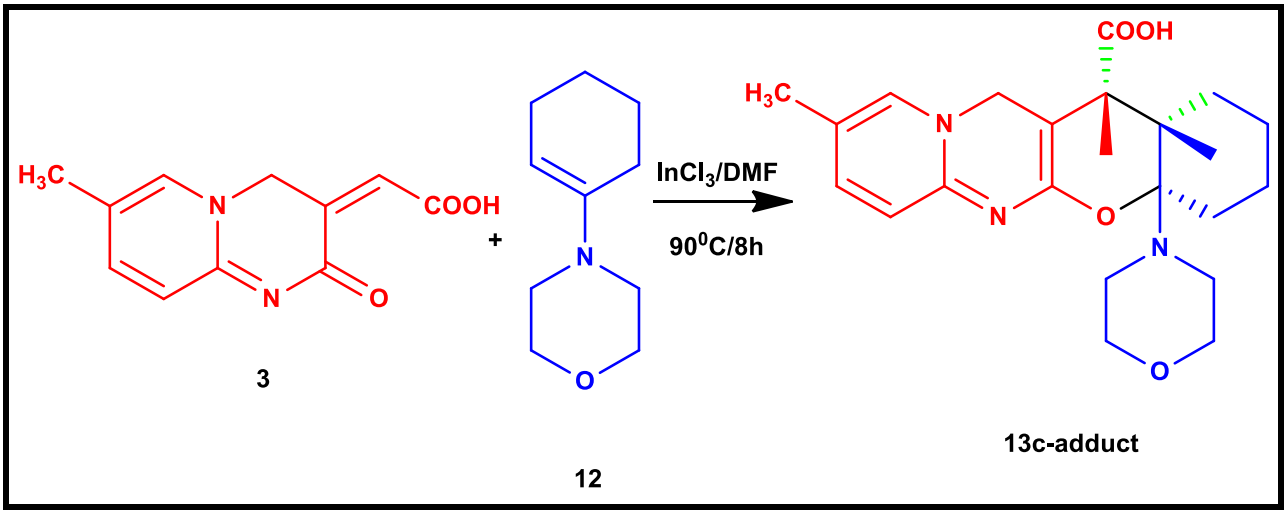

Scheme 16 : Synthesis of 9,13,13*a*-Trimethyl-4*a*-Morpholino-1,2,3,4,4*a*,12,13,13*a*-Octahydrochromeno[2,3-*d*]Pyrido[1,2-*a*]Pyrimidine-13-Carboxylic Acid

TABLE 29:Melting Point and Yield of 9,13,13*a*-Trimethyl-4*a*-morpholino- 1,2,3,4,4*a*, 12,13,13*a*-Octahydrochromeno[2,3 *d*]Pyrido[1,2-*a*]Pyrimidine-13-Carboxylic Acid (13c)

Diene	Dienophile	Temp./Time	Product	Yield/M. P
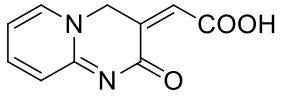	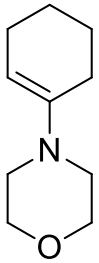	90˚C/8	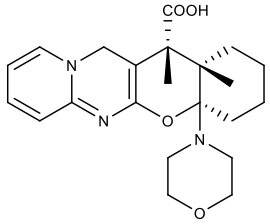	25% /340˚C above
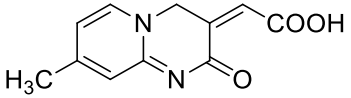		90˚C/10	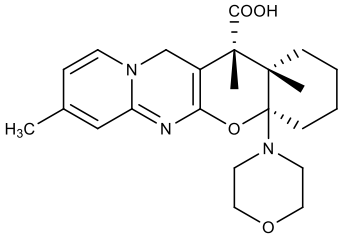	23% /340˚C above
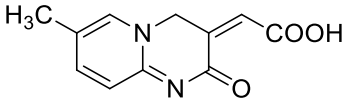		90˚C/9	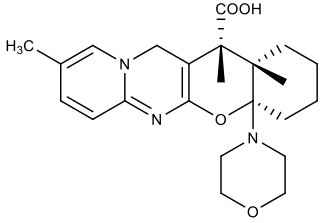	30%/ /340˚C above

4.6.1 SPECTRAL CHARACTERIZATION OF THE SYNTHESIZED CYCLO ADDUCT(13c)

4.6.1.1 FT-IR SPECTRUM

The IR spectrum of compound **13c** showed the expected absorption bands of C=N at 1586 cm^{-1}corresponding to the pyridopyrimidine nucleus. A broad intense O-H stretching band centered at 3379 cm^{-1} was overriding spectral feature of the carboxylic acid. This was also confirmed by the presence of strong intense O-H in plane bend at 1378 cm-^{1} along with medium intense O-H out of plane bend at 1053cm^{-1}.

The strong and medium intense bands at 1760 cm^{-1} and 1240 cm^{-1} were attributed to the -C=O and -C-O stretch of the carboxylic acid moiety respectively. The absence of strong absorption band at 1680-1700 cm^{-1} confirmed the formation of the product. **(Figure 58)**

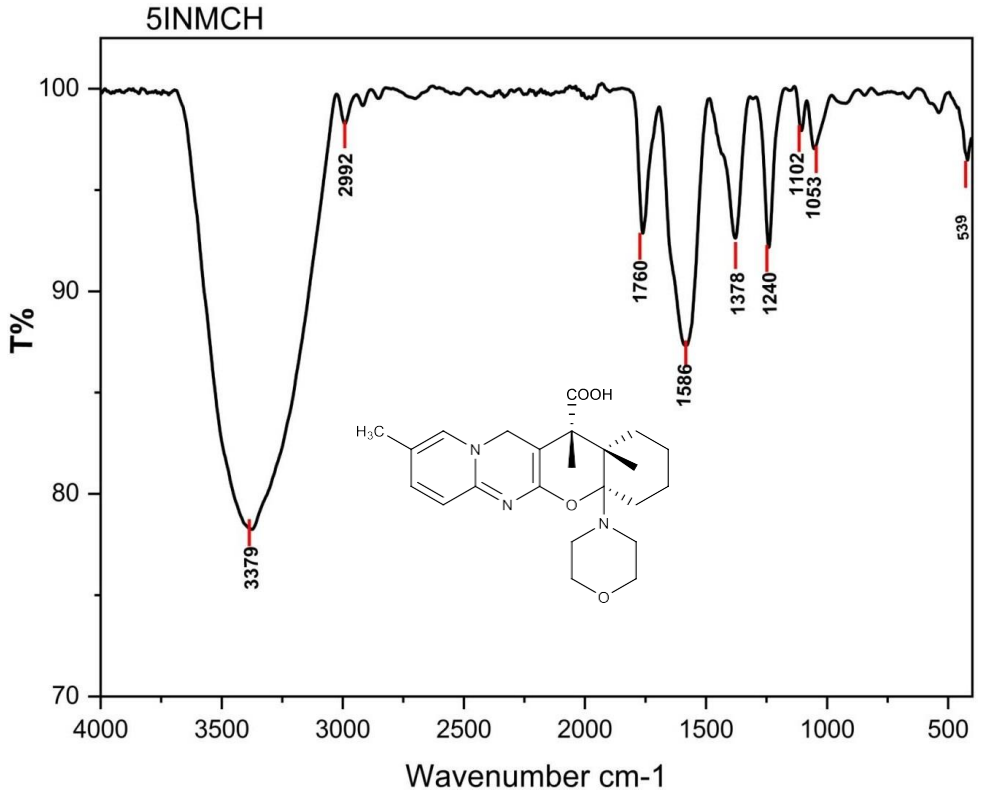

FIGURE 58 : FTIR Spectrum of 9,13,13*a*-Trimethyl-4*a*-Morpholino-1,2,3,4,4*a*, 12,13,13*a*-Octahydrochromeno[2,3-*d*]Pyrido[1,2-*a*]Pyrimidine-13-Carboxylic Acid (13c)

4.6.1.2 ^{1}H NMR SPECTRUM

The proton NMR **(Figure 59)** spectrum of compound **13c** displayed 15 sets of protons. The proton attached to C-14 give rise to a doublet δ 6.3 with coupling constant J=12.0 due to coupling with C-13. The proton attached to C-13 carbon gave a quintet at δ 6.5 with coupling constant J=12.0 due to coupling with proton attached to C-13 and C-18 carbons respectively. The proton attached to C-18 carbon resonated at δ 6.2 as quartet with coupling constant J=12.0, 6.0 due to coupling of protons attached to C-13 and C-17 carbons respectively. The COOH proton appeared at δ 12.4. Other aromatic ring protons were registered at δ 10.4-9.2.

TABLE 30:

^{1}H NMR Assignments of 9,13,13*a*-trimethyl-4*a*-morpholino-1,2,3,4,4*a*,12,13,13*a*-octahydrochromeno[2,3-*d*]pyrido[1,2-*a*]pyrimidine-13-carboxylic acid (13c)

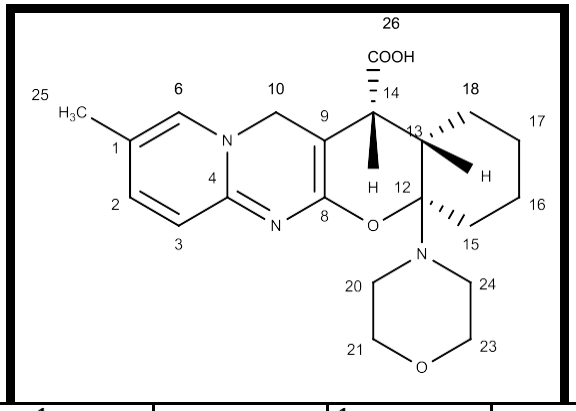

^{1}H Shift in ppm	No. of ^{1}H/ Multiplicity	J value (mz)	^{1}H Shift in ppm	No. of ^{1}H/ Multiplicity	J value (mz)
10.6	H^{2} /d	12.0	5.7	H^{17} /q	6.0/12.0
10.5	H^{3} /d	12.0	6.2	H^{18} /q	6.0/12.0
9.2	H^{6} /s		6.7	H^{20} /t	12.0
5.8	H^{10} /s		6.9	H^{21} , H^{23} /t	12.0
6.5	H^{13} /q	12.0	6.6	H^{24} /t	12.0
6.3	H^{14} /d	12.0	4.8	H^{25} /s	
5.2	H^{15} /t	6.0	12.4	H^{26} /s	
5.6	H^{16} /q	6.0/12.0			

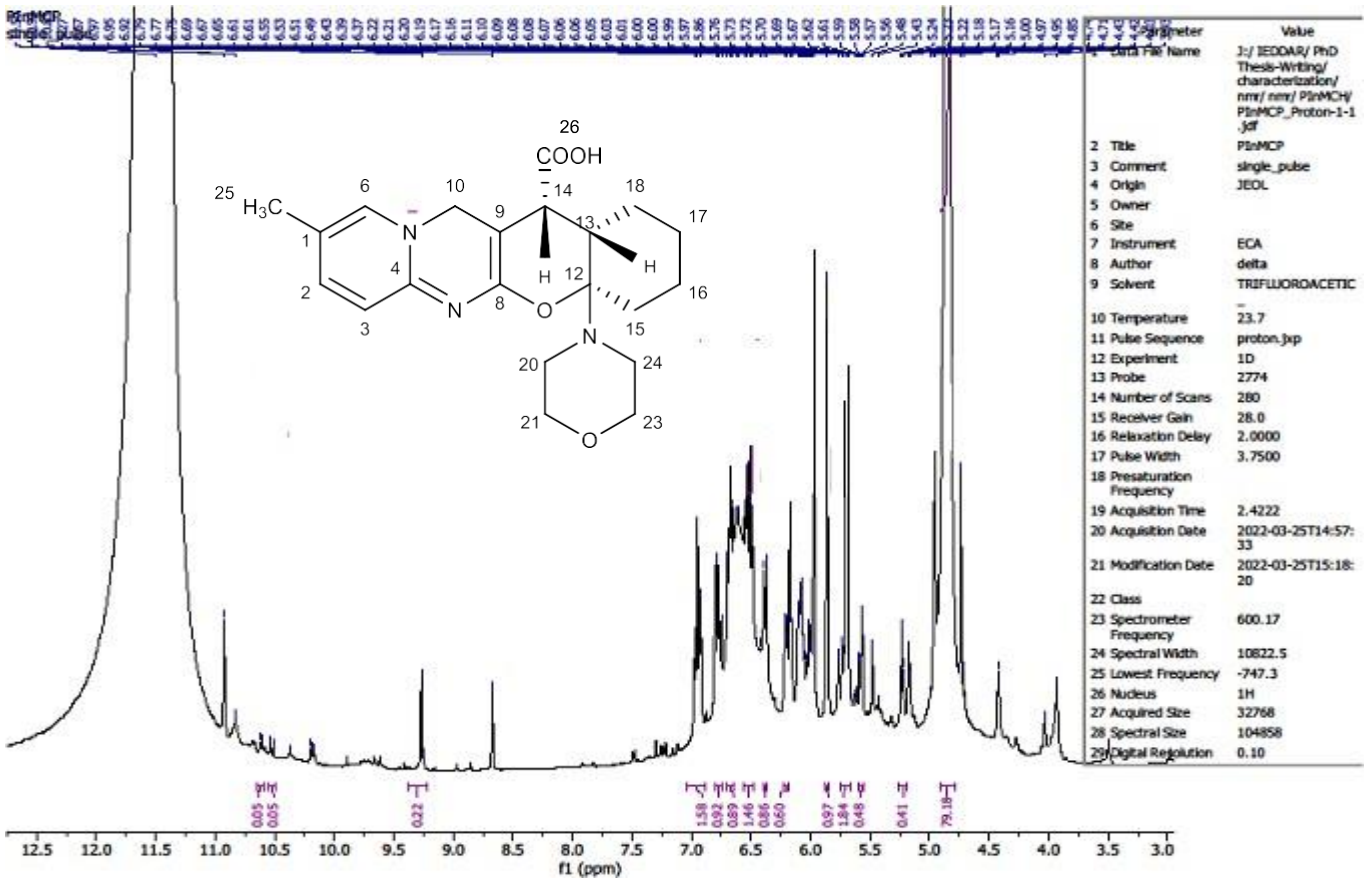

FIGURE 59 : ^{1}HNMR Spectrum of 9,13,13*a*-Trimethyl-4*a*-Morpholino-1,2,3,4,4*a*,12,13,13*a*-Octahydrochromeno [2,3-*d*]Pyrido[1,2-*a*] Pyrimidine-13-Carboxylic Acid (13c)

^{1}HNMR Spectrum of 9,13,13*a*-Trimethyl-4*a*-Morpholino-1,2,3,4,4*a*,12,13,13*a*-Octahydrochromeno[2,3-*d*]Pyrido[1,2-*a*] Pyrimidine-13-Carboxylic Acid (13c)

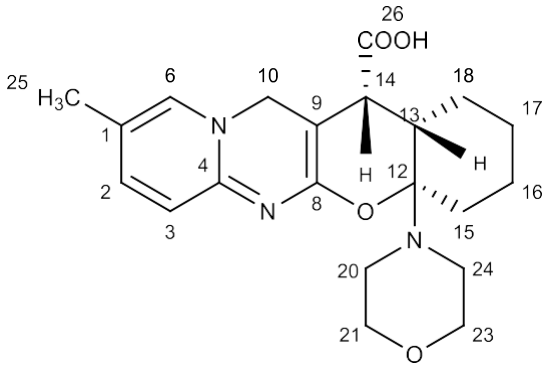

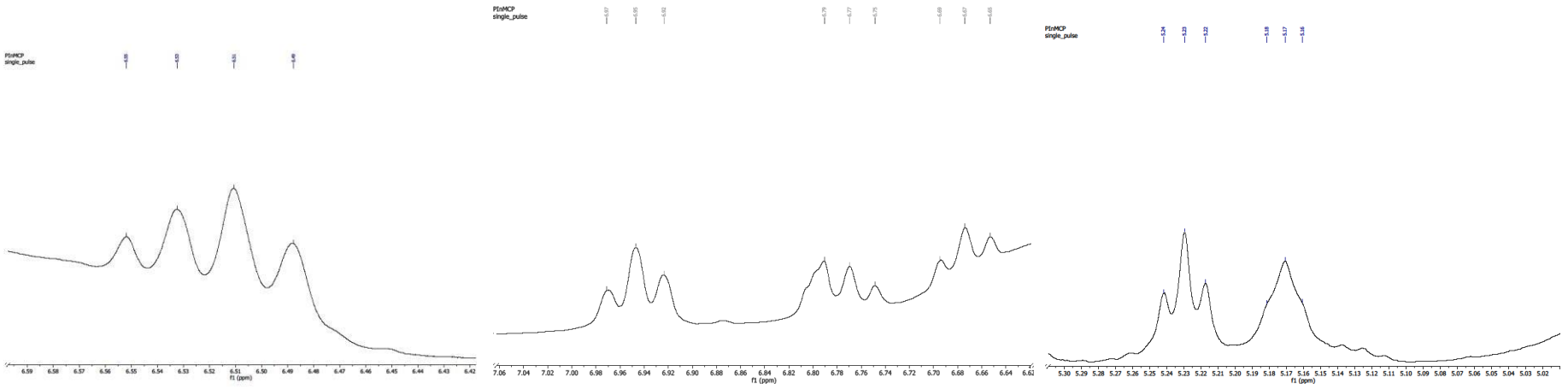

4.6.1.3 MASS SPECTRUM

Further evidence for the structure **13c** was obtained from the mass spectrum which showed M+1 peak at m/z **414.24.** Hence the assigned structure of the **13c** was confirmed. (**Figure 60)**

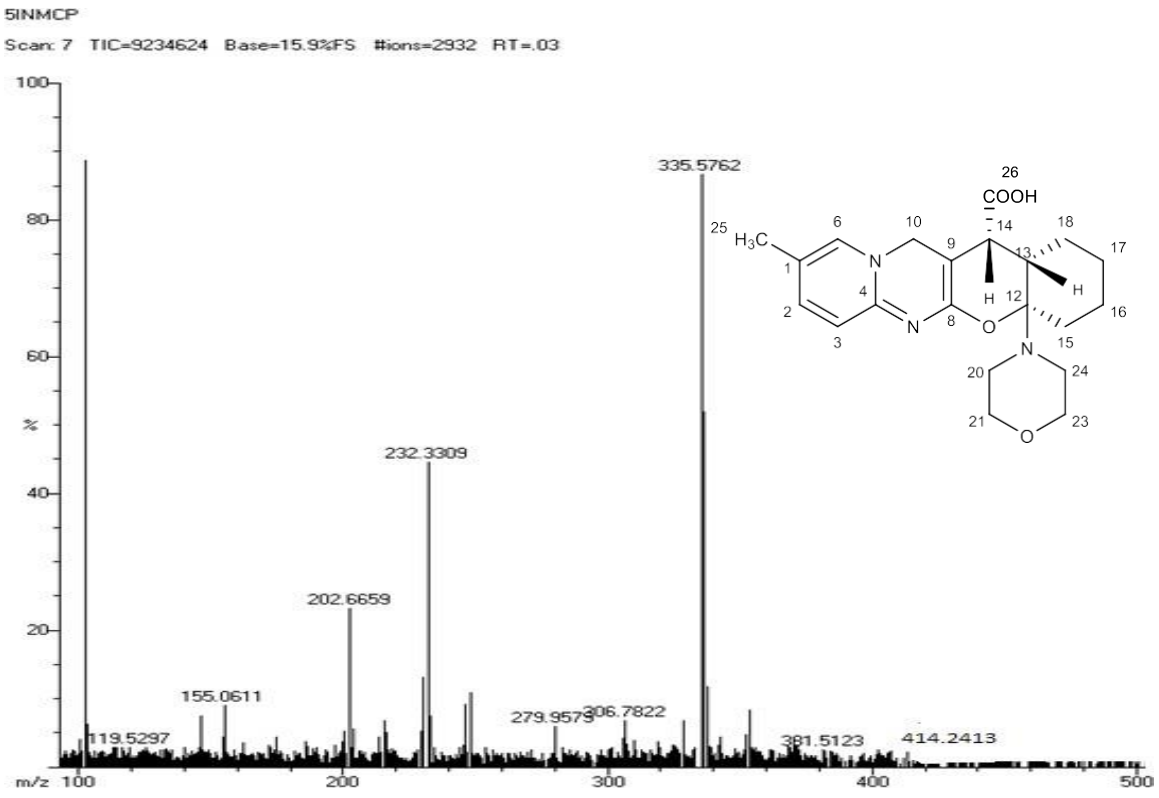

FIGURE 60 : Mass Spectrum of 9,13,13*a*-Trimethyl-4*a*-Morpholino-1,2,3,4,4*a*, 12,13,13*a*-Octahydrochromeno[2,3-*d*]Pyrido[1,2-*a*]Pyrimidine-13-Carboxylic Acid (13c)

4.7. COMPUTATIONAL STUDIES

To get an insight into the mechanistic pathway of the studied IEDDAR between diene 2-oxo-2*H*-pyrido[1,2-*a*]pyrimidin-3(4*H*)-ylidiene Acetic acid **(3)** and various dienophiles **(4,6,8,10 and 12)** computational calculations were performed using Gaussian16W software programme by Density functional theory (DFT)/B3LYP technique with the 6-311+g(d,p) basis set .

4.7.1. Normal DA versus IEDDA [4 + 2] cycloaddition reaction

The reactivity of DA reaction is based on the strength of interaction between LUMO and HOMO of the dienophile and diene respectively.

The [4 + 2] cycloaddition reaction of diene with dienophile can proceed via two ways:

- ✓ Pairing of HOMO of the diene, with LUMO of the dienophile, in normal electron demand cycloaddition
- ✓ Pairing of HOMO of the dienophile, with LUMO of the diene, in inverse electron demand cycloaddition. **(Sharma *et al.*, 2008)**

To anticipate the course of the reaction Fuki's FMO approach was followed. In this method the energy gap between LUMO of the diene and HOMO of the dienophile Lde-Hdo and the energy gap between LUMO of the dienophile and HOMO of the diene Ldo-Hde were calculated using DFT method.

HOMO and LUMO energies of the diene **(3)** and the dienophiles **(4,6,8,10 &12)** are tabulated in **Table 31 & Figure 61.** For all the studied reacting pairs **3+4,3+6,3+8,3+10** and **3+12** smaller energy gap was observed for LUMO of the diene **(3)** and HOMO of the dienophiles **(4,6,8,10 &12).** Hence the electron flow will be from dienophile **(4,6,8,10 &12)** to diene **(3).** This demonstrated that the reaction followed IEDDA pathway.

Table 31 : Calculated HOMO and LUMO energy gap of diene (3) and dienophiles (4,6,8,10,12).

Diene/dienophile	HOMO (eV)	LUMO (eV)	Ldo-Hde (eV)	Lde-Hdo (eV)
2-oxo-2H-pyrido[1,2-a]pyrimidin-3(4H)-ylidiene Acetic acid **(3)**	-6.4028	-2.3682		
Butyl Vinyl ether **(4)**	-6.2711	0.11075	6.5136	3.9029
1-phenyl-3-methyl-pyrazolone **(6)**	-6.6197	-1.0468	5.3560	4.2515
1-methyl-1-cyclohexene **(8)**	-6.3759	0.03020	6.4330	4.0077
3,4-Dihydro-2H-pyran **(10)**	-6.0975	0.02803	6.43086	3.7293
1-morpholinocyclohexene **(12)**	-5.2934	-0.07157	6.3313	2.9252

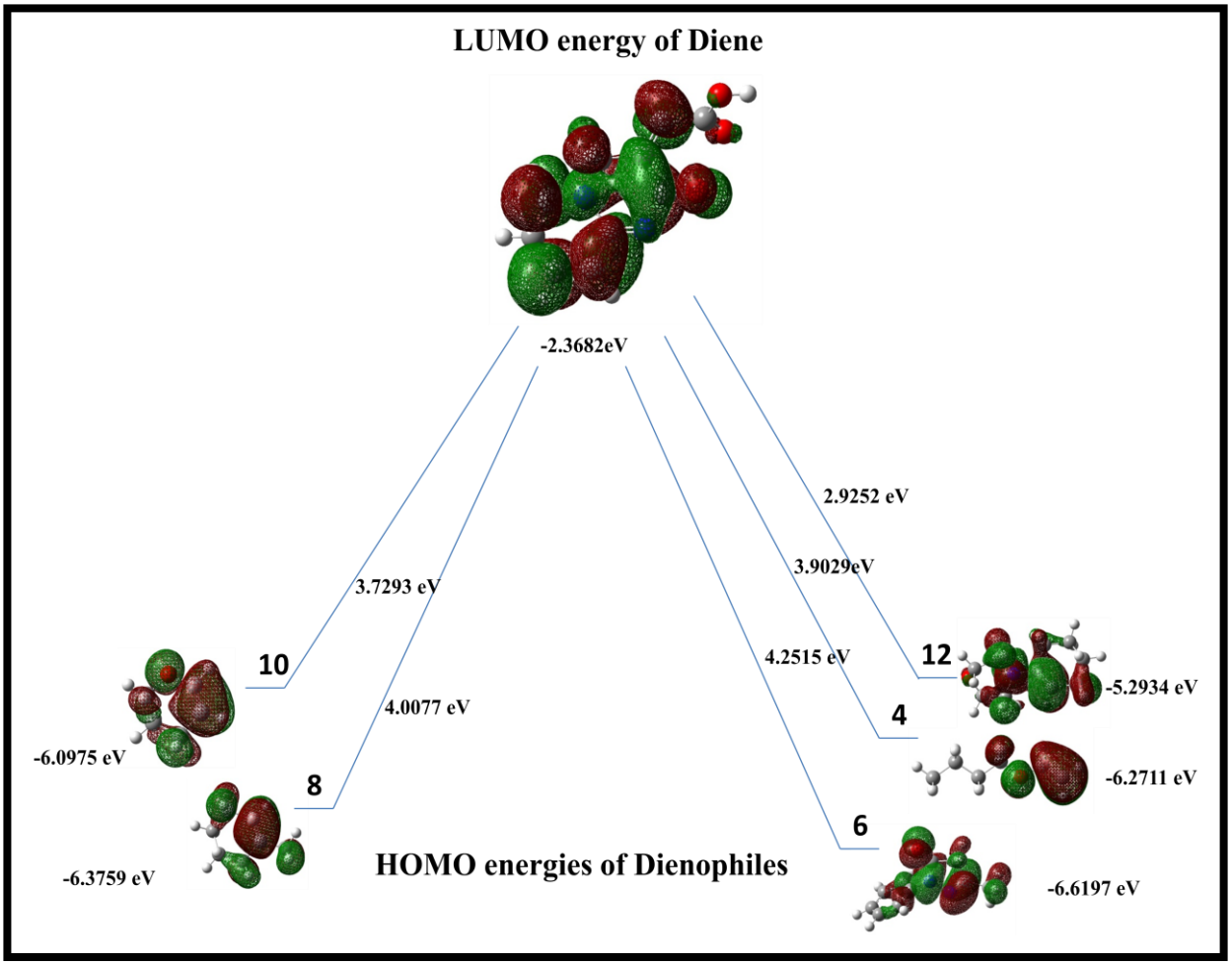

Figure 61:

Energies of HOMO and LUMO of diene (3) and dienophiles (4,6,8,10 &12)

4.7.2 Effect of Lewis Acid Catalyst on LUMO energy of Diene (3)

A plot of FMO energy of diene **(3)**, and dienophiles **(4,6,8,10 &12)** for catalyzed and uncatalyzed reaction is depicted in **Figure (62)**. The catalyst indium (III) chloride decreased the LUMO energy of the diene **(3)** to an extent of 0.6304eV. This explained the enhanced reactivity of IEDDA reaction of the studied reaction pairs in presence of indium (III) chloride catalyst. Hence further computational calculations were performed for the diene complexed with the catalyst indium (III) chloride.

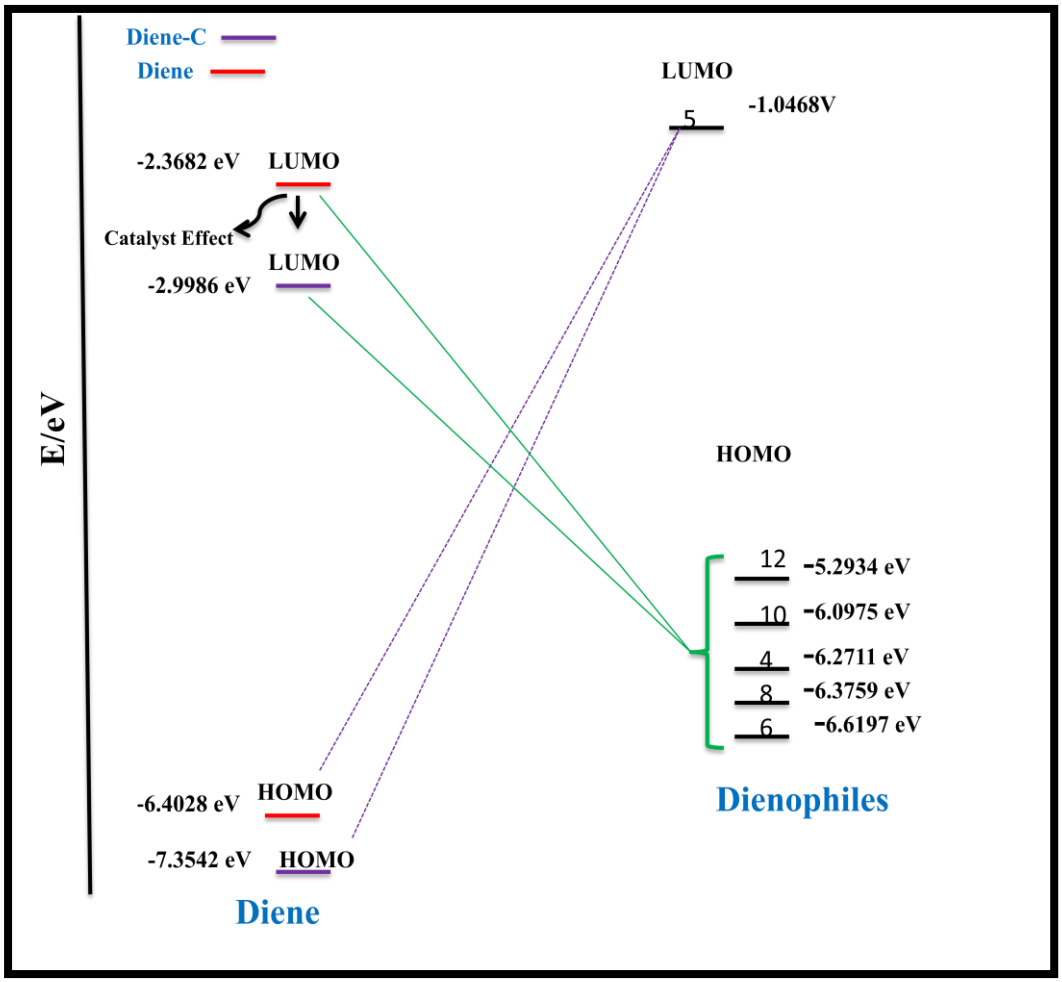

Figure 62: Graphical representation HOMO & LUMO energy gap between diene (3) with Indium (III) **chloride and without catalyst and Dienophiles (4,6,8,10 & 12)**

4.7.3 Global reactivity indices

The overview of calculated electronic parameters, viz electronic chemical potential (μ), chemical hardness (η), global electrophilicity index (ω) and *N* max are presented in **Table 32.** The electronic chemical potential represents the feasibility of a molecule to exchange electron density with the environment. The electronic chemical potential (μ) for the diene **(3)** was found to be 0.161165a.u while for dienophiles **(4,6,8,10& 12)** it ranged from -0.09261 to -0.14087a.u. The higher electronic chemical potential for the dienophiles suggested the flow of the electrons from dienophiles to diene **(Sharma, *et al.*, 2008).**

Electrophilicity index ω value is an indicator for the elctrophilic or nucleophilic nature of the compounds. The calculated values of electrophilicity index ω of dienophiles **(4,6,8,10& 12)** varied from 0.01827 to 1.37172eV, while for the diene **(3)** it was found to be

2.38298eV. The greater value of ω for diene **(3)** complexed with indium (III) chloride implied its high electrophilic nature. Therefore, it acts as an acceptor of electrons, which supported the IDEEA reaction pathway. The increased electrophilicity of diene **(3)** indicated the coordination of carboxyl oxygen atom at C_{11} position of the diene with indium (III) chloride thus making it more electrophilic.

N max is a parameter that quantifies the maximum electronic charge that an electrophile may accept from the environment. Species with large *N*max values would be excellent electrophiles **(Samba *et al.*, 2021).** The calculated *N*max value for diene **(3)** was 1.08675, which was found to be higher than that of dienophiles **(4, 6, 8, 10& 12)**. The above results explained that the diene **(3)** was more electrophilic and thus it reacts through IEDDA reaction mechanism with dienophiles**(4,6,8,10& 12).**

Table 32: Global reactivity indices for Diene (3) and Dienophiles (4, 6, 8, 10& 12).

Diene/dienophile	**HOMO**	**LUMO**	**μ (a.u)**	**Ƞ (a.u)**	**ω(eV)**	**N_{max}**
2-oxo-2H-pyrido[1,2-a]pyrimidin-3(4H)-ylidiene Acetic acid **(3)**	-0.23530	-0.08703	-0.161165	0.1483	2.38298	1.08675
Butyl Vinyl ether **(4)**	-0.23046	0.00407	-0.113195	0.23937	0.72829	0.47289
1-phenyl-3-methyl-pyrazolone **(6)**	-0.24327	-0.03847	-0.14087	0.19683	1.37172	0.71569
1-methyl-1-cyclohexene **(8)**	-0.23431	0.00111	-0.1166	0.23641	0.78244	0.49321
3,4-Dihydro-2H-pyran **(10)**	-0.22408	0.00103	-0.11153	0.23633	0.71612	0.47192
1-morpholinocyclohexene **(12)**	-0.24327	-0.03847	-0.14087	0.19683	1.37172	0.71569

4.7.3 Investigation of the regioselectivity of IEDDA reaction

In the IEDDA reaction of diene **(3)** with dienophile **(4)** two regioisomers are possible depending upon the mode of interaction of oxygen of C_2 carbonyl group of diene **(3)** with that of C_1(bearing EDG) of dienophile **(4)** or with C_2 carbon of the dienophile **(4) (Scheme-17).**

To investigate the aforementioned formation of regiosiomers Natural bond analysis (NBO) analysis were performed.

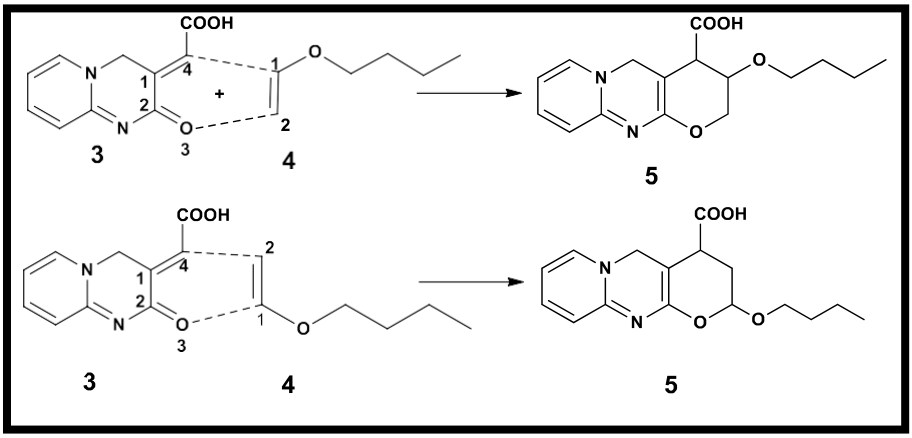

Scheme 17: Possible Regioisomers for the IEDDA reaction of (3) and (4)

NBO analysis is a method to illustrate non-covalent interaction occurring between the functional group of the reacting species. It calculates the atomic charges of the atoms present in a molecule. These charges may be used to predict molecular polarizations, from which mechanisms of the reaction can be explained **(Samba *et al.*, 2021)(Ge *et al.*, 2019).**

The calculated NBO charges are presented in **Table 33.** From the table it was clear that NBO charge for C_2-terminus of the dienophile **(4)** is higher (3.70095) than that for the C_1 terminus (2.54623). Similarly, NBO charge of the diene **(3)** is higher at the O_3-terminus (-1.6952) as compared with the C_4 terminus (−1.6952). Therefore, the most favourable regioisomeric channel was that associated with C_2–O_3 and C_1–C_4 reaction coordinates, which was in good agreement with the anticipated and experimental outcome **(Figure-63)**. The same trend was observed for other dienophiles **(6,8,10, &12)** with diene **(3).**

Table 33: NBO atomic charge of the diene (3) and dienophiles (4,6,8,10 &12)

Diene 3	NBO charge	dienophile 4	NBO charge	dienophile 6	NBO charge	dienophile 8	NBO charge	dienophile 10	NBO charge	dienophile 12	NBO charge
C1	-0.08849	**C1**	**0.15662**	**C1**	**0.31147**	**C1**	**-0.00125**	**C1**	**0.12327**	**C1**	**0.28294**
C2	0.62643	**C2**	**-0.50548**	**N2**	**-0.32830**	**C2**	**-0.22464**	**C2**	**-0.27573**	**C2**	**0.20373**
O3	**-0.66469**	O3	-0.58539	C3	-0.53424	C3	-0.59394	H3	0.19565	H3	0.19474
C4	**-0.02297**	H4	0.17644	N4	-0.34238	C4	-0.40431	O4	-0.60031	C4	-0.39497
C5	0.80186	H5	0.20669	C5	-0.61101	H6	0.19258	C5	-0.41314	N5	-0.55788
O6	-0.61723	H6	0. 19980					H6	0.21238	C6	-0.36807
O7	-0.68273										

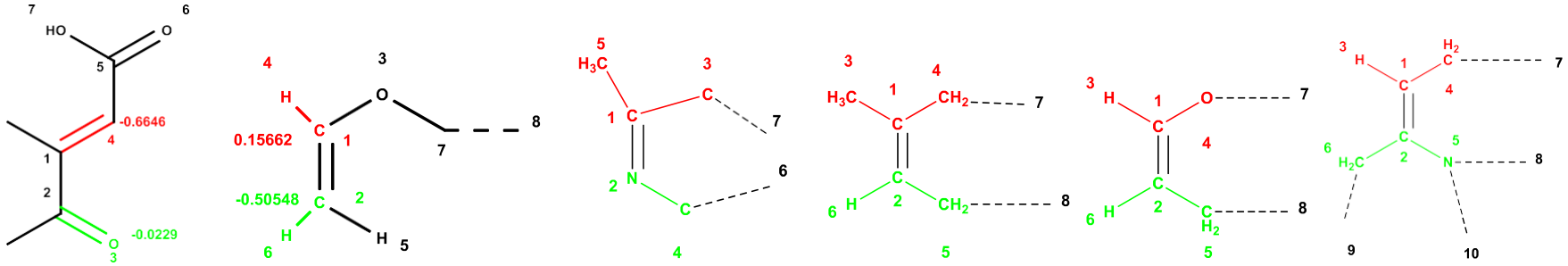

3 **4** **6** **8** **10** **12**

Figure 63: Atomic labels with charges of diene (3) and dienophiles (4, 6,8,10 &12)

4.7.4 Mechanism of the reaction

From the inspection of FMO analysis, and NBO charge analysis the following concerted mechanism was proposed for the IEDDA reaction (**Scheme-17**). Lewis acid catalyst indium (III) chloride coordinated with the carboxyl oxygen at C_{11} position of the diene **(3)** to form active catalyst complex with decreased LUMO energy. This provided a better interaction of the diene **(3)** with HOMO of the dienophile **(4)**. Subsequently cycloaddition occurred by the formation of two sigma bonds.

- Oxygen of C_2 carbonyl carbon of the diene **(3)** and C_2 carbon of the dienophile **(4)**
- C_{10} carbon of the diene **(3)** with C_2 carbon bearing EDG of the dienophile **(4)**

In the cyclic transition state and afforded the cycloadduct **(5) Figure 64.**

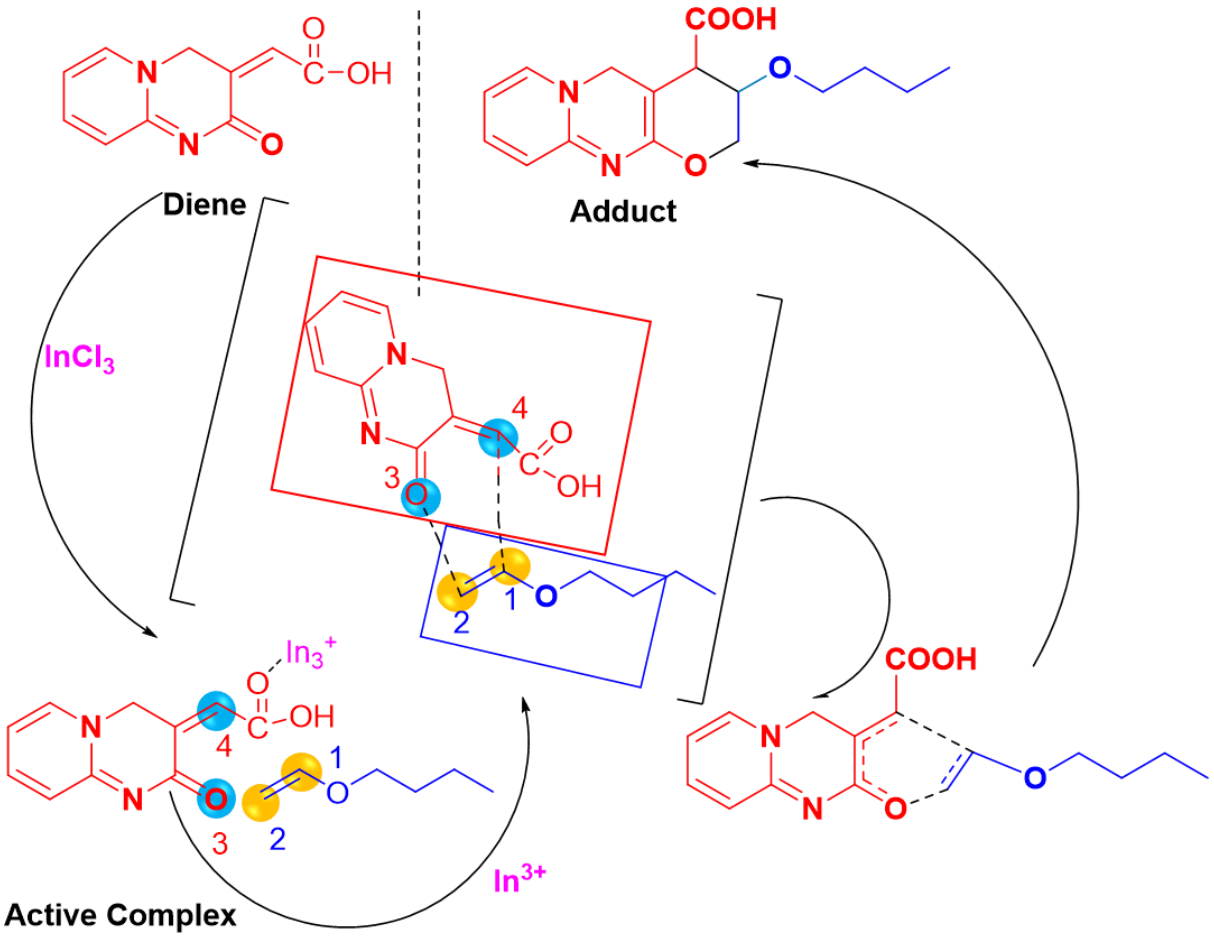

Figure 64: Proposed mechanism for indium (III) chloride catalysed IEDDA reaction

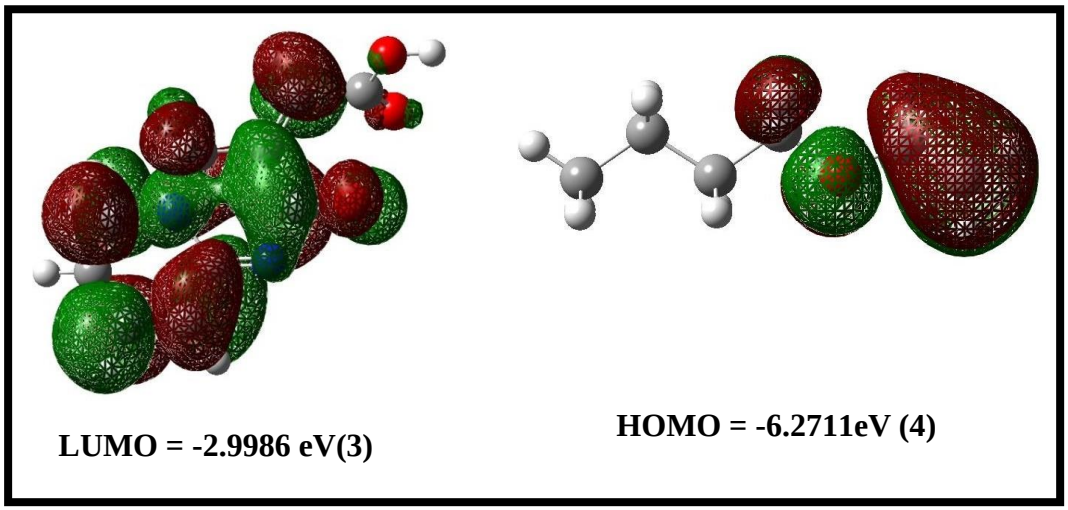

Figure 65: Geometry-optimized structures and orbital energies for diene(3) and dienophile(4) by B3LYP/ 6-311+g(d,p)

4.7.5 Transition States of the IEDDA reaction of diene (3) with dienophile (4)

To confirm the above said concerted mechanism and to analyse the various possible modes of cycloaddition of diene **(3)** with dienophile **(4)** *Ab initio* calculations were performed using DFT method. The IEDDA reaction of diene **(3)** with dienophile **(4)** may lead to the formation four possible adducts (two *endo* and two *exo*) depending upon the approach of dienophile **(4)** towards the diene **(3)** during the course of the reaction. **(Scheme-18) Figure 66** depicts the optimized geometries of all the four possible transition state.

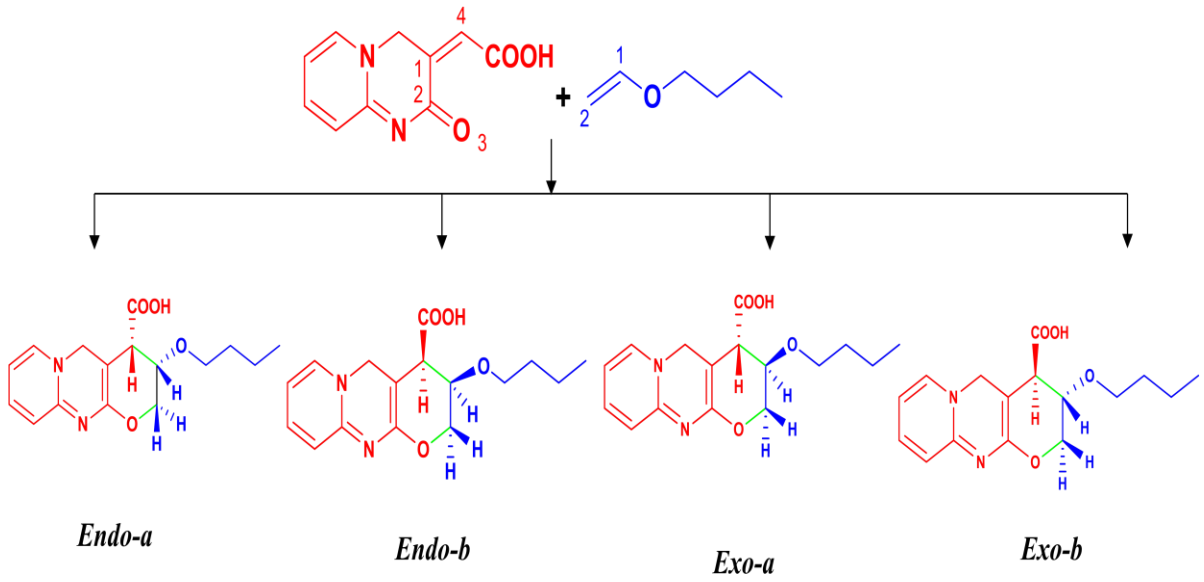

Scheme 18 : Possible products formed in the reaction of diene (3) with dienophile(4)

Bond lengths for the newly forming sigma bonds for the transition states TS_1 to TS_4 are tabulated in **Table-34.** The difference in the bond lengths (Δd) of the newly forming sigma bonds in the IEDDA reaction α give the extent of the synchronicity of the transition state. The parameter α gives the degree of asynchronocity of the reaction. **(Domingo *et al.*, 2014)(Tamilmani *et al.*, 2005).** The observed Δd and α were found to be low. **(Table-34)** for all the transition states indicating the synchronicity in the bond formation. This confirmed the proposed concerted mechanism of IEDDA reaction.

Table 34: Bond length of the newly formed sigma bonds in TS

TS	Bond length $d(C_2\text{-}O_3)$Å	Bond length $d(C_4\text{-}C_2)$ Å	$\Delta d = d(C_2\text{-}O_3) - (C_4\text{-}C_2)$ Å	α Å
TS-I	1.863	2.209	0.346	0.08467
TS-II	2.171	1.927	0.244	0.0595
TS-III	1.898	2.127	0.229	0.0569
TS-IV	1.889	2.186	0.297	0.07288

The origin of *endo* and *exo* selectivity can be explained on the basis of energy barrier ΔG++ observed for the IEDDA reaction **(Yu *et al.*, 2017).** The computed Gibbs free energy profile to afford *endo* **5a** *endo* and *exo* **5a** *exo* cyclic adducts are shown in **Figure-67.** The energy barrier for the formation of *endo* adduct was 16.96 $kcal^{-1}mol$ while for *exo* adduct it was found to be 17.02 $kcal^{-1}mol$ respectively. A very small energy difference of 0.06 $kcal^{-1}mol$ between the *endo* and *exo* adducts **5a** illustrated the formation of diastereoisomers in the ratio 1:1 experimentally.

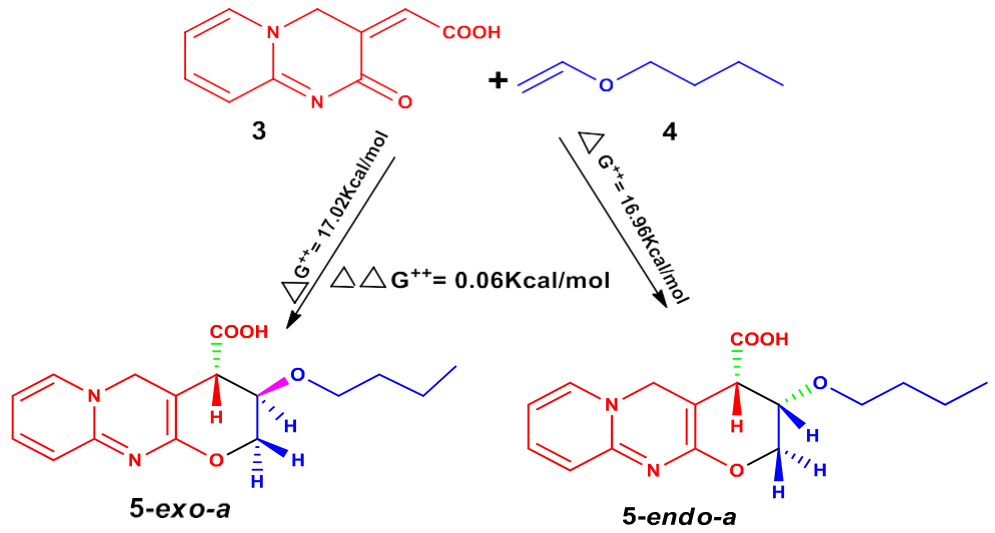

Figure 66: Calculated energy barriers for *endo* and *exo* IEDDA reaction of diene(3) and dienophile(4)

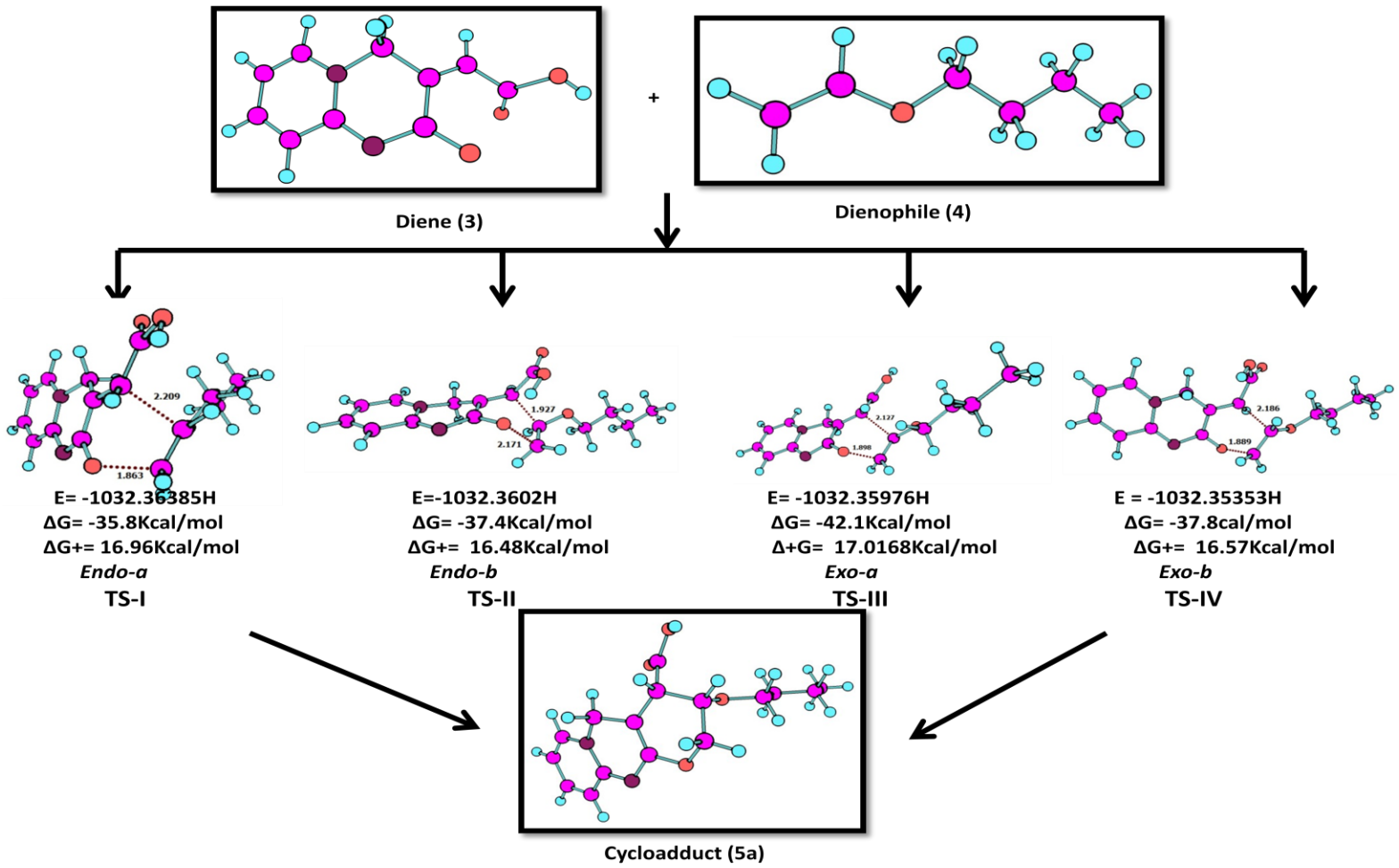

Figure 67: Transition structure of *endo* and *exo* adducts for diene(3)and dienophile(4)

Similarly for the reaction of diene **(3)** with dienophile **(8)** was found to be synchronous and the energy barrier for exo adduct **(9a)** was found to be 15.38 $kcal^{-1}mol$ which was slightly higher than for *endo* adduct **(9a)** 15.09 $kcal^{-1}mol$ respectively. This agreed well with the obtained experimental results (6:1 *endo*:*exo*). The bond length and optimized geometries of transition states for the IEDDA reaction of diene **(3)** with dienophile **(8)** are presented in **Table 35 and Figures 68 and 69**

Table 35: Bond length of the newly formed sigma bonds in TS

TS	Bond length $d(C_2\text{-}O_3)$ Å	Bond length $d(C_4\text{-}C_2)$ Å	$\Delta d = d(C_2\text{-}O_3) - d(C_4\text{-}C_2)$ Å	α Å
TS-I	2.328	1.861	0.467	0.1114
TS-II	2.054	2.066	0.012	0.0029
TS-III	2.440	1.968	0.472	0.1071
TS-IV	2.053	2.059	0.006	0.0014

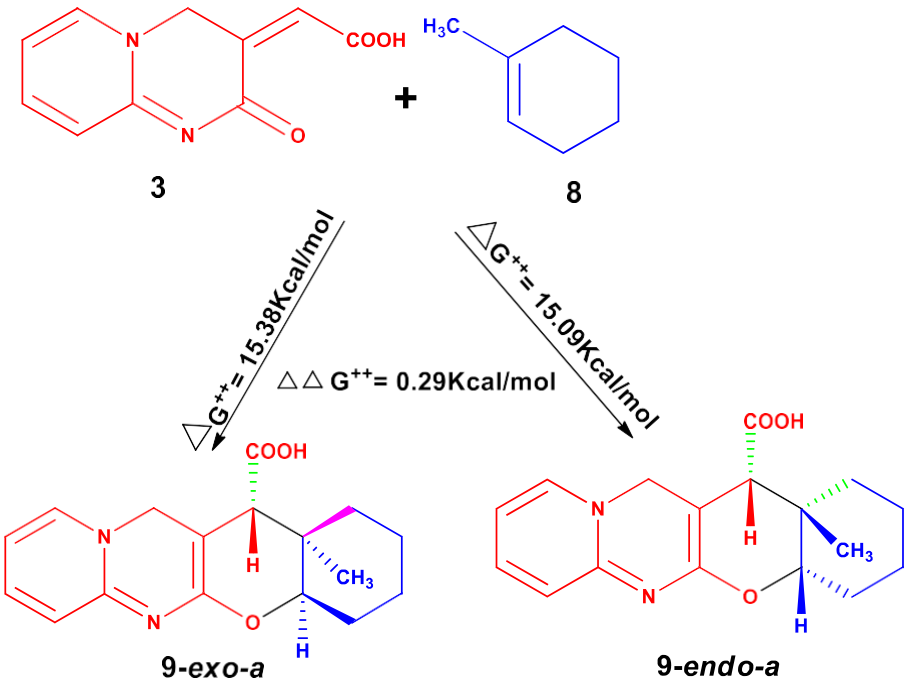

Figure 68 : Calculated energy barriers for *endo* and *exo* IEDDA reaction of diene(1) and dienophile(8)

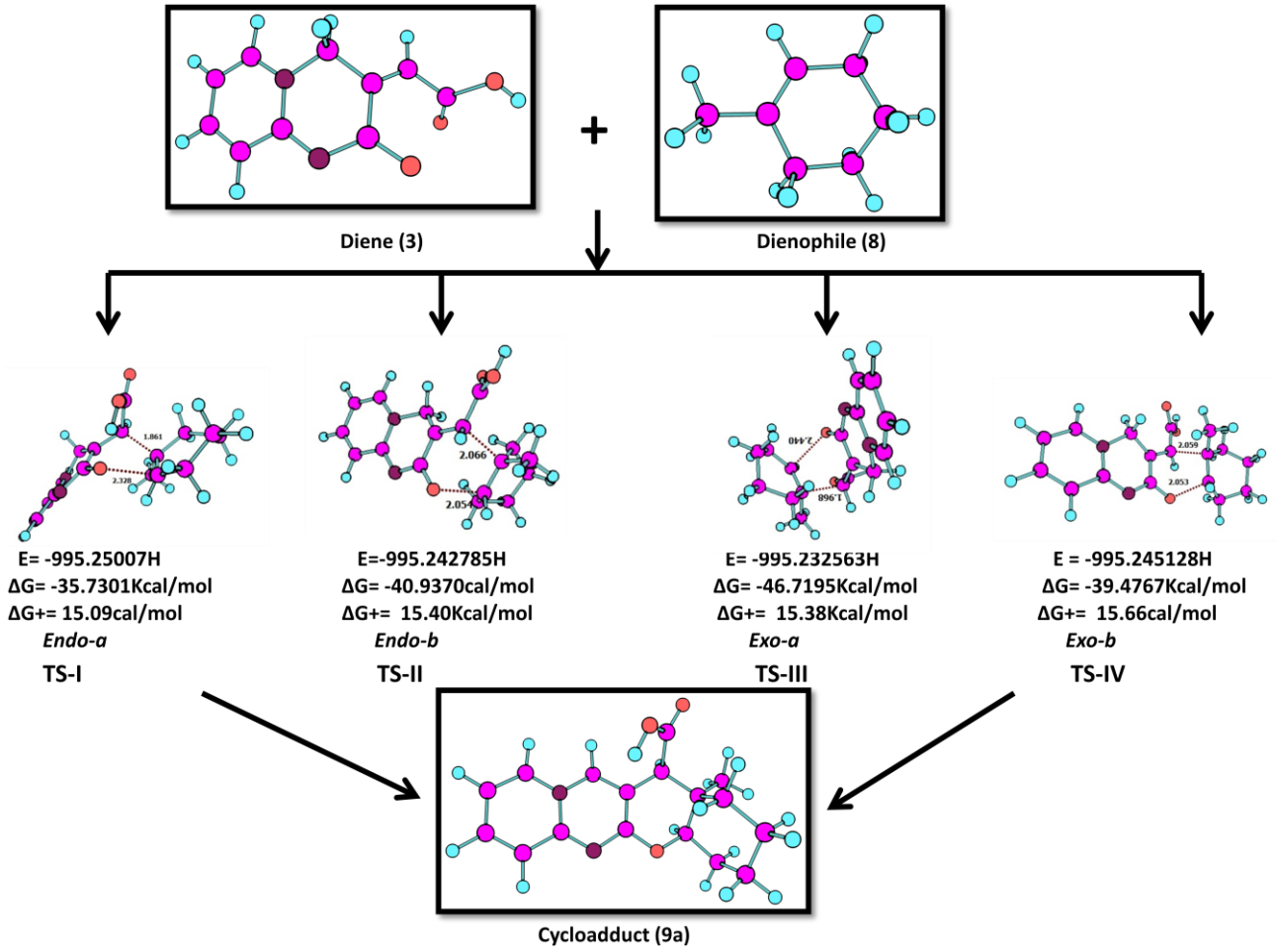

Figure 69 : Transition structure of *endo* and *exo* adducts for diene(3)and dienophile(8)

4.7.6 The intrinsic reaction coordinates (IRC)

The intrinsic reaction coordinate (IRC) method has been used extensively in quantum chemical analysis and prediction of the mechanism of chemical reactions **(Tormena *et al.*, 2010)**. IRC path was traced to check the energy profiles connecting each transition state to the associated minima energy of the product/reactant for [4+2] IEDDA cyclo addition reaction of diene **(3)** with dienophiles **(4 &8).** The obtained intrinsic coordinates and total energy along the IRC path were depicted pictorially in **Figures 70** The IRC plots for diene **(3)** with dienophile **(4)** showed smaller energy difference between the transition states of *endo* and *exo* pathway. These results agreed well with the experimental outcome (1:1 *endo*: *exo ratio*). In contrast higher energy difference between the two transition states *exo* and *endo* was observed in the IRC plots for diene **(3)** with dienophile **(8)** which again coincides with the experimental observation (6:1 *endo*: *exo ratio*).**Figure 71**

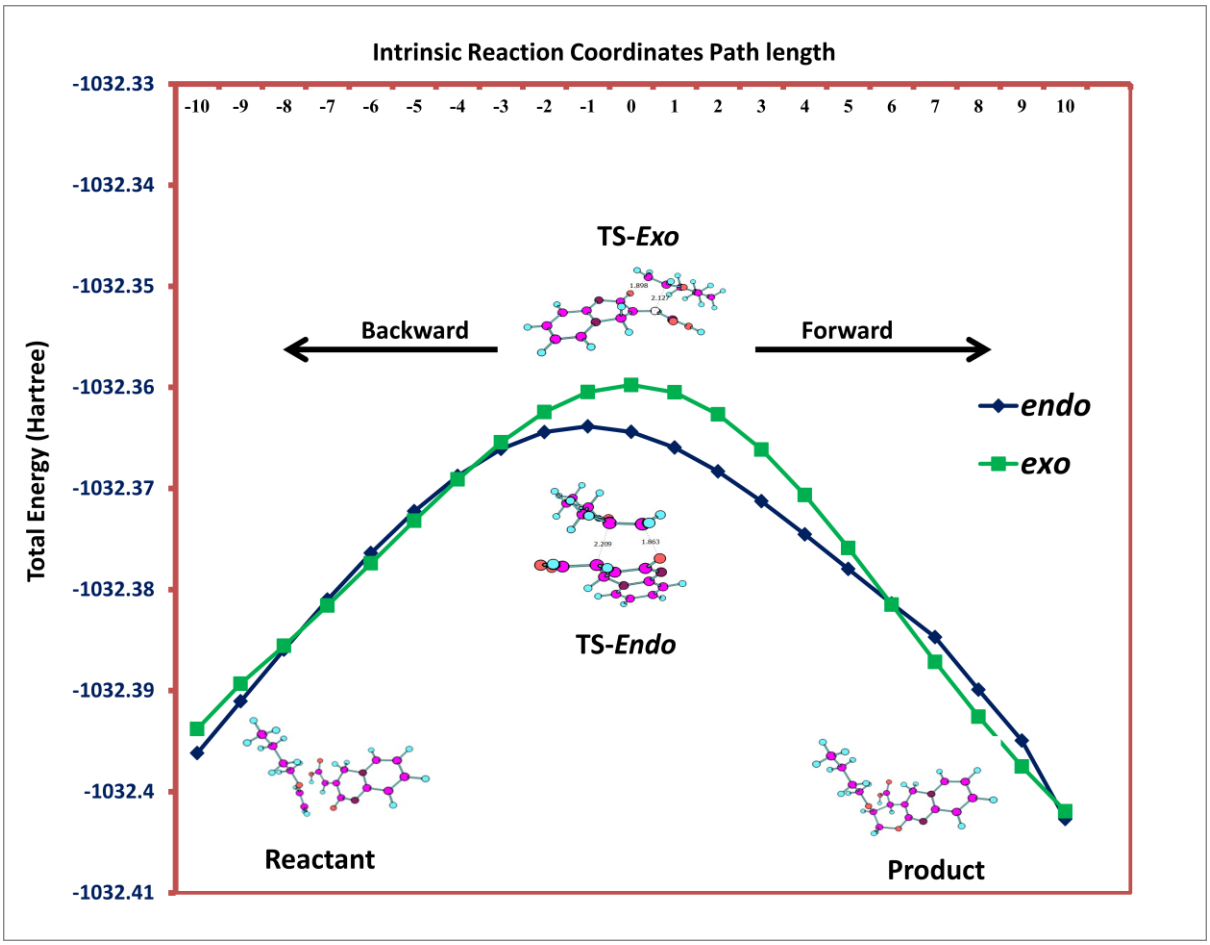

Figure 70: IRC plots for the IEDDR for the *Endo and Exo*-adduct (5a)

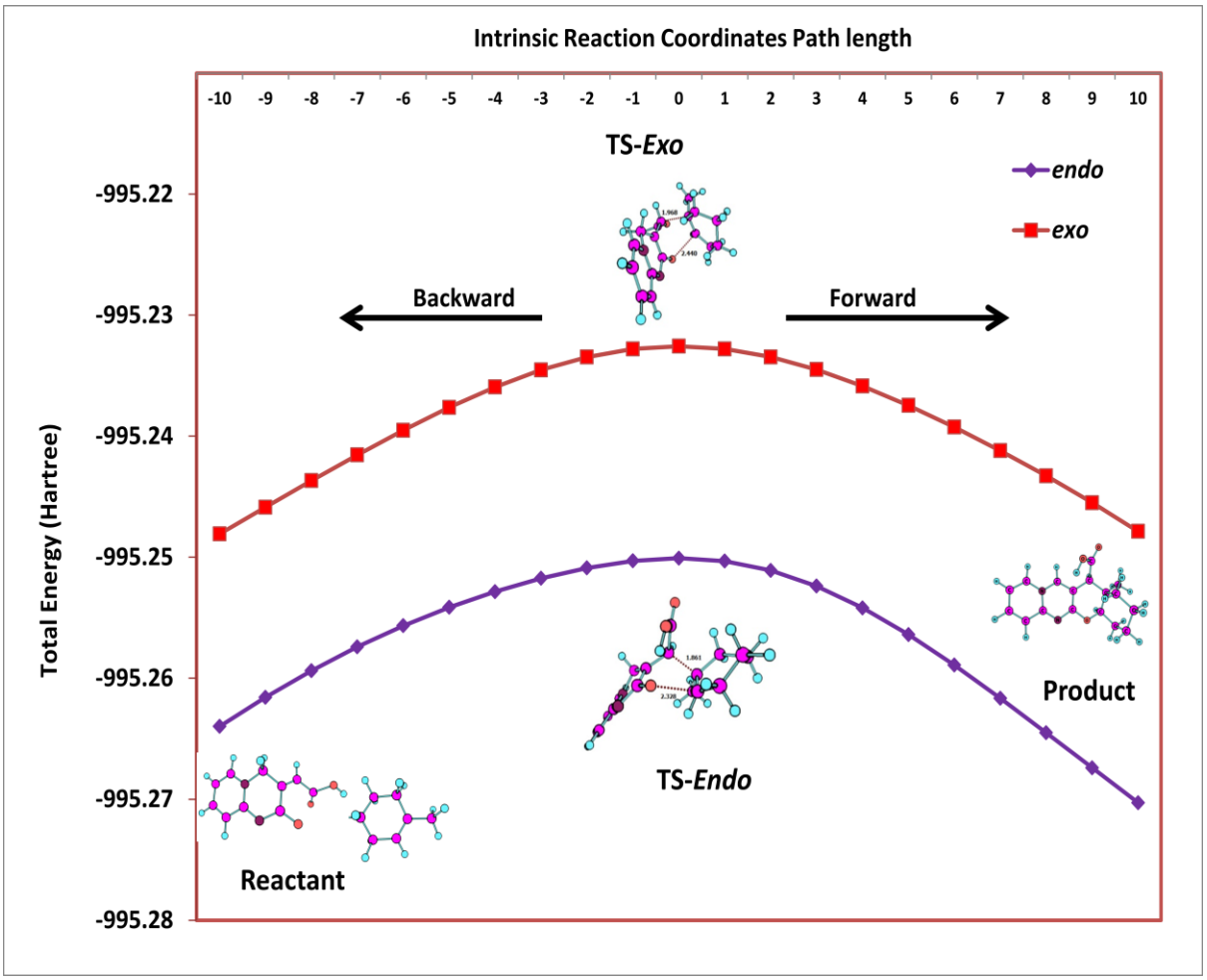

Figure 71: IRC plots for the IEDDR for the *Endo and Exo*-adduct (9a)

4.8 BIOLOGICAL ACTIVITY

4.8.1 Anti-bacterial activity

The synthesized compounds (5a, 5c, 7a, 7c, 9a, 9c, 11a, 11c, 13a and 13c) were evaluated for their *in-vitro* antibacterial activity against *Staphylococcus aureus* and *Escherichia coli by* disc diffusion method against the standard drug Kanamycin with different concentrations like 20-100µg. The compounds exhibited zone of inhibition ranging from 8-18mm and 10-27 mm for *Staphylococcus aureus* and *Escherichia coli* respectively **(Table 36 & 37)** The tested compounds exhibited moderate activity against both bacteria. The compounds 7a and 13a demonstrated maximum zone of inhibition (18mm) against *Staphylococcus aureus* at 100µg concentration.

TABLE 36:

ZONE OF INHIBITION OF SYNTHESIZED COMPOUNDS AGAINST *Staphylococcus aureus* TESTED BY DISC DIFFUSION ASSAY

Compounds	Zone of Inhibition				
	Staphylococcus aureus				
	20 µg/disc	**40 µg/disc**	**60 µg/disc**	**80 µg/disc**	**100 µg/disc**
Kanamycin	14 mm	18 mm	20 mm	20 mm	24 mm
(5a)	0 mm	8 mm	10 mm	12 mm	14 mm
(5c)	11 mm	11 mm	13 mm	14 mm	15 mm
(7a)	0 mm	15 mm	13 mm	16 mm	18 mm
(7c)	0 mm	0 mm	0 mm	11 mm	15 mm
(9a)	0 mm	11 mm	14 mm	14 mm	14 mm
(9c)	11 mm	12 mm	165mm	16 mm	16 mm
(11a)	0 mm	12mm	13 mm	14 mm	15 mm
(11c)	0 mm	0 mm	10 mm	11 mm	16 mm
(13a)	0 mm	11 mm	14 mm	16 mm	18 mm
(13c)	11 mm	13 mm	14 mm	15 mm	15 mm

★ **Negative Control (DMSO)-** 0mm

FIGURE 72

ANTIBACTERIAL ACTIVITY OF SYNTHESIZED COMPOUNDS AGAINST *Staphylococcus aureus* AND *Escherichia coli*

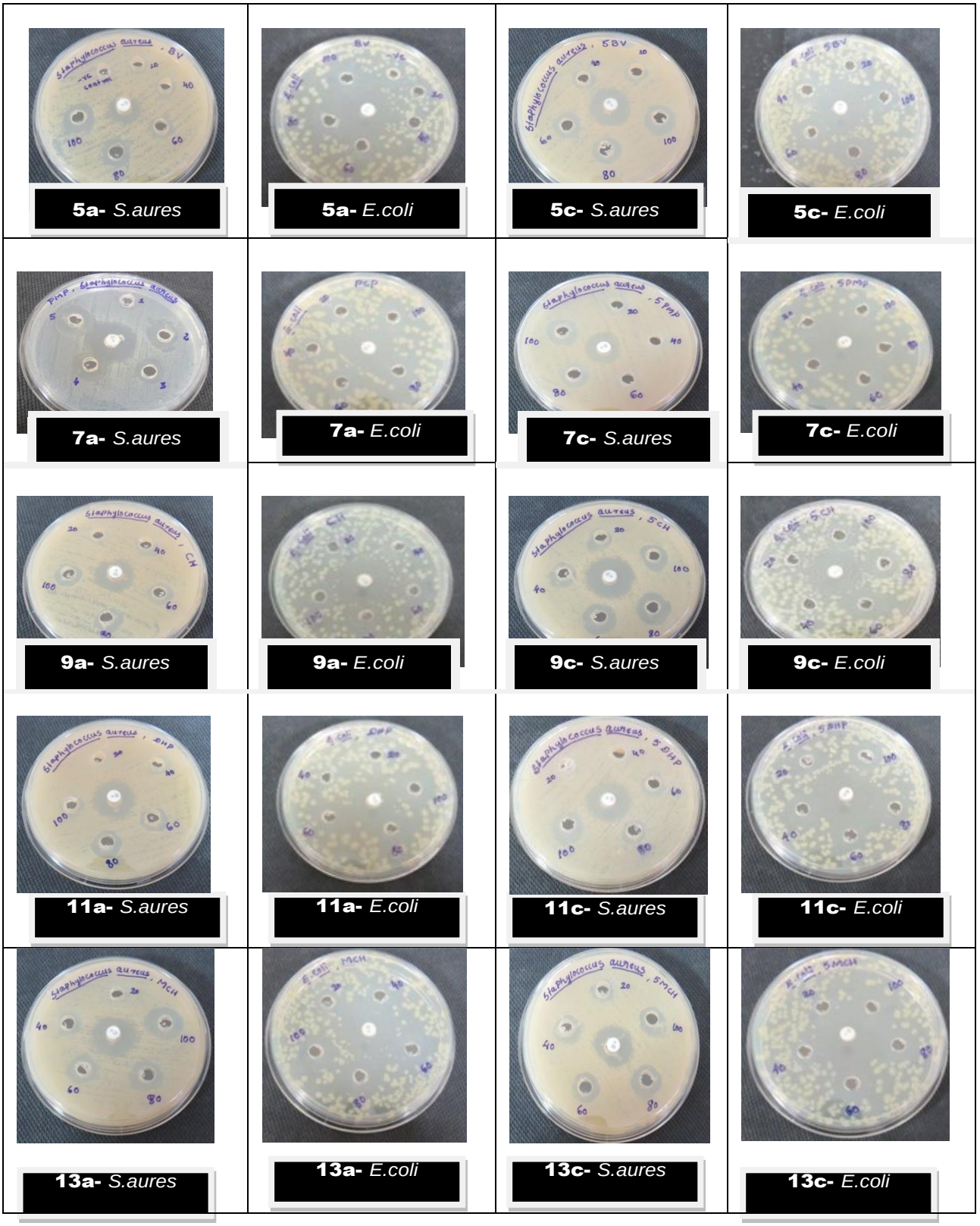

Among all the tested compounds, compounds 7a and 5c demonstrated maximum zone of inhibition (21mm and 27mm) against *Escherichia coli* at 100µg. The high potency of 7a may be due to the presence of pyrazolone ring **(Zhao et al., 2020)**.

TABLE 37

ZONE OF INHIBITION OF SYNTHESIZED COMPOUNDS AGAINST *Escherichia coli* TESTED BY DISC DIFFUSION ASSAY

Compounds	**Zone of Inhibition**				
	Escherichia coli				
	20 µg/disc	**40 µg/disc**	**60 µg/disc**	**80 µg/disc**	**100 µg/disc**
Kanamycin	20 mm	22 mm	22 mm	23 mm	25 mm
(5a)	0 mm	14 mm	16 mm	18 mm	20 mm
(5c)	13 mm	18mm	18 mm	25mm	27mm
(7a)	10 mm	15 mm	18 mm	20 mm	21 mm
(7c)	12 mm	15 mm	16 mm	18 mm	15 mm
(9a)	0 mm	0 mm	18 mm	18 mm	16 mm
(9c)	0 mm	10 mm	20 mm	18 mm	20 mm
(11a)	18 mm	20 mm	22 mm	18 mm	18 mm
(11c)	12 mm	13 mm	17 mm	18 mm	20 mm
(13a)	0 mm	10 mm	15 mm	16 mm	20 mm
(13c)	0 mm	15mm	20 mm	20 mm	20 mm

★ **Negative Control (DMSO)-** 0mm

FIGURE 73

ZONE OF INHIBITION PLOT OF SYNTHESIZED COMPOUNDS AGAINST *Staphylococcus aureus* AND *Escherichia coli* TESTED BY DISC DIFFUSION ASSAY at 100µg/disc

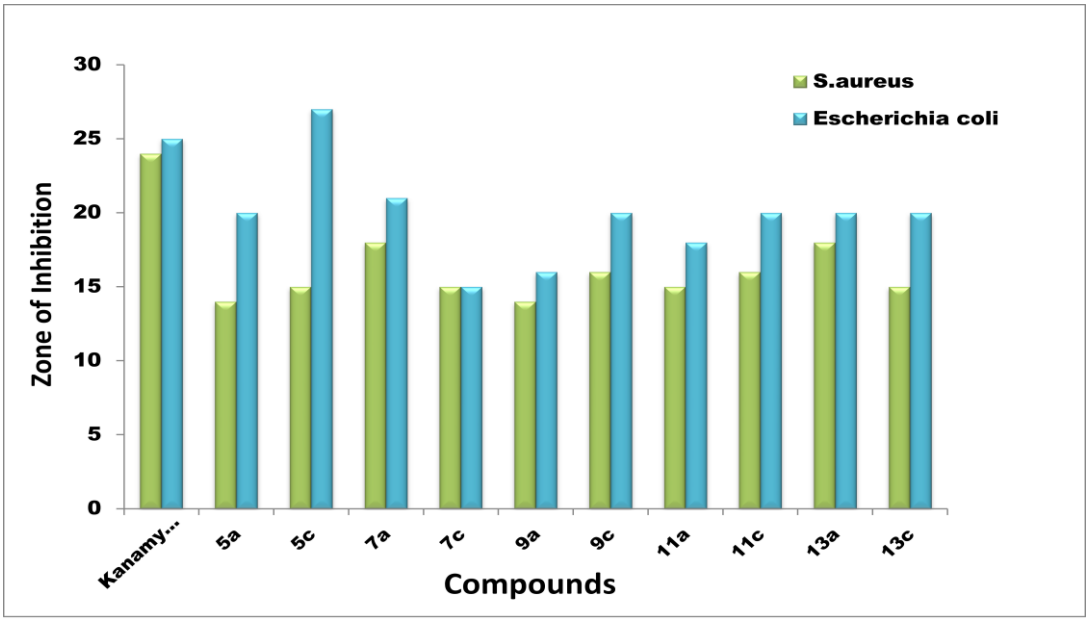

4.9 MOLECULAR DOCKING

Docking studies were carried out for the compounds (5a, 5c, 7a, 7c, 9a, 9c, 11a, 11c, 13a and 13c), for which the activity studies were done. The following proteins were selected for the study

- For *Staphylococcus aureus* the selected target protein was Dihydrofolate reductase (DHFR) enzyme (PDB-2W9S)

- For *Escherichia coli* the selected target protein was Uridine diphospho-N-Acetylenolpyruvyl Glucosamine reductase enzyme (PDB-1MBT).

The docking produced nine distinct positions for each compound, along with the appropriate binding energy scores; the best-docked poses with the lowest energy from a total of nine poses for each compound were retained. **Table 38 &39** shows the docking findings of the investigated adducts. According to the findings, the investigated compounds interacted extensively with the amino acids of the target site Dihydrofolate reductase and Uridine diphospho-N-Acetylenolpyruvyl Glucosamine reductase, with binding energies ranging from

-8.6 to -6.6 kcal/mol, which is nearly similar to the binding energy of the conventional drug Kanamycin.

TABLE 38

DOCKING INTERACTIONS BETWEEN LIGANDS AND DIHYDROFOLATE REDUCTASE

Compounds	Hydrogen Bonds	H-Bond Length(Å)	H-bond with	Hydrophobic Interactions	Binding Energy (kcal/mol)
5a	1	2.23	LYS29A	GLN19F,GLN33A	-6.6
5c	1	3.20	LYS29A	ASN18F,GLU48F	-6.7
7a	3	2.58,3.20, 2.62	SER67E, HIS69E,GLN140B	HIS69C,LEU141B, ASP142B	-7.9
7c	3	2.94,2.40,2.55	LYS32A,LYS52A,ARG57A	PRO25A,LEU34A, PHE117B	-8.3
9a	3	2.75,2.10,2.34,2.44, 3.53	LEU54C,ASN56C, ARG57C	PRO53C, ARG58C	-7.6
9c	3	3.02,2.40, 2.98	GLN65E,GLN140B, GLU 143B	LEU141B	-7.5
11a	3	2.90,2.40,2.69, 2.96	GLN65E,GLN140B, HIS69E	HIS69C	-7.1
11c	3	3.09,2.53, 3.31	GLN65E,HIS69E, GLN140B	LEU141B	-7.4
13a	3	2.83,3.31, 2.37	GLN65E,GLN140B, GLU 143B	ASP142B,GLU 143B	-7.3
13c	3	2.85,3.30, 2.40	GLN65E,GLN140B, GLU143B	ASP142B, GLU143B	-7.5
Standard	4	3.14,3.12, 2.83, 2.88	HIS23A,ASN56C, ARG57C,ASN59C	-	-9.2

Compound **7a** (-7.9 and -8.6 kcal/mol) and 7c (-8.3 and -8.6 kcal/mol) showed the best binding energies with the target receptors Dihydrofolate reductase and Uridine diphospho-N-Acetylenolpyruvyl Glucosamine reductase. For the Dihydrofolate reductase the compound 7a **(Figure 74)** formed three strong H-bonds with SER67E, HIS69E, GLN140B residues respectively and it formed five strong H-bonds with GLY191A, SER229A, ASN233A, TYR254A(2) for Uridine diphospho-N-Acetylenolpyruvyl Glucosamine reductase. It made three hydrophobic interactions with the residues for Dihydrofolate reductase and four for Uridine diphospho-N-Acetylenolpyruvyl Glucosamine reductase.

Compound **7c (Figure 74**) formed three H-bond with the residues LYS32A, LYS52A, ARG57A for 29WS and to the residues SER229A, ASN233A, TYR254A, GLY266A, GLN288A for Uridine diphospho-N-Acetylenolpyruvyl Glucosamine reductase respectively. It formed three hydrophobic interactions with the residues of Dihydrofolate reductase and one for Uridine diphospho-N-Acetylenolpyruvyl Glucosamine reductase respectively.

The antibacterial activity of the synthesized adducts may be explained in terms of hydrogen bonding and hydrophobic interactions. The synthesized compounds may be effective at interacting with the target proteins, hence the synthesized adducts may serveas lead compounds for further studies.

TABLE 39

DOCKING INTERACTIONS BETWEEN LIGANDS AND URIDINE DIPHOSPHO-N-ACETYLENOLPYRUVYL GLUCOSAMINE REDUCTASE

Compounds	Hydrogen Bonds	H-Bond Length(Å)	H-bond with	Hydrophobic Interactions	Binding Energy (Kcal/mol)
5a	4	3.14, 2.65, 2.47, 2.34	TYR125A, ARG214A,SER229A, ASN233A	LYS217A, LEU218A, LEU291A	-6.6
5c	3	2.21, 2.02, 3.42	ASN233A, GLY266A, GLY288A	TYR125A, TYR190A	-6.7

Compounds	Hydrogen Bonds	H-Bond Length(Å)	H-bond with	Hydrophobic Interactions	Binding Energy (Kcal/mol)
7a	5	3.45, 2.07, 2.57, 2.88, 3.44	GLY191A, SER229A, ASN233A, TYR254A(2)	TYR125A, TYR190A, ARG214A, LEU218A	-8.6
7c	5	2.55, 2.65, 2.75, 2.15, 2.90	SER229A, ASN233A, TYR254A, GLY266A, GLN288A	TYR190A	-8.6
9a	3	2.31, 2.48, 2.30	TYR125A, SER229A, ASN233A	TYR190A, TYR254A	-7.6
9c	2	2.25, 2.40	TYR125A, GLY288A	TYR125A, TYR190A, ARG214A, LEU218A	-7.9
11a	2	2.18, 2.48	TYR125A, GLN288A	ARG214A, LEU218A	-7.6
11c	2	2.67, 2.20	TYR254A, GLN288A	LEU218A, ALA264A	-7.4
13a	4	2.01, 3.40, 2.21, 3.63	TYR125A, LYS217A, SER229A, GLN288A	LEU218A	-8.6
13c	4	2.07, 3.38, 2.22, 3.62	TYR125A,LYS217A, SER229A, GLU288A	TYR125A, LEU218A	-8.5
Standard	6	3.66, 2.82, 2.04, 3.24,2.23, 2.43	GLY123A, TYR125A, ARG214A, SER229A, ASN233A, GLN288A	-	-9.0

FIGURE 74:

2D AND 3D REPRESENTATION OF THE INTERACTIONS OF THE COMPOUNDS WITH DIHYDROFOLATE REDUCTASE AND URIDINE DIPHOSPHO-N-ACETYLENOLPYRUVYL GLUCOSAMINE REDUCTASE

2D representation of the compounds with Dihydrofolate reductase	3D representation of the compounds with Dihydrofolate reductase	2D representation of the compounds with Uridine diphospho-N-Acetylenolpyruvyl Glucosamine reductase	3D representation of the compounds with Uridine diphospho-N-Acetylenolpyruvyl Glucosamine reductase
5a 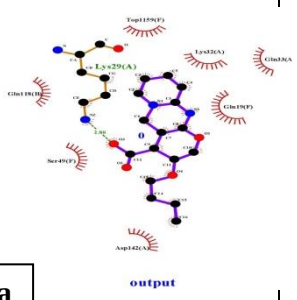	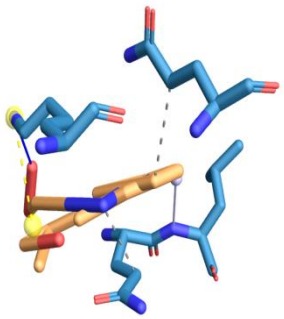	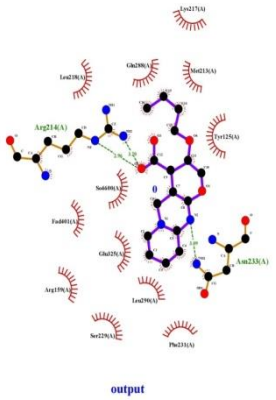	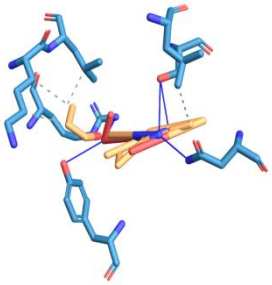
5c 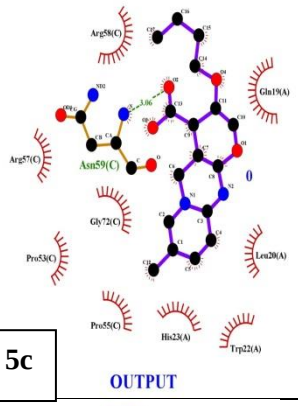	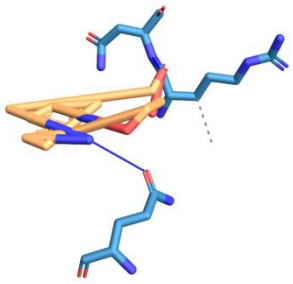	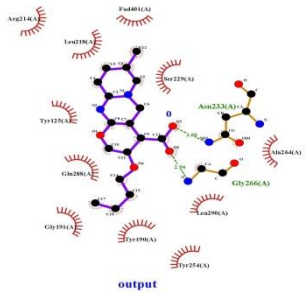	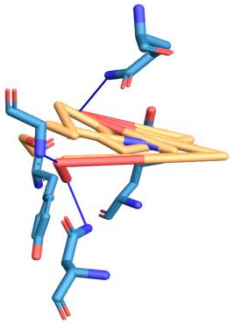
7a 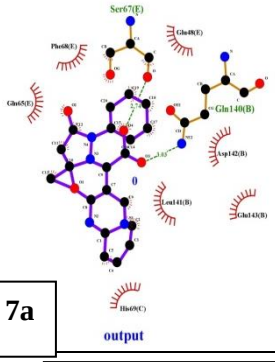	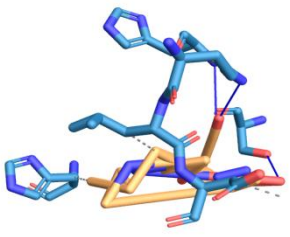	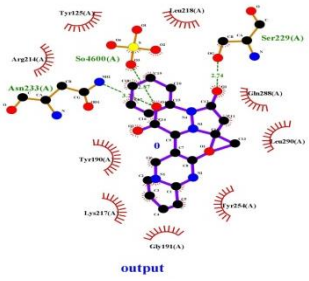	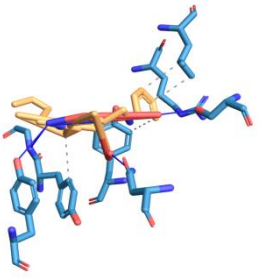

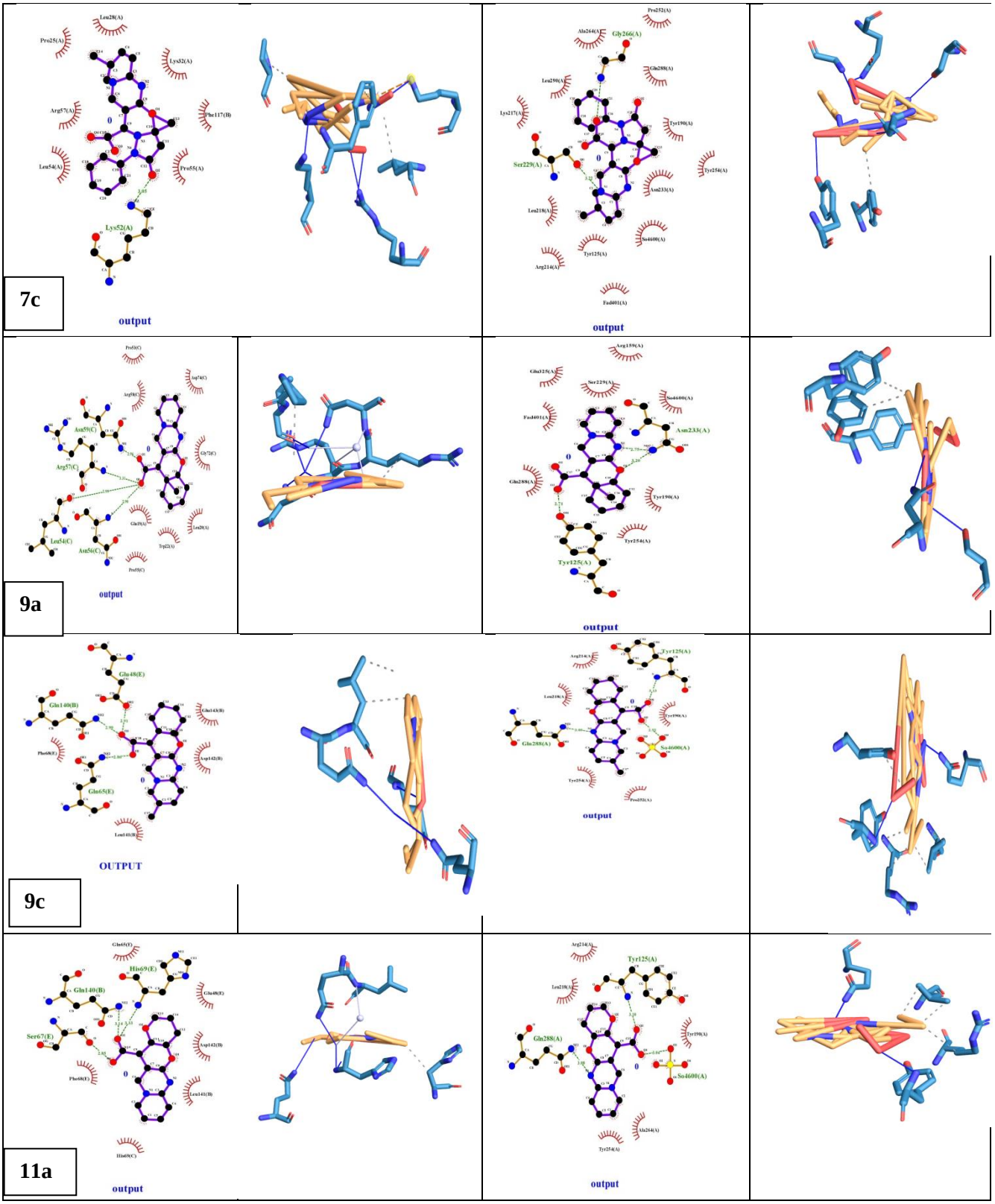
7c
output
output
9a
output
output
9c
OUTPUT
output
11a
output
output

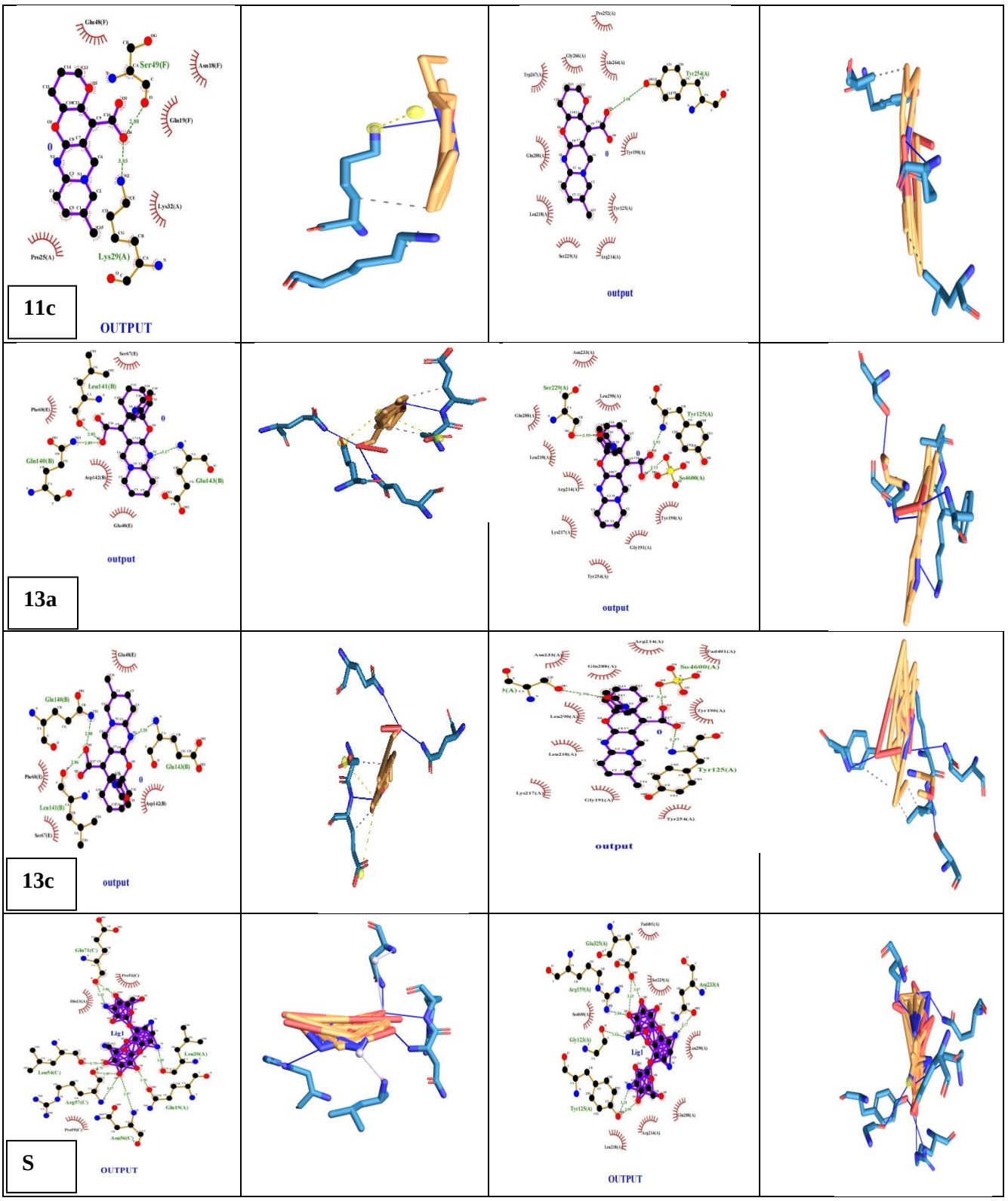
11c
OUTPUT
output
13a
output
output
13c
output
output
S
OUTPUT
OUTPUT

4.10 LIPINSKI'S RULE OF FIVE (ADME)

All newly synthesized showed potential activities against *Staphylococcus aureus* and *Escherichia coli*. Therefore, to ensure that the modified compounds are viable drugs, *in-silico* pharmacokinetic parameters were carried out**.** ADME parameters and molecular properties such as Molecular Weight (MW), Rotatable bonds (RB), Molar refractivity (MR), Hydrogen bond donor (HBD), Hydrogen bond acceptor (HBA), Topological polar surface area (TPSA), Blood brain barrier penetration (BBB), Hydrophilicity (ClogP), and bio-availability were predicted using SwissADME tool. All of the compounds satisfied Lipinski's rule and the values of molecular properties are tabulated in **Table 40**.

The overall polarizability of a mole of a substance is related to molar refractivity. The molar refractivity value should be between 40 and 130 for good absorption and oral bioavailability. The Molar refractivity of the studied compounds lied within its range i.e 76.03-109.8 **A^o.** This indicated that the synthesized compounds have good intestinal absorption and oral bioavailability.

The TPSA aims to predict drug transport properties like intestinal absorption and BBB penetration. When TPSA's quantitative value is below 140 $Å^2$, it becomes a reliable predictor of intestinal absorption, and when it is below 60 $Å^2$, it shows good blood-brain barrier penetration **(Agarwal *et al.*, 2021).** The value of TPSA of the entire studied compound lied in the range 63.82-114.01 $Å^2$ which is under the 140 $Å^2$ upper limit of TPSA, indicating that intestinal absorption was good and since TPSA values were larger than 60 $Å^2$, the proposed derivatives do not penetrate the blood-brain barrier well, as evidenced by the BBB determination.

The ability of molecules to penetrate the outer layer of the skin is described by skin permeability (Kp). For the synthesized compounds studied log Kp values were found to be within the permissible range of – 9.79 to − 7.01 limit. The bio availability's of all the compounds ranged from 0.55-0.85. This indicated that all the compounds have good binding affinity thus suggesting that these have the potential to behave as an orally active drug.

TABLE 40: ADME PARAMETERS OF SYNTHESIZED COMPOUNDS

Compounds	MW g/mol ≤500	RB ≤10	HBA ≤10	HBD ≤5	MR <120 A^o	TPSA (Å^2)	ClogP ≤ 5	Log S	GI absorption	BBB	P-gp	CYP1A2 inhibitor	Logk$_p$ (cm/s)	Drug likeness (Lipinski Violation)	Bio-availability Score
5a	304.34	5	5	1	82.95	73.05	2.09	soluble	High	No	No	No	-7.70	Yes	0.85
5c	318.37	5	5	1	87.92	73.05	2.70	soluble	High	No	No	No	-7.84	Yes	0.85
7a	378.38	2	6	1	87.37	109.04	2.43	soluble	High	No	No	No	-9.58	Yes	0.56
7c	392.41	2	6	1	87.37	114.01	2.69	soluble	High	No	No	No	-9.72	Yes	0.56
9a	300.35	1	4	1	84.30	63.82	2.21	soluble	High	No	Yes	NO	-7.01	Yes	0.85
9c	314.38	1	4	1	89.26	63.82	2.45	soluble	High	No	Yes	NO	-7.16	Yes	0.85
11a	288.30	1	5	1	76.03	73.05	1.82	soluble	High	No	No	No	-8.10	Yes	0.85
11c	302.33	1	5	1	80.99	73.05	2.10	soluble	High	No	No	No	-8.24	Yes	0.85
13a	371.43	2	6	1	104.8	76.29	2.48	soluble	High	No	Yes	No	-9.64	Yes	0.55
13c	385.46	2	6	1	109.8	76.29	2.74	soluble	High	No	Yes	No	-9.79	Yes	0.55